國立交通大學

材料科學與工程學系

博士論文

2-羥基乙基丙烯酸甲酯複合物奈米結構與控制釋放行為之研究

Nanostructural evolution and controlled release behavior of SiO_2/pHEMA and Cu/pHEMA hybrids

研究生：劉彥妤

指導教授：陳三元 博士

中華民國九十八年一月

中文摘要

就許多醫療器材而言，改善其與血液接觸所產生之相容性至今日仍是相當重要的議題。高分子是目前最被廣泛應用於製造醫療元件的材料，通常需藉由改質來改善其血液相容性。許多文獻指出，表面改質方法如電漿表面改質或是肝素接枝法都已被廣泛且成功的運用在與血液接觸的元件上；然而，材料表面為較容易損壞之部分，對於需要植入體內之醫療元件，其可能因腐蝕、與血液接觸或因個人生活型態迥異而造成不同物理環境，產生非預期之化學作用，其更須具備長期穩定之特性。因此，考量醫療元件整體之功用及其在臨床治療上所面臨之問題，材料表面改質及材料整體改質仍具有許多研究及發展的空間。

本論文之研究主旨，即在於利用奈米級無機粒子與金屬粒子之混摻，探討其對於高分子水膠微結構以及整體性質之改變，與此複合材料於藥物釋放以及血液相容性上之討論。論文主體分為兩部分：

第一部分探討奈米級矽分散粒子與矽醇水合前驅物，對於 2-羥基乙基丙烯酸甲酯高分子載體其微結構以及其在血液相容性之影響。我們利用即時(in-situ)光聚合法，成功製備出矽/2-羥基乙基丙烯酸甲酯 (SiO_2/pHEMA and Silanol/pHEMA) 複合材。從電子顯微鏡可知，複合材料孔洞隨無機物含量遞增，含有 4%奈米 SiO_2 粒子之複合材有最佳機械性質。此外，水膠複合材之膨潤度隨無機物含量遞增，當無機物含量由 2% 增加至 9%，藥物擴散速率提高約 100 倍。經由血小板貼覆測試可知 SiO_2/pHEMA 複合材具有相當良好之血液相容性。

第二部分探討奈米級金屬銅粒子，對於 2-羥基乙基丙烯酸甲酯高分子載體其微結構以及其在血液相容性之影響。我們利用即時(in-situ)光聚合法，將銅離子均勻分散於 2-羥基乙基丙烯酸甲酯高分子載體中，其後並以化學還原法，製備得到 Cu(0)-pHEMA 複合材。由穿透電子顯微鏡可知，隨溶劑與單體莫耳比增加，可得奈米級銅顆粒均勻分散於高分子載體，顆粒大小約為 5~10nm。此外，並探討 Cu(0)-pHEMA 複合材中，銅溶解擴散模式以及其對於內皮細胞成長之影響。由結果可知，銅離子可經由

Cu(0)-pHEMA 複合材中以穩定緩慢的模式釋放，可經由複合材料組成之變化，控制銅離子釋放濃度。於體外實驗，與控制組相較，當每日銅釋放量約為 10ppm 時，可提升內皮細胞增長量至 120%；若每日銅釋放濃度高於 20ppm，則會產生毒化情形。

最後，探討 Cu(0)-pHEMA 複合材之電化學特性，與其行氧化作用使 GSNO (Nitrosoglutathione)還原產生一氧化氮(NO)之反應探討。由循環伏安測試我們可得一氧化電流(-320mV vs. Ag/AgCl)，Cu(0)-pHEMA 複合材具有氧化能力。由交流阻抗分析得知，隨 Cu(0)-pHEMA 複合材中之銅含量之增加至 1%, 阻抗可降低至 6438 ohm。在定電位測試中可知，Cu(0)-pHEMA 複合材可將 GSNO (Nitrosoglutathione)還原產生一氧化氮(NO)。

這個以奈米複合材微結構來控制藥物釋放之血液相容元件的研究具有很好的前瞻性。在本研究中，與血液接觸之相容性以及藥物釋放之性質同等重要，而了解複合材中無機奈米顆粒在微結構變化、表面組織及生物相容特性所扮演的角色，將有助於我們發現新的科學現象並設計更新穎的材料以應用在材料科學、生物醫學以及藥物釋放學上。

關鍵詞: 2-羥基乙基丙烯酸甲酯、矽、銅、複合材料、藥物控制釋放、血液相容、表面電性

Abstract

Use of medical devices with clinically acceptable blood compatibility has gained increasing attention over the years. This has been consciously alerted due to a current understanding that the devices used to contact with human blood has been criticized to having insufficient anti-blood clotting surface for short-to-long term invasion medication. Therefore, development of new biomaterials with improved blood compatibility has continuously attracted great attention.

In this thesis, the incorporation of inorganic (silica) and metal (Cu) nanoparticles into the poly(2-hydroxyethyl methacrylate) (pHEMA) matrix to form inorganic/organic nanocomposites for drug controlled release and blood compatibility was achieved.

The first part in this thesis, an in-situ method is developed successfully to mix well-dispersed silica colloidal suspension and silica sol-gel solution with HEMA monomers following photopolymerization to form a nanocomposite. The incorporation of SiO_2 nanoparticles and Silanol into pHEMA matrix revealed a significant effect on the reaction rate of crosslinking during polymerization, resulting in composites with varying nanoporous structures. The nanocomposites showed improved tensile strength, and the platelet adhesion property remained as excellent as that of neat pHEMA, which encourages the use of such composites for antithrombotic applications. Drug diffusion characteristics in the composites can be well modulated by controlling the concentrations of SiO_2 nanoparticles and silanol and water in the starting stage of synthesis.

In the second part, a novel in-situ synthesis method is developed where a hybrid system based on HEMA monomers that were photopolymerized in the presence of Cu^{2+} precursor was prepared through an in-situ synthesis, following an in-situ chemical reduction of the Cu^{2+} precursor to form resulting metallic Cu-containing hybrid. The cell proliferation, surface potential, and interaction with blood of the Cu-pHEMA hybrid nanocomposites was

systemically discussed. From the results, coordinated interaction between Cu(II) with the hydroxyl groups within the pHEMA matrix was confirmed by the infrared spectral analysis and considerable improvement of the thermal stability of the Cu(0)-pHEMA hybrids. Localization of the metallic copper particles within pHEMA network structure as a result of those intermolecular interactions gives rise to the formation of discretely distributed nanocrystallites with a particle size ranging from 10 to 25 nm in diameter. A relatively slow and sustained release of the Cu (in form of cupric ion) from the hybrids for a time period over 10 days was measured, which also illustrated a Cu(II)-induced proliferation of the endothelial cells. The hybrids also showed negative surface charge and considerable improvement in blood compatibility compared to neat pHEMA.

Finally, the electrochemical properties of the Cu-pHEMA hybrid nanocomposites were investigated by cyclic voltammetry (CV) and alternating current (AC) impedance measurements. The generation of nitric oxide in aqueous by Cu(0)-pHEMA hybrid was also tested. From the results, the Cu(0)-pHEMA hybrid exhibits an oxidation current at -310mV. The charge transfer resistances (R_{CT}) of Cu(0)-pHEMA hybrids are estimated to be reduced from 11743 to 6438 ohm, respectively as the content of nano copper particle in polymer matrix increased to 1 wt%. The reduction currents of Cu(0)-pHEMA hybrid varied with the concentration of nitrosoglutathione. With increasing levels of nitrosoglutathione (GSNO), the amount of NO generation increased.

Keywords: 2-hydroxyethyl methacrylate, silica, copper, hybrid, drug controlled release, blood compatibility, surface charge, and electrochemical properties

Contents

Figure captions

Table captions

Chapter 1

Introduction

Improved compatibility with blood is one of the key features for a variety of medical devices. The materials used currently to manufacture the medical devices are mostly polymers, which are not inherently compatible to human blood but require a subsequent modification for clinical uses. However, conditions become more stringent for a number of implantable devices, such as vascular grafts/stents, artificial heart valves, etc. since those devices may suffer from a variety of stresses, flowing fields, and site-specific physiological conditions. Some of the devices require not only surface but also bulk to be biologically compatible; they also need sufficient strength to keep long-lasting service performance during the life time of the patients. Therefore, development of new biomaterials with improved blood compatibility has continuously attracted great attention.

The design and preparation of hydrogels have attracted a great deal of interest in biomedical engineering, pharmaceutical applications, and biomaterials science because of their tunable chemical and three-dimensional (3D) physical structure, good mechanical properties, high water content, and biocompatibility. These unique properties offer great potential for the utilization of hydrogels in tissue engineering, biomedical implants, drug delivery, and bionanotechnology [1-5]. Among all, it has been noticed that methacrylate monomers consisting of an alkyl group, an acrylate ester group, and a functional carboxyl group can react with a wide range of monomers and functionalized molecules providing flexible polymer chains. Methacrylate hydrogels are prepared by interconnecting the lineal polymeric chains with cross-linkers establishing a three-dimensional network of strong chemical bonds. For example, the synthesis of Poly(2-hydroxyethyl methacrylate), i.e., pHEMA, is a favorable biomaterial because of its excellent biocompatibility and physicochemical properties similar to those of living tissues [6-7]. It also exhibits good

chemical and hydrolytic stability and good tolerance for entrapped cells. Because of these unique characteristics, pHEMA is one of the most extensively studied materials in tissue engineering, and has also been widely used as the backbone for synthesizing stimuli-responsive hydrogels. The presence of hydroxyl and carboxyl groups makes this polymer compatible with water, whereas the hydrophobic methyl groups and backbone impart hydrolytic stability to the polymer and support the mechanical strength of the matrix [8].

During the last decade, considerable attention was paid to inorganic–organic hybrid materials because their solid state properties could be tailored in relation to the nature and relative content of their constitutive components. These organic–inorganic composites possess a complicated structure, including phases of the organic and the inorganic polymer and a third phase, which is a product of interaction between the organic and the inorganic components [9]. Recently, the development of hydrogel hybrid with nano-sized materials such as inorganic clays [10-11], carbon nanotubes [12], and polyaniline nanosticks [13] has also been of increasing interest in the field of biomaterials science. Composite materials containing metal (M) and semiconductor (SC) nanoparticles, immobilized in polymer matrices are under intense studies due to fundamental novelty and technological importance. The interconnection of inorganic and organic ingredients by either chemical, or physical interaction upon in-situ polymerization provides not only a featured nanostructure in the resulting hybrid, but also correspondingly offers unique properties that are frequently not able to achieve through individual components. Therefore, it is more interesting and potentially clinically important if a hybrid system can be developed where the constituting component is able to provide desirable functional reaction to deactivate clot-forming proteins in human blood and further reduce or eliminate platelet deposition and aggregation. Moreover, drug controlled delivery could be achieved in this hybrid.

In this thesis, the introduction of inorganic (silica) and metal (Cu) nanoparticles into the pHEMA matrix to form inorganic/organic nanocomposites for drug controlled release and

blood compatibility was achieved. It can be categorized into two parts: Part 1. An in-situ method is developed successfully to mix well-dispersed silica colloidal suspension (Chapter 4) and silica sol-gel solution (chapter 5) with a HEMA monomer following photopolymerization to form a nanocomposite. In part 2, a novel in-situ synthesis method is developed where a hybrid system based on the use of HEMA monomers that were photopolymerized in the presence of Cu^{2+} precursor was prepared through an in-situ synthesis, following an in-situ chemical reduction of the Cu^{2+} precursor to form resulting metallic Cu-containing hybrid.

1.1 Silica-base pHEMA nanocomposites (Part 1)

It can be expected that the incorporation of a silica nanophase into the pHEMA matrix can not only enhance the mechanical properties of the resulting composites but also regulate the release kinetics of the drug from within. Until today, the effects of the variation of the structure of the composite on the diffusion characteristics of a molecule, i.e., a drug, have not been systematically investigated in detail. In addition, the effect of silica nanophase on the hemocompatibility of pHEMA is still unclear. Hence, in chapter 4, nanoporous SiO_2/pHEMA nanocomposites were synthesized in situ by incorporating silica colloid with a HEMA monomer, following a UV-induced photopolymerization. The evolution of nanostructure and drug release behaviors of the hydrogel composite was thoroughly studied.

In addition, the incorporation of polymeric components to sol gel derived materials may constitute an important tool to provide modified chemical reactivity [14] or more compatible media for encapsulation of biological molecules and medicines [15]. The silanol group could provide an active site for further reaction of the surface modification [16] or be a catalyst for the nucleation of other bioactive materials [17]. Because of the activity of silanol, the variation and the modification of the structure and chemical bonding of the hybrid could be expected. Therefore, in chapter 5, silanol group was produced and incorporated with HEMA monomer to form a hybrid membrane for drug controlled release.

The hydroxyl group of the hybrid was verified by controlling the hydrolysis degree of silanol and the composition of the hybrid.

1.2 Copper-base pHEMA nanocomposites (Part2)

Copper has been well-recognized as a physiologically important element for human health and from a number of clinical practices. Copper deficiency has been known to associate with complications such as Wilson's disease, thrombotic disorder, etc. In the meantime, copper is also a widely known element that is able to enhanced repairing efficacy with optimal dose for skin and bone growth as a result of proangiogenic action that favors the development of new vessels after surgery [18-21]. . Copper has also been widely known to enhance the antifertility effect of an intrauterine device (IUD); great efforts have been made to improve the copper-containing intrauterine device (Cu-IUD) and to investigate corrosion behavior of copper *in vivo* and *in vitro* [22]. All of those studies, from in-vivo to clinical practices, have pointed out that a stringent control of copper concentration level, either for the maintenance of health or acting as therapeutic purposes, is essentially critical. For the development of Cu-containing composites, although not extensively studied so far, has been reported for years. However, limitation of copper ion content and the stability of ion release from the hydrogel system are still heavily concerned.

In chapter 6, structural evolution of the Cu-containing composite has been elucidated in terms copper release and its effect on the proliferation or inhibition of human endothelial cells and smooth muscle cells were also investigated.

In chapter 7, the Cu-containing nanocompoistes were characterized by transmission electron microscopy (TEM), X-ray photoelectron spectroscopy (XPS), and streaming potential measurements. Interaction between blood and hybrids were examined in terms of platelet adhesion test.

Finally, in chapter 8, Cyclic voltammetry (CV) and alternating current (AC) impedance

measurements demonstrated that the electrochemical properties of Cu/pHEMA composite could be changed by alternating the synthesis condition. In this study, the nano-sized metal or metal oxide particles could disperse uniformly in polymer matrix and to react with ionic group in the aqueous solution by the charge transfer from the interfacial surface of nano copper particles. In this paper, an experimental study of different electro-chemical and physical aspects of electrochemical sensitive Cu/pHEMA composite was presented.

Chapter 2

Literature Review and Theory

2.1 pHEMA nanocomposites hydrogel

Since the pioneering work of Wichterle and Lim in 1960 on cross-linked HEMA hydrogels [23], and because of their hydrophilic character and potential to be biocompatible; hydrogels have been of great interest to biomaterial scientists for many years. Poly(2-hydroxyethyl methacrylate), i.e., pHEMA, has been extensively studied because of its relatively high capability of water uptake, non-toxicity, and favorable compatibility to tissues and blood, which renders itself as an attractive biomaterials for many biomedical applications such as drug delivery vehicles, contact lenses, antithrombotic devices, and implants [24-25]. However, there are still some disadvantages of the pHEMA hydrogels in utilization such as its poor mechanical properties after swelling. Hence, numerous studies have been conducted to modify pHEMA with the aim of improving its mechanical properties [26-28], electro-responsive properties [29] and to elicit better physiologic responses [30]. To deal with the challenge of producing high mechanical strength hydrogels, researchers have taken many approaches: (1) using special comonomers or altering their composition [31], changing the type and concentration of cross-linking agent [32], and optimizing polymerization conditions [33]; (2) inducing a double network (DN) structure for various combinations of hydrophilic polymers [34]; (3) introducing interpenetrating polymer networks (IPN) into hydrogels [35]; (4) synthesizing organic/inorganic hybrid nanocomposite hydrogels [36]; (5) adopting the method of material reinforcement [26].

In the past few years, nano-composites have attracted considerable attention from both fundamental research and application points of view [37-38]. Nano-structured composites, mixed at the molecular level or near molecular level, are much different from the conventional composites with incorporation of a variety of additives in the polymer

matrices [39]. In inorganic–organic nano-composites, strong chemical bonds (covalent or ionic) or interactions such as van der Waals forces, hydrogen bonding, or electrostatic forces, often exist between the organic and inorganic components. This usually leads to some novel nanocomposites with improved performance properties, which may have large potential applications in the fields of optics [40], electrical devices [41], mechanics [42], photoconductors [43], and so on. In order to meet practical requirements, certain properties of pHEMA such as mechanical properties, thermal stability, wettability, diffusion mechanism of solutes (such as biomolecules or drugs), and affinity to specific biomolecules can be tailored and regulated by the incorporation of nanomaterials and manipulated through controlling the composition of inorganic or organic ingredients, nanostructure, nature of inorganic and/or organic components, etc. [44-46].

2.1.1 Silica/pHEMA nanocomposites

Since the mid-1980s, when the first sol-gel derived hybrids were obtained by mixing linear polymer chains with silica precursors [47], many works have been conducted trying to probe structure and to explore potential applications of this type of materials, as demonstrated by several review papers [48-50]. This low temperature process, which is particularly well suitable to combine with organic species, offers an interesting way of preparing hybrid materials. The most commonly used silica precursor is tetraethoxysilane (TEOS). The sol–gel reactions involving this silicon alkoxide can be summarized as follows:

(i) Hydrolysis

$$\equiv Si-O-C_2H_5 + H_2O \rightarrow \equiv Si-OH + C_2H_5OH \qquad (1)$$

(ii) Condensation

$$\equiv Si-OH + HO-Si\equiv \rightarrow \equiv Si-O-Si\equiv + H_2O \qquad (2)$$

and/or

$$\equiv Si-OH + C_2H_5-O-Si\equiv \rightarrow \equiv Si-O-Si\equiv + C_2H_5OH \qquad (3)$$

If these sol– gel reactions are complete, full condensed silica is obtained through a chemical process that can be summarized by the following equation:

$$Si(O-C_2H_5)_4 + 2\,H_2O \rightarrow SiO_2 + 4C_2H_5-OH \qquad (4)$$

At high pH values, where condensation reactions are favored, discrete, large, and highly condensed silica particles are produced, whereas low pH conditions favor hydrolysis reactions and lead to a finer ramified polymeric silicate structure. A wide variety of types of organic polymers have been employed in the syntheses of hybrids of silica [51]. Particularly the polymer pHEMA is an interesting choice because, in addition to being easily soluble in the water-alcohol mixtures employed in sol-gel method, its pendant hydroxyl groups lead to the formation of hydrogen bonds and eventual condensation with silanol groups [52, 45], thus favoring the production of structurally homogeneous materials within a wide range of compositions[53]. Many studies have been devoted to the preparation of pHEMA-based composite materials with organic HEMA monomers and inorganic precursors such as tetramethoxysilane (TMOS) or tetraethoxysilane (TEOS) through sol-gel processes [54-55].

One of the most important problems in studying the hybrid nano-composite materials is their structural analysis. The correlation between material evolution and composition–structure–property dependence, as well as the processes of nanostructure formation, aggregation and development of self-organized materials has been investigated. The nanostructure surface of silica and hybrids has been studied by several research groups [56-57]. The nano-structure of the hybrid, either with the nano-silica uniformly dispersing in the polymer phases or with phase separation of inorganic and organic phases occurring, depends on the processing conditions such as the type of catalyst, the pH value, the water quantity, the solvent system, and the reaction temperature [58]. In order to investigate the type and the extent of the interactions between inorganic and organic domains, which play a determinant role in controlling the properties of hybrid materials, Fontana et al [59] have characterized the hybrids obtained from the polymerization of pHEMA, modified by silicon

tetraethoxide (TEOS) by Raman and Brillouin spectroscopes to explain tentatively the changes of the properties, included of Brillouin scattering and refractive index, were on the basis of the structural change in the polymeric network, due to the presence of the inorganic domains. Moreover, Wu wt al. [60] have used XRD, FT-IR, BET, SEM and AFM techniques to investigate the influence of the main silica precursors and the type and quantity of organic components (HEMA) on the structure of hybrid materials by sol-gel synthesis. It was found that the type of precursors is of paramount importance for the formation of strong chemical bonds between inorganic and organic components of synthesized materials.

In inorganic/organic nano-coomposites, the inorganic molecules and organic molecules interconnect by chemical covalent bonds, hydrogen bonds or physical interaction. The formation of covalent bonds such as Si-C or specific secondary interactions such as hydrogen bonds between organic and inorganic moieties may be a technique for structural control. Structural control by introducing hydrogen bonds into a system depends on the use of polymers containing specific functional groups susceptible to interacting with Si–OH groups of silica gel. Particularly the polymer pHEMA is an interesting choice because its hydroxyl groups, in addition to forming hydrogen bonds, will eventually form Si–O–C bonds by condensation with silanol groups [61-62], although Si–O–C bonds may be, theoretically, unstable to hydrolysis under sol–gel conditions [52]. On the other hand, the formation of covalent bonds between organic and inorganic moieties may be a technique for structural control. Some studies [63] developed during the past years have emphasized the insertion of covalent bonds linking organic polymers and silica network by introducing coupling agents, which contain both polymerizable and hydrolysable groups. In order to improve the understanding of structural control of hybrid materials synthesized from mixtures of tetramethoxysilane, water and pHEMA, Costa and Vasconcelos [64] introduced a bonding agent 3-methacryloxypropyltrimethoxysilane (MTMOS) in prior to sol–gel

reactions to evaluate the effect of primary interactions between organic and inorganic components. The results reveled that thhe presence of MTMOS prevented crack formation and macroscopic phase separation, though the formation of larger fluctuating composition domains with increasing pHEMA content.

An alternative way to synthesize the inorganic/organic hybrids is by directly mixing inorganic colloidal particles with polymers. The inorganic colloidal particles can be pre-produced through the sol–gel process with a pure inorganic precursor such as alkoxysilanes. Vigier et al. [45] compared two types of pHEMA/silica nano-composites prepared by undergoing free radical polymerization of HEMA either in the presence of HEMA-functionalized SiO_2 nano-particles (Type 1) or during the simultaneous in situ growing of the silica phase through the acid-catalyzed sol– gel polymerization of tetraethoxysilane (TEOS) (Type 2). They demonstrated that Type 1 systems exhibit classical particle-matrix morphology, but where particles tend to form aggregates. Type 2 systems possess a finer morphology characterized by a very open massfractal silicate structure, which is believed to be bicontinuous with the organic phase at a molecular level. Similar discovers were also observed by Yang et al. [65] that the structure of the colloidal silica/pHEMA hybrid consisted of nano-silica uniformly dispersed in the pHEMA phase with slight inter-molecular hydrogen bonding. Furthermore, the structure of TEOS/pHEMA hybrid was similar to a semi-interpenetrated network with pHEMA chains tethered into the nano-silica network by inter- and intra-molecular hydrogen bonding. Consequently, the TEOS/pHEMA hybrid gels exhibited a smoother surface, higher transparency, and better thermal stability than the colloidal silica/pHEMA hybrid gels.

2.1.2 Metal/pHEMA nanocomposites

Recently, polymer-protected nanoparticles have been synthesized successfully [66, 67]. Polymer-protected, nano-sized metals are the subject of increasing attention because they have high potential for application in many technologies, such as the controlled release of

drugs, catalysis, and electron or energy storage [68]. There are different ways to produce such materials: treatment of polymers by metal vapours; reduction of metal salts or their reactions in polymer solutions; incorporation of metal salt solutions in micropores of stretched polymer films; various polymerisation processes of metal-containing monomer systems, etc. As an intermediate between molecular and bulk states, inorganic nano-particles often exhibit unique properties (e.g., electrical, optical, magnetic, catalytic), which are, in addition, dependent on their size [69]. But, this also makes them perfect building blocks for preparation of composite nanostructures with adjustable performances. A polymer is a good choice for the matrix material since it enables an easy processing of the obtained nanocomposites into technologically useful forms. Furthermore, depending on the preparation procedures, polymer matrices can be used to control the size and shape of the inorganic nanofiller. Under certain conditions, nanoparticles of metals can be induced to undergo self-organization into three-dimensional super-lattices [70]. Such nanoparticle assemblies open the door to "tunable" materials, in which optical and electronic properties can be controlled by both the initial cluster sizes and the manner in which the clusters are organized to form larger structures.

It is important to note that the HEMA monomer can likewise act as a ligand due to the presence of the pendant –OH group. Moreover, the pHEMA chains may intertwine amongst the nanoparticles and act as "polyligands" resulting in supramolecular structures. In addition, the HEMA monomer which is approximately 5 Å in width, can find its way into the interior of the nano-particles through the porous structure/windows. Harmon et al. [71] indicated that the cross-linking density increased in the pHEMA nanocomposites suggesting that there is an interaction taking place between the nanoparticles and HEMA; they believe that this interaction is physical (H bonding). In this case the pHEMA–nanparticle nanocomposites may form structures similar in concept to polyrotaxanes. Polyrotaxanes are macromolecules in which a linear component is treaded through a cyclic component; the ends of the linear

component are capped with bulky end groups to prevent slippage [72, 73]. Threading of the linear component through the macrocycle is a statistical event; however, driving forces such as electrostatic attraction, hydrogen bonding and hydrophobic–hydrophilic interactions have been shown to favor threading as well; it should be noted that no covalent bonding exists between the two components in the rotaxane. If the linear component is not capped the system is called a pseudorotaxane; dethreading occurs in pseudorotaxanes and as a result they are much less thermodynamically stable than true rotaxanes.

Currently, several successful methods have been carried out to obtain functional metal nanoparticle/pHEMAl nanocomposites. For example, atom transfer radical polymerization (ATRP) is a recently developed "living" radical polymerization method, which is particularly versatile for the polymerization of various vinyl monomers, such as styrene, methacrylates, acrylates and acrylonitrile [74]. Wang groups [75] developed a kind of polymer-metal complexes which were obtained after the introduction of Cu^{2+} cations into the pHEMA brushes by the complexing bond between Cu^{2+} cations and the hydroxyl groups in pHEMA brushes. However, the homogeneous dispersion of metal nanoparticles in these hydrogels is a key challenge due to the easy agglomeration of nanoparticles and the high viscosity of hydrogels [76]. Recently, several approaches have been reported to obtain composites with well-fined size and morphology of the metal nanoparticles [77, 78]. A more effective approach reported by Wang et al. [79] is the in situ reduction of metal ions in the hydrogel. In this method, the metal ions were anchored in the hydrogel network by the functional groups of the hydrogels before in situ reduction. It can effectively inhibit the aggregation of the metal particles. This method requires the particular modification of the hydrogel with functional groups capable of interacting with the metal precursor ions. However, in most cases, those functional groups, such as thiol, pyridyl and amine, are not environmentally friendly. Therefore, the deprotonized carboxylic acid groups (COO^-) of the pH responsive hydrogel were used directly as the anchoring reagent of the silver (Ag) ions

[80] to prepared successfully novel pH-responsive Ag nanoparticle / p(HEMA–PEGMA–MAA) composite hydrogels by in situ reducing the anchored Ag+ ions.

2.2 pHEMA nanocomposites for drug delivery system

It would be most desirable for drug release to match a patient's physiological needs at the proper time and/or the proper site. This is why there is a great interest in the development of controlled delivery systems [81]. In particular, the application of polymeric systems provides, in a great number of selected cases, a clear optimization in the dosage methods to get the desired therapeutic result in the required target, as well as the optimization of the control drug release in order to obtain the maximum result and the minimum adverse effects. The release of a drug incorporated in a polymeric system takes place by migration of the solute to the medium that surrounds the system by molecular diffusion through the support or by diffusion through micropores of the polymeric matrix. This makes the solute solubility in the polymer an important factor in the control of its migration. Drug diffusion from monolithic systems can be analyzed using Fick's Second Law of Diffusion [82].

Diffusion-controlled polymeric matrix devices have been among the most widely used drug delivery systems, mainly due to their low manufacturing cost. However, in conventional matrix devices, where the drug to be released is dispersed or dissolved uniformly through the polymer, the diffusional distance increases with time (as drug is released), and hence, the release rate decreases. To circumvent this disadvantage of first-order diffusion behavior, various approaches have been developed to achieve constant release rates in polymeric matrix devices, including variations in geometry [83], development of surface eroding polymers [84], and design of devices combining several release mechanisms [85]. Swelling-controlled release systems [86] are capable of delivering drugs at constant rates over an extended period of time. In these systems, the rate of drug

delivery is controlled by the balance between drug (solute) diffusion across a concentration gradient, the polymer relaxation occurring as the cross-linked polymer imbibes water, and the osmotic pressure occurring during the swelling process [87]. Swelling-controlled release systems are based on the principles, where a polymeric carrier can counterbalance normal Fickian diffusion by hindering the release of an imbedded solute or drug, leading to an extended period of drug delivery under zero-order release conditions, Case II transport [88]. Swelling and relaxational behavior of p(HEMA-co-MMA)) polymers were observed by Davidson and Peppas [89] who determined polymer relaxation times by mechanical stress relaxation experiments and used them to calculate the diffusional Deborah number (De), a dimensionless parameter relating solvent uptake to macromolecular relaxation. Franson and Peppas [90] observed the swelling front motion using polarized light to view stressed regions in p(HEMA-co-MMA) and related gels when exposed to water. They noted the importance of gel history on the swelling behavior. After a dry sample was swollen to equilibrium, some macromolecular chains could be disentangled to yield a different structure and different swelling kinetics upon subsequent swelling processes. In addition, Water and solute or drug transport in p(HEMA-co-MMA) was investigated to determine the effects of polymer morphology, composition and solute properties on transport behavior [91]. Anseth et al. [92] developed a novel approach to immobilize nonuniform initial drug concentration profiles in multilaminated matrix devices utilizing photopolymerization techniques. Solution polymerization of HEMA and diethylene glycol dimethacrylate (DEGDMA) in the presence of a model compound, acid orange 8 (AO8), was conducted using UV light and photoinitiators to construct a laminated matrix device. The results indicate that a zero-order release pattern can be approximated by employing a suitable nonuniform initial drug concentration profile. Penetrant uptake behavior into crosslinked polymers has been investigated over the past several decades, with notable contributions made to the understanding of deviations from classical Fickian diffusion [93, 94]. This

general behavior, known as anomalous transport, is bound by pure Fickian diffusion and Case II transport which have been observed in several polymer/penetrant systems [95].

Another powerful approach for controlling drug delivery is to incorporate the drug into biodegradable polymeric matrix, which can achieve a controlled and sustained fashion through the drug diffusion or/and the polymeric carrier degradation. Sustained drug release from a degrading hydrogel is obtained when the initial mesh size of the network is smaller than the size of the drug molecules, since the latter cannot leave the gel before the network has been degraded [96]. Currently, there is a major interest in pulsed drug delivery in which the pharmaceutical device releases the drug at a preprogrammed time [97]. Pulsed drug release can be achieved by creating a rigid, semipermeable membrane around the degradable gel particle. During degradation the gel gradually liquefies, and the swelling pressure Π_{sw} increases. When Π_{sw} exceeds the tensile strength of the membrane, it ruptures [98], followed by a sudden release of the drug. Demeester et al. [99] had demonstrated that the chemical composition of the network (dex-HEMA content and the number of HEMA groups on the dextran chains) strongly affects the degradation rate of dex-HEMA hydrogels. These observations are important to design degrading hydrogel systems with tailored swelling pressure profile for pulsed drug delivery.

Drug delivery technology can be brought to the next level by the fabrication of smart materials into a single assembled device that is responsive to the individual patient's therapeutic requirements and able to deliver a certain amount of drug in response to a biological state. Such smart therapeutics should possess one or more properties such as proper drug protection, local targeting, precisely controlled release, self-regulated therapeutic action, permeation enhancing, enzyme inhibiting, imaging, and reporting. This is clearly a highly challenging task and it is difficult to add all of these functionalities in a single device. Hence, Lee et al. [100] attemped to develop an intelligent system for drug protection, self-regulated oscillatory release, and targeted uni-directional release based on

hydrogels. In the study, a pH-sensitive hydrogel together with a pHEMA barrier was used as a gate to control drug release. In addition, pHEMA coated with poly(ethylene oxide)/poly(propylene oxide)/poly(ethylene oxide) (PEO–PPO–PEO) surfactant was utilized to enhance mucoadhesion on the device surface. Herein, the pHEMA layer not only affects the folding direction but also serves as a barrier to protect the model drugs. In addition, Roma´n et al. [101] designed one kind of "polymeric drugs" based on copolymers of HEMA, and five methacrylic derivatives which incorporate ibuprofen or ketoprofen in their chemical structure by means of labile ester bonds. The use of polymeric systems with pharmacological activity provides very good local activities reducing the toxicological risks, and in addition could act as release systems of the pharmacological active residue, controlled by chemical reactions, mainly hydrolytic processes under enzymatic catalysis [102].

Recently, much attention has been focused on delivery systems which can deliver drugs on demand in response to an external signal. In these systems, release could be pulsatile, periodic or in direct response to some signal generated by the disease state itself. Intelligent materials have been a focus for therapeutic and diagnostic uses [103]. The concept of intelligent drug-delivery systems for clinical therapy could be considered by combining the homeostasis theory and chronopharmacology of drugs [104]. Therefore, intelligent drug-delivery systems not only act as a rate-controlling system for drug release but also deliver the drug when it is required, i.e. they are time-controlled [105]. The use of thermoresponsive hydrogels has received much attention in recent years. Ansari et al. [106] reported the use of thermotropic liquid crystals (LCs) embedded in pHEMA membranes as a temperature-controlled drug release system. The use of thermoresponsive liquid-crystal-embedded membranes has also been studied before [107]. However, the use of thermotropic liquid crystals as thermoresponsive drug-delivery systems is rare. Temperature-related properties of thermotropic liquid crystals are both sharp and positive,

i.e. they can control drug release in response to minute temperature changes.

2.3 Blood compatibility of pHEMA nanocomposites

Antithrombogenic biomaterials have been of great interest in the development of artificial internal organs. When a foreign material is exposed to blood, we first observe the activation of clotting factors or the adhesion and activation of platelets, and finally the formation of non-soluble fibrin network or thrombus. The most popular methods for improving hemocompatibility are the modification of the materials themselves into antithrombogenic materials. To be biocompatible materials used in medical applications must meet certain criteria and regulatory requirements. What actually happens is that when a material comes in contact with the flowing blood, the earliest event that happens at the solid-liquid interface is believed to be the adsorption of blood proteins which is further followed by a number of consequential processes such as the activation of intrinsic coagulation, the adhesion and aggregation of platelets and the activation of the complement system [108]. Since the first attempt in 1950s to develop blood-compatible materials with a negatively-charged surface for artificial vessels, continuous efforts to design biomaterials with superior blood compatibility have been made by various research groups. Such efforts created various polymer surfaces with good blood compatibility, for instance, the surfaces composed of nonionic hydrophilic polymer [109, 110], biomembrane-like polymer [111], and microphase-separated block copolymer [112-113]. To explain the compatibility of these materials, a number of mechanisms have been proposed, because one material has one mechanism different from the others. Moreover, these mechanisms are qualitative and inadequate to explain various phenomena of blood compatibility of the materials. That is, a universal mechanism that can explain the reason for the blood compatibility has not been proposed yet. However, it is known that cells and proteins generally display a low tendency for adhesion to hydrogel surfaces because of the low interfacial free energy of the hydrogels

when in contact with body fluids [114]. One of the most extensively studied hydrogels in biomedical applications is poly(2-hydroxyethyl methacrylate), [p(HEMA)], a thermoset that is not enzymatically degraded or hydrolysed by acidic or alkaline solutions [115-117]. In addition, numerous studies have been conducted to modify p(HEMA) with the aim of improving its mechanical properties [118-120], its electro-responsive properties and to elicit better physiologic responses [121].

A series of complex interactions occur when blood comes into contact with an artificial surface. The interaction between the biological environment (e.g., hard or soft tissue, blood, body liquids, or saliva) and biomaterials take place on the surface of the materials. The biological response of the living tissues against the biomaterials depends on the surface properties, such as the chemical composition, surface energy, resistance to corrosion, and tendency to denature of the neighboring proteins. Therefore, the surfaces of biomaterials are believed to play a vital role in determining biocompatibility [122]. In addition, physicochemical surface properties of biomaterials, such as the chemical composition, wettability, surface energy, semiconductivity, and surface charge, also play important roles in these interactions [123]. Therefore, the surface modification of synthetic polymeric materials in contact with blood is a new research area [124]. Since 1985, HEMA has been polymerized in presence of 2-mercaptoethylamine to an amino-semitelechelic pHEMA [125]. Both prepolymers were linked together by coupling reaction between -NH_2 and -NCO groups, resulting in an ABA type block copolymer. Further, animal experiments showed that this ABA type block copolymer has good blood compatibility and excellent permeability for uric poisonous substances. The surface modification method can be grouped into general categories: physical adsorption, grafting coupling, and grafting copolymerization. Grafting copolymerization of hydrophilic polymer chains to the cellulose surface has been considered to be a promising method for improving blood compatibility [126]. Kwon et al. [127] has found that hemodialysis, acrylic acid, HEMA grafted cellulose

film by radiation grafting technique can effectively improve the surface blood compatibility of cellulose film. In addition, synthesis of poly(HEMA-co-acrylic acid) [128] and poly(HEMA-co-acrylamide) [129] in the presence of gelatin results in semi interpenetrating polymer networks (IPNs) showed remarkable water sorption potential and a fair level of blood compatibility.

Protein adsorption on surfaces of biomaterials and medical implants is an essential aspect of the cascade of biological reactions taking place at the interface between a synthetic material and the biological environment [130]. The anticoagulation activity was evaluated using protein adsorption, platelet adhesion and coagulation time including activated partial thromboplastin time (APTT), prothrombin time (PT), fibrinogen time (FT), and thrombin time (TT). Concerning the protein adsorption process, the fundamental electrostatic interactions between ceramic particles and proteins are only fragmentarily investigated and not well understood [131]. Thus, realizing the potential significance of blood protein–material interaction in biomaterial science, Mishra et al. [132] aimed at studying adsorption of bovine serum albumin (BSA) and fibrinogen (Fgn) onto the surfaces of pHEMA-silica nanocomposites. It was indicated that the nanocomposites surfaces show a fair level of blood compatibility especially at higher and lower content of pHEMA and silica, respectively.

2.4 Effect of copper particles on blood compatibility

It has been noticed that the use of organic-metal compound such as lipophilic Cu complex [133] or metallic Cu particles [134] embedded in the polymeric matrix where a catalytic generation of nitric oxide generated from the composite surface has received promising outcomes in-vitro where both the lipophilic Cu complex or copper particle were employed as a catalyst to activate the redox chemistry by reduction of the nitrite or

S-nitrosothiols into nitric oxide in blood and has successfully mimicking the nitric oxide forming activity of endothelial cell or other cells.

In addition, the proangiogenic activity of a hyaluronan-based 50% hydrogel (Hyal-50%) enriched with copper ions (Cu(II)) has also been reported where the Cu-containing hydrogel was mixed with freeze-dried bone and inserted in subcutaneous pockets. The angiogenesis results showed a significant higher vascular density in Hyal-50%-Cu(II) and Hyal-50%- Cu(II) plus freeze-dried bone group when compared to other groups [18].

Besides, it is interesting that using of n-type oxides (e.g., CuO), which behave as a semiconductor, provides a thromboresistant surface [135]. Briefly, Platelets and blood were found to react strongly with p-type biomaterials while little or no sign of interaction with n-type biomaterials was demonstrated. It might be due to that p-type semiconductors have a higher oxidative potential than n-type semiconductors.

Moreover, from the view of nutrition, copper has been well-recognized as a physiologically important element for human health and from a number of clinical practices. The copper content of adult is about 1.4 ~ 2.1mg of copper per kilo of dry body and the copper concentration in the group of apparently healthy human was 0.85 ± 0.19 (μg Cu/ml)[]. The deficiency of copper has been known to associate with complications such as Wilson's disease, thrombotic disorder, etc. In the meantime, copper is also a widely known element that is able to enhanced repairing efficacy with optimal dose for skin and bone growth as a result of proangiogenic action that favors the development of new vessels after surgery [19-21]. It has to pay attention that copper ions stimulate proliferation of human umbilical artery and vein endothelial cells but not human dermal fibroblasts or arterial smooth muscle cells [22]. Incubation of human umbilical vein endothelial cells for 48 h with 500 μM $CuSO_4$ in a serum-free medium in the absence of exogenous growth factors

results in a twofold increase in cell number, similar to the cell number increase induced by 20 ng/ml of basic fibroblast growth factor under the same conditions.

From these evidence, therefore, either being a catalyst for producing nitric oxide in the blood vessel or a activation factor for blood vessel repairing and the stimulation of endothelial cells, copper particles or copper ion must play an important role in coagulating mechanism.

Chapter 3

Experimental

3.1 Flowchart of Experiment Process

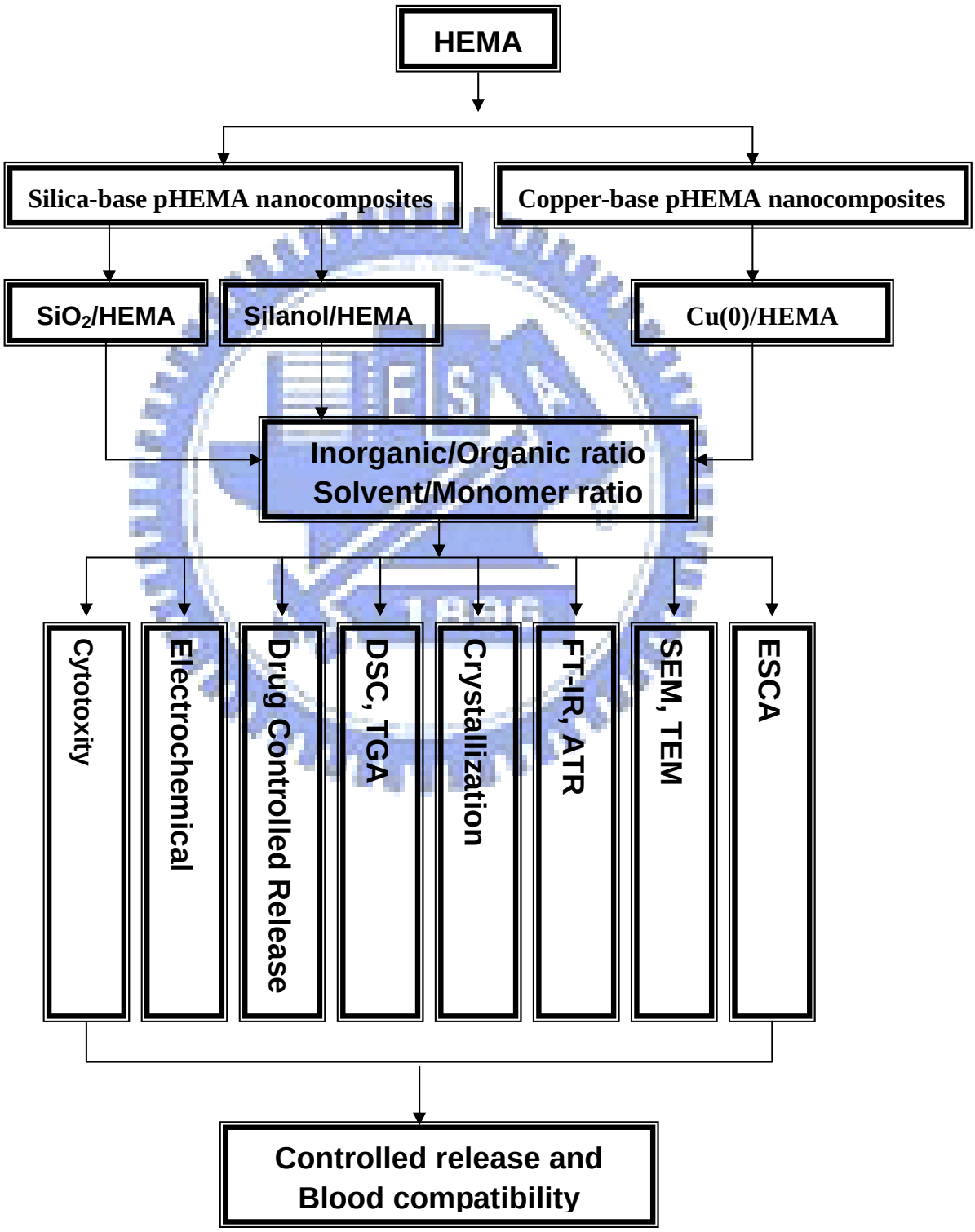

3.2 Materials and Equipment

Materials

Name	Source	
2-hydroxyethyl methacrylate (HEMA)	Tokyo Kasei Kogyo Co., Ltd., Japan	
benzoin methyl ether (BME)	Tokyo Kasei Kogyo Co., Ltd.	
ethylene glycol dimethacrylate (EGDMA)	Showa Chemical Co., Ltd., Japan	
Nanosilica suspension	(ChangChun group, Taiwan)	particle size ranging from 10 to 12 nm and 20% solid content
Vitamin B_{12}	Sigma-Aldrich, Inc. USA	
Phosphate-buffered saline (PBS)	Sigma-Aldrich, Inc. USA	
glutaraldehyde	Fluka, Sigma-Aldrich, Inc. USA	
Alcohol	Sigma-Aldrich, Inc. USA.	99.5%
Darocur 1173	Ciba	
tetramethoxy silane (TMOS)	Sigma-Aldrich, Inc. USA	
Pyranine	Fluka, Sigma-Aldrich, Inc. USA	
Polyvinylpyrrolidone (PVP)	Sigma-Aldrich, Inc. USA,	Average mol wt 10,000, analytical grade
$CuSO_4$	Sigma-Aldrich, Inc. USA	analytic grade
Hydrazine	Sigma-Aldrich, Inc. USA	analytic grade
Heparin	Sigma-Aldrich, Inc. USA	Grade I-A, cell culture tested, ≥140 USP units/mg, powder
Endothelial cell growth supplement (ECGS)	Sigma-Aldrich, Inc. USA	from bovine pituitary, cell culture tested
TES	Sigma-Aldrich, Inc. USA.	Biotechnology performance certified, cell culture tested
ascorbic acid	Sigma-Aldrich, Inc. USA.	Cell culture tested

insulin	Sigma-Aldrich, Inc. USA	Chemically defined, recombinant from *Saccharomyces cerevisiae*, solution, sterile-filtered, cell culture tested
apo-transferring human	Sigma-Aldrich, Inc. USA	Powder, γ-irradiated, cell culture tested
sodium selenite	Sigma-Aldrich, Inc. USA	Lyophilized powder, γ-irradiated, cell culture tested
fetal bovine serum	Biological Industries, Israel	Lot: 215029
medium 199	GIBCO®, Invitrogen™ cell culture	Medium 199 (1X), liquid
F-12K medium	GIBCO®, Invitrogen™ cell culture	F-12K Nutrient Mixture, Kaighn's Modification (1X), liquid
L-glutamine	GIBCO®, Invitrogen™ cell culture	L-glutamine-200 mM (100X), liquid
HEPES	GIBCO®, Invitrogen™ cell culture,	HEPES Buffer solution (1M)
Sodium diethyldithiocarbamate trihydrate	Sigma-Aldrich, Inc. USA	
AlamarBlue™ assay	AbD Serotec Ltd, Oxford, UK	
Nitrosoglutathione (GSNO)	Sigma-Aldrich, Inc. USA	

Equipments

Name	Type	
Field-emission scanning electron microscopy (FE-SEM,).	JAM-6500F, JAM-6700F	
Transmission electron microscope (TEM)	Philips Tecnai 20 (Holland, The Netherlands)	operated at 200 keV
Ultramicrotome	Leica EM UC6	
Tensile mechanical test	MTS Tytron 250 and TestStar IIs systems	
Differential scanning calorimeter (DSC)	Perkin Elmer	
Atomic force microscopy (AFM)	NanoScope Multimode atomic force microscope (Digital Instruments, Inc.)	
UV-VIS spectrometer	SP-8001, Metertech Inc.	
digital thickness gauges	ASTM D926	
Fourier transformed infrared ATR spectra (FTIR-ATR)	Perkin Elmer Spectrum, USA	ZnSe prism 16 scans from 4000 to 650 cm^{-1} region and 4000 to 8500 cm^{-1}
thermogravimetric analyzer (TGA).	DuPont 2050	
fluorescence spectrophotometer	(F-4500, Hitachi, Ltd. Japan)	
analytical semi-micro precision balance	PRECISA XS225A Series, Switzerland	precision: 0.0001g
X-ray diffraction		Cu Kα X-radiation of wavelength 1.54 Å
ELASA spectrophotometer	GDV DV990 BV4	
potentiostat	CH instruments, CHI, model 614A	

3.3 Characteristics Analysis

Field-emission scanning electron microscopy (FE-SEM)

The morphology and structures of the samples were examined by field-emission scanning electron microscopy (FE-SEM, JAM-6500F).

Transmission electron microscope (TEM)

Microstructure observations were performed using a Philips Tecnai 20 (Holland, The Netherlands) transmission electron microscope operated at 200 keV.

The ultrathin sections of the composites were prepared using a Leica EM UC6 Ultramicrotome with EMFCS cryoattachment at room temperature. The cross-sections measuring approximately 100 nm in thickness were obtained by using a diamond knife. The ultrathin films of the composites were directly placed on the copper grids.

Tensile mechanical test

The tensile mechanical properties of the hybrid composites were measured in wet state by first immersing the composites in water for 2 hr and then evaluating through a complete system of MTS Tytron 250 and TestStar IIs systems in a crosshead speed of 10 $mm \cdot min^{-1}$ at 25°C. The initial cross section (10 mm^2) was used to calculate the tensile strengths and the tensile modulus. Five parallel measurements were carried out for each sample.

Differential scanning calorimeter (DSC)

The phase transitions of water in the polymer were measured with a differential scanning calorimeter (DSC, Perkin Elmer), equipped with a low-temperature cooling apparatus. The hydrated sample (5–10 mg) was placed in an aluminum pan. The sample was first cooled to –60°C and then heated to 20°C at the rate of 5.0°C/min. The heating process was

monitored.

Atomic force microscopy (AFM)

The topology of the pHEMA and hybrids surfaces was studied by atomic force microscopy using a NanoScope Multimode atomic force microscope (Digital Instruments, Inc.). The images were recorded with standard tips in contact mode at a scan rate of 1.0 Hz. The root-mean-square (RMS) surface roughness of the membranes was also determined.

Fourier transformed infrared ATR spectra

Fourier transformed infrared ATR spectra (FTIR-ATR, Perkin Elmer Spectrum, USA) of the hybrids were obtained with a multiple internal reflectance apparatus where ZnSe prism is used as an internal reflection element. The spectra were obtained with an average of 32 scans from 4000 to 650 cm^{-1} region and 4000 to 8500 cm^{-1}.

X-ray diffraction (XRD)

The crystal structure of Cu precipitates in the pHEMA matrix was characterized using X-ray diffraction utilizing Cu Kα X-radiation of wavelength 1.54 Å, at scanning rate of 0.1 s^{-1} in the 2θ range from 20 to 70.

Thermogravimetric analyzer (TGA)

The dynamic weight loss test of hybrids were conducted on a DuPont 2050 thermogravimetric analyzer. All tests were conducted in a N_2 purge (25 ml/min) using sample weights of 8~10 mg over a temperature range 40^{o}C to 600 ^{o}C at a scan rate of 10 ^{o}C/min. The morphology and structures of the Silanol/pHEMA composites were examined by field-emission scanning electron microscopy (FE-SEM, JAM-6500F).

X-ray photoelectron spectroscopy (XPS)

The chemical states of Cu(0)-pHEMA hybrid was determined by X-ray photoelectron spectroscopy (Thermo, VG350, UK) equipped with Mg K_α at 300W power at the anode. A survey scan of varying 0.1 eV for Cu 2p3/2 was taken.

3.4 Methods

In Vitro Release Kinetics

The procedure for drug release tests has been demonstrated in an earlier study [136]. In brief, the test was performed in a vessel containing 2 compartment chambers of equal volume; 1 chamber (considered as the donor side) contained 90 ml of 2000 ppm vitamin B_{12} in PBS (pH 7.4) and the other chamber was loaded with only drug-free PBS (pH 7.4). Each chamber was mechanically stirred during the test. The concentration of vitamin B_{12} in the medium was measured by a UV-VIS spectrometer (SP-8001; Metertech Inc.) at 361 nm. The permeability was calculated according to Eqn. (3-1) [136]:

$$\ln\left(\frac{C_{10}}{C_1 - C_2}\right) = \frac{2[DH]At}{\delta V} \qquad (3\text{-}1)$$

where H is the partition coefficient, D is the effective diffusion coefficient, A is the effective area of the membrane, δ is the thickness of the membrane which was measured by digital thickness gauges (ASTM D926) with 5 parallel measurements for each sample, V is the solution volume (90 ml), C_{10} is the initial concentration (at t = 0) of the drug in the donor solution. C_1 and C_2 are the concentrations in the donor and receptor chambers, respectively, at a given time period (t = t) of diffusion. By plotting $\ln[C_{10}/(C_1 - C_2)]$ versus time, the permeability [DH] can be obtained from the slope of the line. The apparent partition coefficient (H) of vitamin B_{12} for pHEMA, p(water/pHEMA), and SiO_2/pHEMA composite membranes can be determined as follows [137]. The wet weight (W) of the membranes was recorded after immersing drug-free membranes (1 g) in the release medium (drug-free PBS,

pH 7.4) for 2 days. The wet membranes were then immersed in 10 ml of 2000 ppm vitamin B_{12}-containing medium. The partition coefficient (H) is determined from the initial (C_0) and equilibrium (C_e) concentrations of vitamin B_{12}-containing mediums by Eqn. (3-2):

$$H = 10(C_0 - C_e)/WC_e. \qquad (3\text{-}2)$$

Platelet Adhesion Assessment

Fresh blood was drawn from a healthy adult volunteer. Care was taken to insure that it was free of aspirin and other drugs, such as anticoagulant, that could bias the results. Fresh blood and platelet adhesion tests were performed *in vitro*, to investigate the quantity of the adherent platelets on the Cu(0)-pHEMA hybrid. Cu(0)-pHEMA hybrid, i.e., 20C, with 1cm × 1cm in dimensions were immersed in 0.5ml platelet rich plasma (PRP) solution in the 24-well plate and then incubated at 37°C for 2 hr. After terminating the adhesion test by adding 0.5ml PBS into each well, samples were subsequently rinsed with a PBS buffer solution three times to remove the weakly adherent platelets. The firmly adhered blood components or platelets were fixed using 2.5% glutaraldehyde solution at 4 °C for 1 h. Samples with adherent blood components or platelets were then dehydrated in graded ethanol solutions (30%, 50%, 70%, 95%, and 100% for 15 min, respectively, at room temperature) and dried at 37°C for 24 h. Then, the samples were characterized by field-emission scanning electron microscopy (FE-SEM, JAM-6700F) operated at 5 kV. Four SEM images were taken at a magnification of 500X for each sample and five parallel measurements were carried out for each hybrid. The numbers of platelets on the membrane surface were counted for each image and the counting area could be estimated by the scale bar. So the numbers and the volume fraction of platelet on the membrane surface were quantized. Volume fraction of thrombosis coverage on sample surface was counted on 20 fields chosen at random to obtain good statistic analysis.

Copper ion release test

A characteristic coloring is one of the most distinguishing features for cupric ion chelates and visual absorption spectra can be used to quantify the cupric ion content [138, 139]. Sodium diethyldithiocarbamate (copper reagent) was used to form a yellow chelate with the cupric ion. Spectrophotometric measurements were conducted using five concentrations of $CuSO_4$ solution and adding copper reagent chelating agent. Absorbance (Abs) measurements were made at 1 nm intervals from 350 nm to 600 nm. The absorbance was measured using a UV-VIS spectrometer (001; Metertech I SP-8nc.) The calibration curve showed peak height (Abs) as a function of concentration of cupric ions. An absorption maximum can be observed at 450 nm and determinations were performed at this specific wavelength (450 nm). Absorbance measurements were calibrated using cupric sulphate solution and the copper reagent chelating agent. The release of cupric ion was determined by measuring the cupric ion content in the simulated uterine solutions, expressed as mg/L after 24, 48, 72, 96, 120, 144, 168, 192, 216, and 240 hours. Absorbance measurements were performed as follows: chelate solution was added to 10 mL of Cu(0)/pHEMA hybrid sample incubated solutions (pH=7.4) and the cupric ion content in the buffer solutions was then calculated from the measured absorbance and the calibration curve.

Cell culture

Endothelial cells (ECs, HUVEC, human umbilical vein endothelial cell, BCRC number: H-UV001) were purchased from Food Industry Research and Development Institute (FIRDI), Taiwan. ECs were grown in 90% medium 199 with 25 U/ml heparin, and 30 μg/ml endothelial cell growth supplement (ECGS) adjusted to contain 1.5 g/l sodium bicarbonate and 10% fetal bovine serum. Smooth muscle cell (SMCs, T/G HA-VSMC smooth muscle cell, human normal aorta smooth muscle cell, BCRC number: 60293) were also purchased from FIRDI and were grown in culture medium containing 90% F-12K

medium with modifications-Ham's F12K medium with 2mM L-glutamine adjusted to contain 1.5 g/l sodium bicarbonate supplemented with 10mM HEPES, 10mM TES, 0.05 mg/ml ascorbic acid, 0.01 mg/ml insulin, 0.01 mg/ml transferrin, 10 ng/ml sodium selenite and 0.03 mg/ml ECGS and 10% fetal bovine serum. The cells were incubated in 75 cm^2 culture flask (for ECs, the flask was coated with 1% gelatin (Sigma-Aldrich, Inc. USA) before used) in 5% CO_2 at 37 ^oC and culture medium renewal was carried out about every 2~3 days. After 5~10 days, the cells were removed from the 75 cm^2 culture flask with trypsin (Gibco, Invitrogen, Taipei, Taiwan) into the 96-well culture plates with a cell concentration of 5×10^3 cells/ml for 6 h and then incubated with pHEMA and Cu(0)-pHEMA hybrids for durations of 1 and 2 days.

Cell proliferation assay

The viability and proliferation of ECs or SMCs culture with pHEMA and Cu(0)-pHEMA hybrids at specific durations were determined by *AlamarBlue™* assay (AbD Serotec Ltd, Oxford, UK). *AlamarBlue™* assay is designed to quantitatively measure the proliferation of various human and animal cell lines. *AlamarBlue™* assay was diluted in an amount equal to 10% of PBS volume. At the specified durations (1 and 2 days), pHEMA or Cu(0)-pHEMA hybrids and culture medium were removed from the 96-well culture plate, and 100μl of diluted *AlamarBlue™ assay* was added to each well and the plates were incubated at 37 ^oC under 5% CO_2 for 4 h. The absorbance, or called optical density (OD), of *AlamarBlue™ assay* (color from blue to purple) was measured at 590 nm with an ELASA spectrophotometer. The proliferation of endothelial cells (HUVEC) and smooth muscle cells (T/G HA-VSMC) cultured in medium without the endothelial cell growth supplement (ECGS) was also tested in contrast. All experiments were repeated five times. Data were taken to be significant, when a *p*-value of 0.05 or less was obtained (showing a 95% confidence limit)

Zeta potential measurement

The surface charge (zeta potential) of the pHEMA and hybrid membranes were characterized using a streaming potential apparatus, which has been detailed elsewhere [140]. In brief, an electrolyte solution was prepared with a 10^{-3} M KCl solution (dissolved in ultrapure water) at pH 7.4 where the pH value was adjusted by the addition of 0.1M NaOH or 0.1M HCl solutions. In each experiment, the solution flow through the membrane module was supplied by peristaltic pump and the trans-membrane pressure was controlled between 0.2 ~ 1 bar, while the crossflow velocity of the solution was fixed at 0.1 m/s. For each sample, four values of pressure difference (ΔP) were measured and the data of streaming potential (ΔE) were recorded by a personal computer. The zeta potential ζ was calculated using the Helmholtz-Smoluchowski equation, eq. (3-3), where κ is the liquid conductivity, η is the liquid viscosity, ε_r is the liquid permittivity, ε_o is the permittivity of free space, ΔE is the streaming potential, and ΔP is the hydrodynamic pressure difference. The zeta potential ζ was calculated from the slope of ΔE/ΔP curve which having a R-square of the regression curve larger than 0.99, i.e. $r^2 > 0.99$ for each sample.

$$\zeta = \frac{\kappa\eta}{\varepsilon_r \varepsilon_0} \frac{\Delta E}{\Delta P} \qquad (3\text{-}3)$$

Electrochemical tests

Electrochemical tests were performed using a standard three-electrode, temperature-controlled cell and a microprocessor controlled potentiostat (CH instruments, CHI, model 614A). An Ag/AgCl (in 3M NaCl) electrode was used as the reference and platinum plates were used as the working and counter electrode. Cyclic voltammetry (CV) analysis was carried out in 0.1M NaOH solution at room temperature from -700 to +700 mV, at a rate of 50 mV/sec versus an Ag/AgCl reference electrode. A three-electrode system was used throughout the study. Pt plates were used as the working and counter electrode. Cu/pHEMA film clipped tightly

between working and counter electrode and the surface of the Cu/pHEMA sample was stuck smoothly on each of the electrode. Analysis of cyclic voltammetry tracings and determination of the oxidation potential and the anodic current are reported. An alternating current (AC) impedance measurement technique was employed to investigate the electrochemical kinetics at the Cu/pHEMA- electrolyte interface. The measurement was performed at an open-circuit potential and the frequency was varied in the range of 10^5 Hz to 10^{-2} Hz with an imposed voltage of 5 mV AC (model 614A, CHI). These experiments allow the detection of the properties of the films when submerged in an electrolyte solution. Parameters such as capacitance and resistance are generally recorded. The time constant, τ, is calculated by multiplying the values of capacitance and electrical resistance obtained from the impedance measurements.

Chapter 4

Inorganic/organic Hybrid – SiO_2/pHEMA –Synthesis and Characterization of Nanoporous SiO_2/pHEMA Biocomposites

4.1 Introduction

Inorganic/organic hybrid materials have long been attracted great attentions because they have exhibited synergistic beneficial properties from individual components, this unique characteristic has been widely employed in a vast number of engineering and technical areas especially medical community to producing biomedical devices with improved properties. With the advancement of nanometerials technology, highly uniform hybrid composites, especially surface characteristics, becomes stringently inquired for medical uses, where, except those required sufficient mechanical property for load-bearing uses, a surface contact between the medical devices and tissues or blood in human body is critical for the success of the devices or implants.

In this investigation, SiO_2/pHEMA was synthesized and characterized by directly mixing a well-dispersed silica colloidal suspension with a HEMA monomer following photopolymerization to form a composite structure. This method provides not only a simpler scheme of the synthesis of a SiO_2/pHEMA composite, and furthermore, drug release characteristics can be easily manipulated through the control of nanostructural evolution.

4.2 Fabrication of pHEMA and SiO_2/pHEMA Composite

The pHEMA and SiO_2/pHEMA composite were prepared by free-radical photopolymerization at room temperature. The content of the HEMA monomer, EGDMA, SiO_2 suspension, and the solvent (H_2O) during the polymerization are summarized in Table 1.

The composites of x wt% solvent (H_2O) and y wt% nanosilica particles in the reaction solution are designated as ySixH. The overall nanosilica particles loading was varied in the range of 0 wt% to 9 wt% for the composites, indicated as "y" in the abbreviations in Table 1. The composition of the composites determines the structure of the resulting composite. The concentrations of the initiator and crosslink agent were 0.1 wt% and 2 wt%, respectively, based on the HEMA weight. The reaction solution was well mixed by an ultrasonic degasser for 5 min. The well-mixed and unseparated reaction solution was injected into a mold and then polymerized to form a composite by UV light exposure at 365 nm for 2 h.

Table 4.1 pHEMA and SiO_2/pHEMA composites

Sample name	HEMA (Wt%)	SiO_2 (Wt%)	H_2O (Wt%)
pHEMA	97.5	0	0
35H	62.5	0	35
50H	47.5	0	50
4Si35H	58.5	4	35
9Si35H	53.47	9	35
2Si50H	45.5	2	50
4Si50H	43.5	4	50
9Si50H	38.5	9	50

4.3 Microstructure and Physical Characterization

Fig. 4.1 shows the cross-sectional microstructure of the SiO_2/pHEMA composites with different amounts of H_2O and SiO_2 concentrations during polymerization. It was observed that, in Fig. 4.1(a), sample 35H showed a considerably dense and uniform microstructure with no visually observable voids, which is similar to that of pure pHEMA membrane (0H) (not shown in Fig. 4.1), i.e., without the use of water. However, on increasing the amount of water during the synthesis of pHEMA, i.e., 50H, the resultant samples presented a loose microstructure, as illustrated in Fig. 4.1(b). This is because although water is a good solvent for the HEMA monomer, it become a poor solvent upon polymerization, i.e., for the HEMA polymer or pHEMA. Phase segregation between water and pHEMA phases may accordingly cause a change in the resultant microstructure. In the presence of water, a transparent, homogeneous pHEMA membrane can be obtained only when the concentration of water is below a certain critical value (between 40% and 60%) [141]. When the water concentration exceeds the critical value, phase separation occurs due to the thermodynamic interaction between water and the polymer network, resulting in an opaque, heterogeneous pHEMA hydrogel.

With the incorporation of the silica nanoparticles together with a sufficient amount of water in the starting solution, the resulting composite membranes of 4Si35H and 4Si50H, shown in Fig. 4.1(c) and (d), exhibited a wrinkled structure. In contrast to the sample without SiO_2 particles, 4Si35H and 4Si50H presented a rougher surface morphology. With a further increase in the content of silica nanoparticles, i.e., sample 9Si35H (Fig. 1(e)) showed a nanoporous structure developed in the composite. Similarly, for sample 9Si50H, with higher water and silica nanoparticles contents, a submicroporous structure was developed, as illustrated in Fig. 1(f), indicating that the addition of SiO_2 nanoparticles induced the formation of nano-to-micro pores. The variation in microstructural evolution of the composites suggests that the presence of the SiO_2 nanoparticles does play an important role

in the evolution of nanoporosity during synthesis.

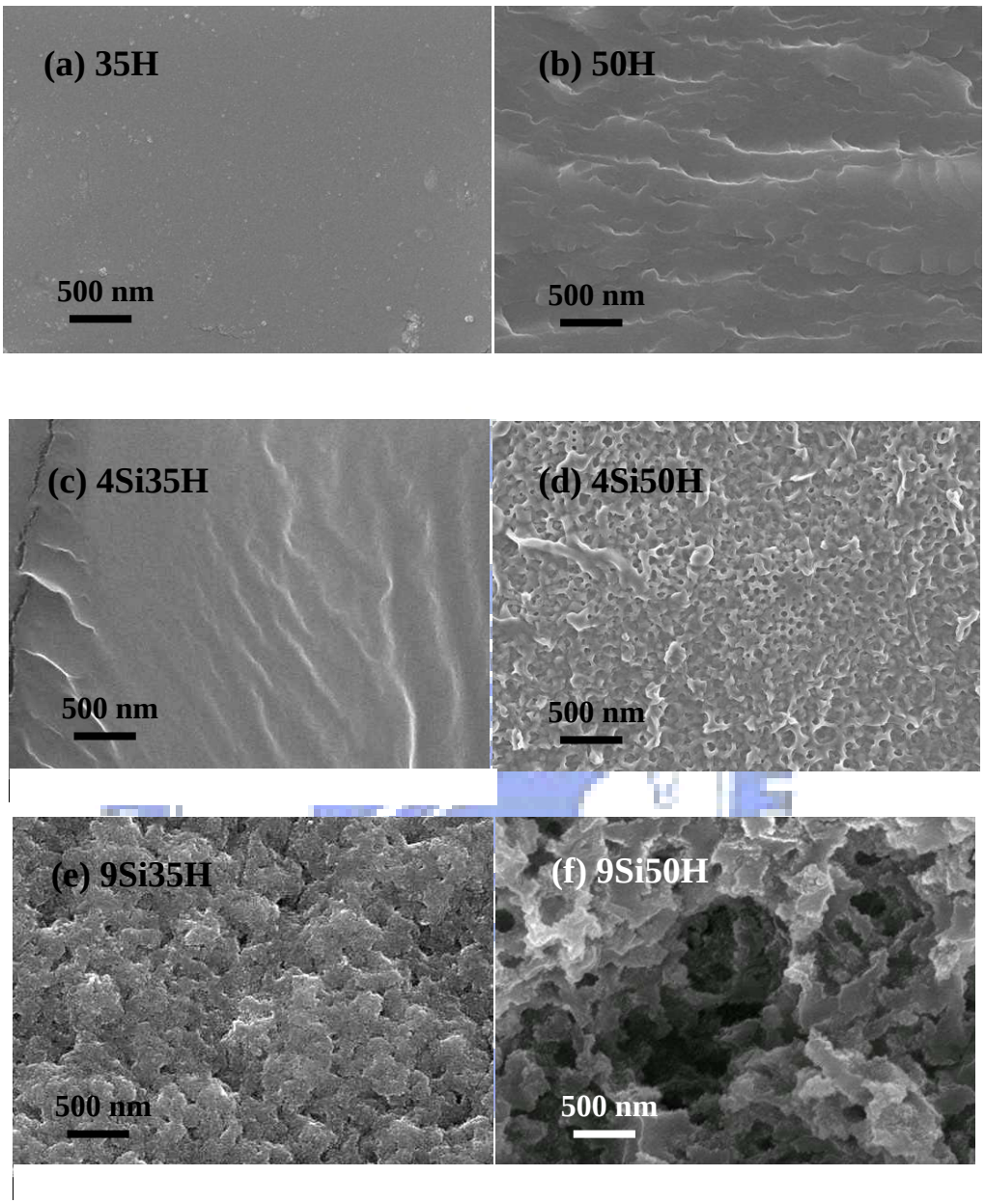

Fig. 4.1 SEM micrographs of cross-section image of various SiO2/pHEMA composites

The development of a nanoporous structure in the presence of the nanoparticles suggests that the nanoparticles may act as a heterodomain that induce phase separation, thus forming nanoporosity in the SiO_2/pHEMA composite. As shown in Fig. 4.1(e), the nanopores developed during UV polymerization were randomly distributed in the composite. These nanopores percolated into a continuous network throughout the composite structure (Fig.

4.1(f)).

Radical polymerization has been known as the reaction responsible for the synthesis of polymeric HEMA; however, this reaction is expected to take place without interference in the regions at a distance away from the site of the SiO_2 nanoparticles, which is termed as a "bulk region." Nevertheless, in the region (termed "domain region") that is close to the vicinity of the nanoparticles, the polymerization rate of the HEMA monomers is catalytically accelerated over the "bulk region." Thus, the monomers near the silica nanoparticles can be cured at a faster rate under UV irradiation than those of the bulk regions [142-144]. Hence, the difference in the rate of polymerization between the "domain regions" and "bulk regions" induced the formation of heterodomains. It is believed that a phase separation should take place once the heterodomains are fully developed; this would result in a nanoporous structure in the final composite. Furthermore, the diffraction efficiency of the UV light can be enhanced by the presence of nanoparticles [145, 146] so that the presence of SiO_2 nanoparticles is expected to accelerate the polymerization rate and accordingly, the regions near the nanoparticles polymerize faster than other regions that are far from the nanoparticles is expected. By increasing the content of SiO_2 nanoparticles, it was found that the formation of porous structure of the membranes was enhanced for the samples of 4Si50H and 9Si50H, as shown in Fig. 4.1(d) and (f). In other words, it indicates that the acceleration of polymerization rate could be enhanced by SiO_2 nanoparticles, inducing the phase separation of polymer and the nanoporous structure.

Figure 4.2 shows that the tensile strength is decreased with increasing water concentration for the samples without silica nanoparticles. This has been explained to be a result of a lower degree of crosslinking during polymerization. However, a considerable improvement in the tensile strength can be detected for the SiO_2/pHEMA composites. It was noted that the tensile strength of the 35H samples increased with the addition of silica

nanoparticles up to 4 wt%. This mechanical reinforcement effect of the silica nanoparticles can be referred to an earlier argument where the silica nanoparticles enhanced the degree of polymerization and possibly interacted with the pHEMA matrix although numerous nanopores were formed in the matrix polymer [142]. Those nanopores appear to have little effect on the deterioration of the tensile strength of the 9Si35H composites, and it is believed that the silica nanoparticles do provide an advantage in mechanical reinforcement. The same scenario is prevalent for other compositions except for the sample 9Si50H for which the tensile strength was decreased compared with that of the sample 4Si90H. The explanation for this exception in the sample 9Si50H is due to the water content exceeding a critical value (40%) during the synthesis of SiO_2/pHEMA where a considerable phase separation may have occurred, resulting in a composite with a higher porosity, as evidenced in Fig. 4.1(f).

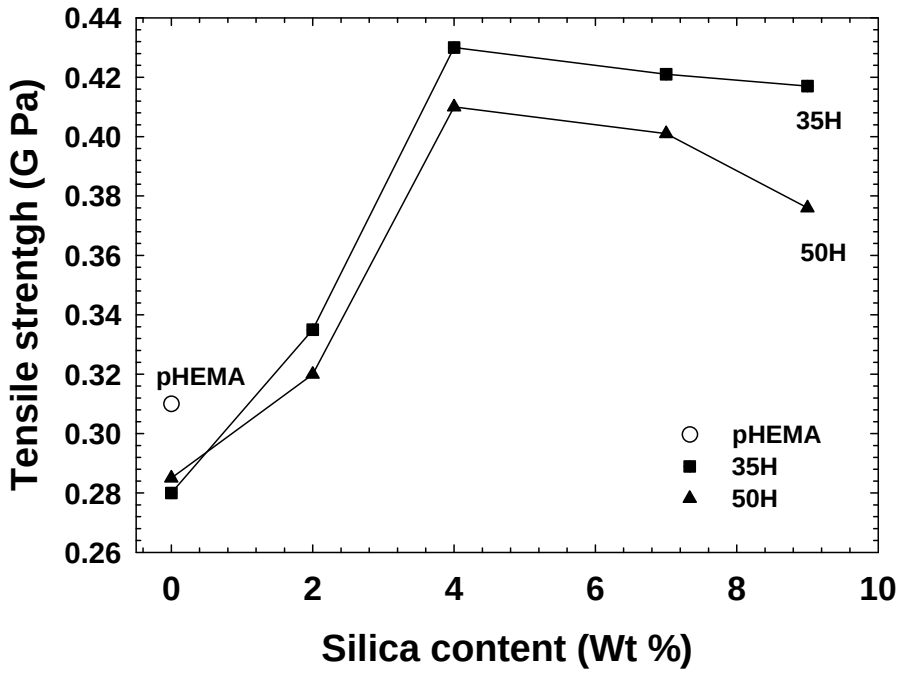

Fig. 4.2 Mechanical properties of pHEMA and SiO_2/pHEMA composites

A further characterization of the composite materials SiO_2/pHEMA, in comparison to pHEMA, was performed by undertaking swelling experiments. The dried composites and

pHEMA were placed in the distilled water and the water uptake was recorded by gravimetric measurement at different time durations. The swelling properties of the composites and pHEMA are shown in Fig. 4.3. Both SiO_2/pHEMA composites of ySi35H and ySi50H series showed higher equilibrium swelling than pHEMA. The water absorption of SiO_2/pHEMA composites increased corresponding to the content of silica nanoparticles and the effect is enhanced by increasing the amount of water in the starting reaction solution as illustrated in the ySi50H curves. The swelling ratio of the hydrogel was observed to be dependent on its free volume, the degree of chain flexibility, cross-linking density, and hydrophilicity [147]. The change in the swelling ratio might be attributed to the presence of hydrophilic nanosilica in the composite and an enhanced ability of water storage as a result of the nanoporous structure developed in the composites. Thus, an increased swelling ratio can be expected [148].

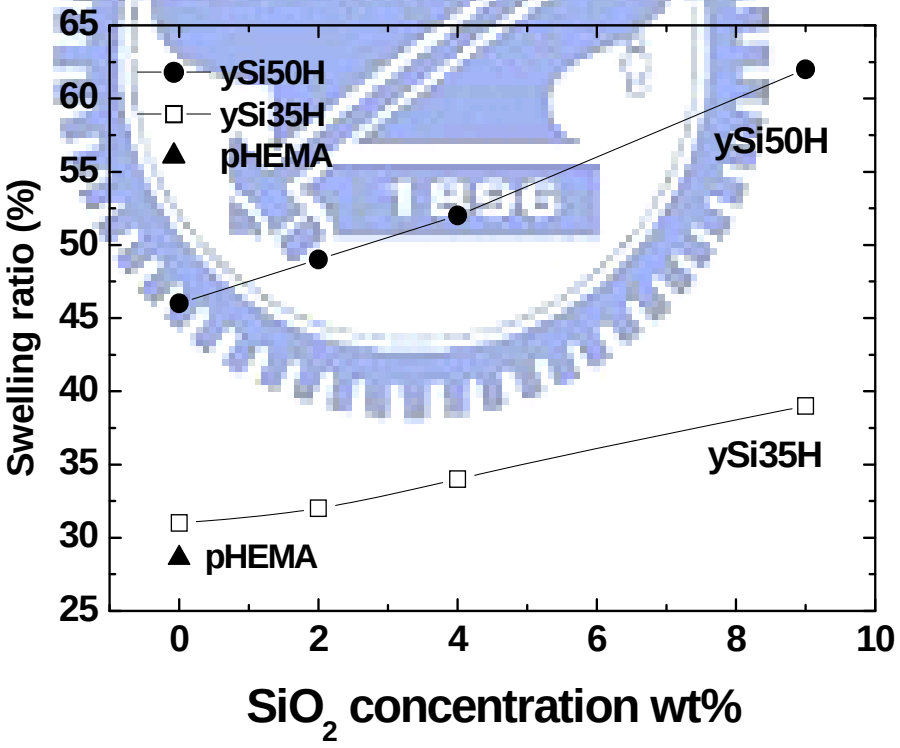

Fig. 4.3 Amount of water absorption of pHEMA and SiO_2/pHEMA composites

4.4 Platelet Adhesion

Platelet reactivity, measured by the degree of adhesion of platelets to a given surface *in vitro,* has been proposed as an indication of thrombogenicity for a given material entity. Number of platelets adhesion on pHEMA and SiO_2/pHEMA composite membranes are shown in Fig. 4.4. Trace amounts of platelets anchored on the surface of the SiO_2/pHEMA composite membrane were detected; these findings closely resembled those observed for the neat pHEMA membrane. A number of surface properties affect platelet adhesion, such as surface roughness, surface charge, and surface energy; the close resemblance between the behavior of platelet adhesion for neat pHEMA and for the composites suggests that these factors may be compromised to some extent with the addition of the SiO_2 nanoparticles and water.

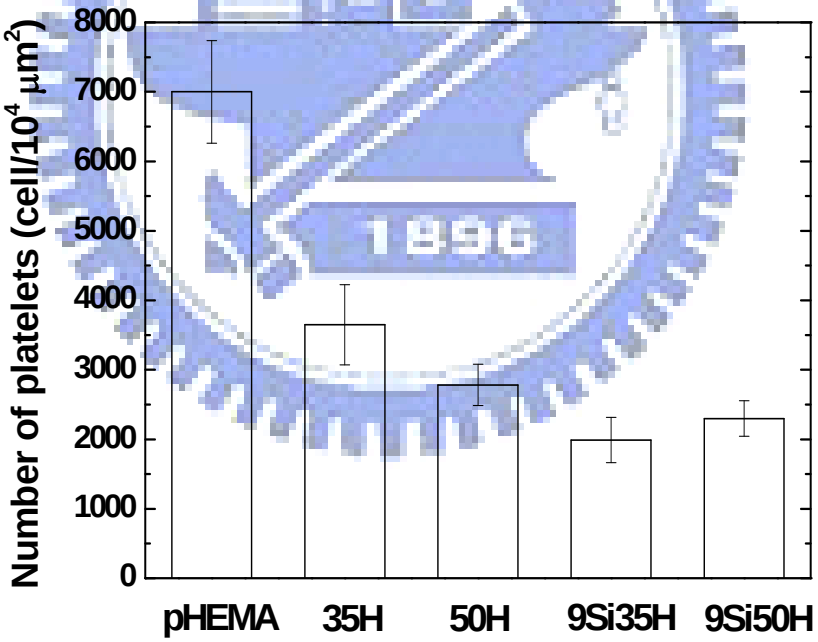

Fig. 4.4 Number of platelets adhering onto surface of pHEMA and SiO_2/pHEMA membranes

From an earlier argument regarding the microstructural evolution following SiO_2 and water incorporation, we examined in particular the surface roughness of the composite surfaces of interest using 3-D AFM, as shown in Fig. 4.5(a) and (b). The root mean square surface

roughness (R_q) in a 10 × 10 μm^2 surface region for 35H pHEMA was approximately 57.1 nm; for the 9Si35H composite (i.e., 9 wt% SiO_2 nanoparticles), it increased to 65.6 nm, that is, by a factor of approximately 7.6% compared to that of 35H pHEMA. This finding indicates that the addition of a small amount of SiO_2 nanoparticles into pHEMA had a little or negligible effect on surface roughness. Although no direct evidence can be provided in this investigation for other surface characters, it was believed that the surface properties may remain intact following a small addition of the nanoparticulate phase. This, together with the aforementioned improved properties, encourages the use of such composites for antithrombotic applications.

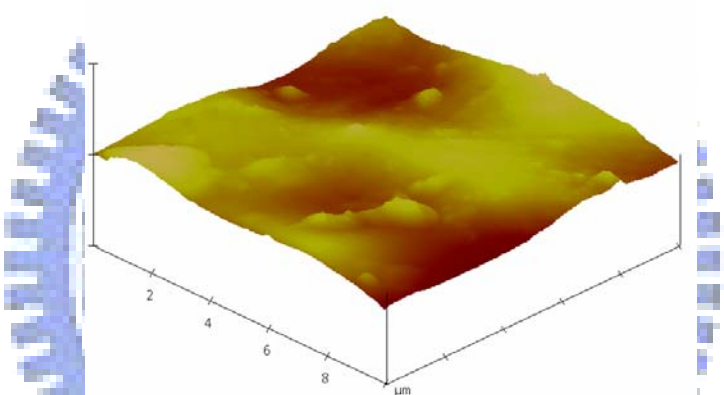

(a) 35H, R_q = 57.1 nm

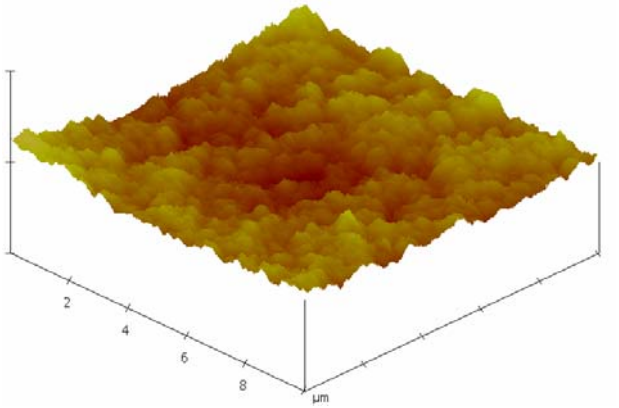

(b) 9Si35H, R_q = 65.6 nm

Fig. 4.5 Tapping-mode AFM images of (a) 35H and (b) 9Si35H

Furthermore, there has been greater evidence to demonstrate that the water state in

polymers exerts a vital role in the biomedical properties of materials [149, 150]. In general, water in a polymer can be classified into 3 types: nonfreezing water, freezing bound water (cold crystallizable water), and free water [151, 152]. Freezing bound water has been reported to play an important role in hemocompatibility [153]. Therefore, it is important to further confirm whether these SiO_2/pHEMA composites have freezing bound water or not. The water structure in the pHEMA and SiO_2/pHEMA composites as obtained by DSC is disclosed in Fig. 4.6.

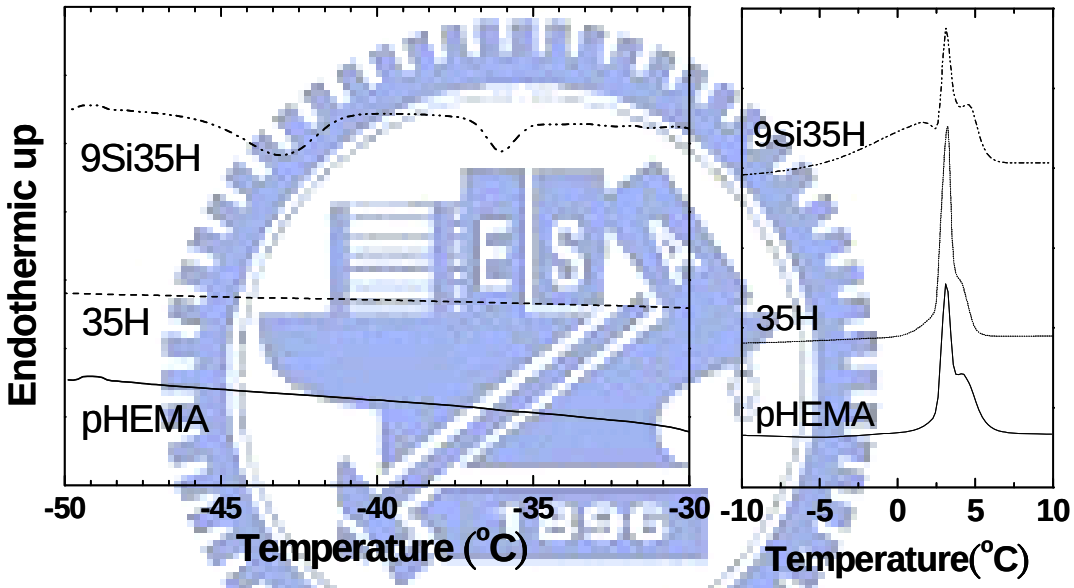

Fig. 4.6 DSC thermogram of pHEMA and SiO_2/pHEMA composites

In the DSC analysis of pHEMA, the only observed peak is the endothermic one at 2°C to 5°C, assigned to the fusion of ice of free water. In the case of the 9Si35H composite, two exothermic peaks at –30°C to –50°C and a broad endothermic peak at –5°C to 2.5°C were observed. The typical exothermic peak at –45°C to –35°C (ΔHcc) on heating was assigned to the cold crystallization of water that was defined as freezing bound water [153]. The result of the melting point indicates that the endothermic peak at –5°C to 2.5°C, ΔHm, is assigned to the fusion of ice of cold crystallized water (freezing bound water). Therefore, the water state in the SiO_2/pHEMA composite is composed of 2 types of water: free water and freezing bound water. It might be caused by the water molecules coordinating with

nano silica particles forming coordinated complex with hydrogen bonds. The freezing bound water existing in the SiO_2/pHEMA composites may provide excellent compatibility with platelets. These analyses are consistent with the aforementioned observation that the addition of SiO_2 nanoparticles does exhibit slightly reduced platelet adhesion.

4.5 Drug Release Characterization

The drug release profiles of the pHEMA and SiO_2/pHEMA composites are shown in Fig. 4.7 wherein vitamin B_{12} was used as a model molecule. The release profiles of vitamin B_{12} for samples pHEMA, 35H, 50H, 4Si35H, 9Si35H, and 2Si50H showed a similar two-stage pattern consisting of a slow release in the first stage and a rapid release in the second stage. From the profile, the permeability of vitamin B_{12} is almost unchanged at the beginning but slightly increased in the second stage. Both stages follow a steady-state linear diffusion mode. The two-stage release profile may be attributed to the variation of the partition coefficient H that is a function of the concentration of the permeant dissolved in the membrane [154].

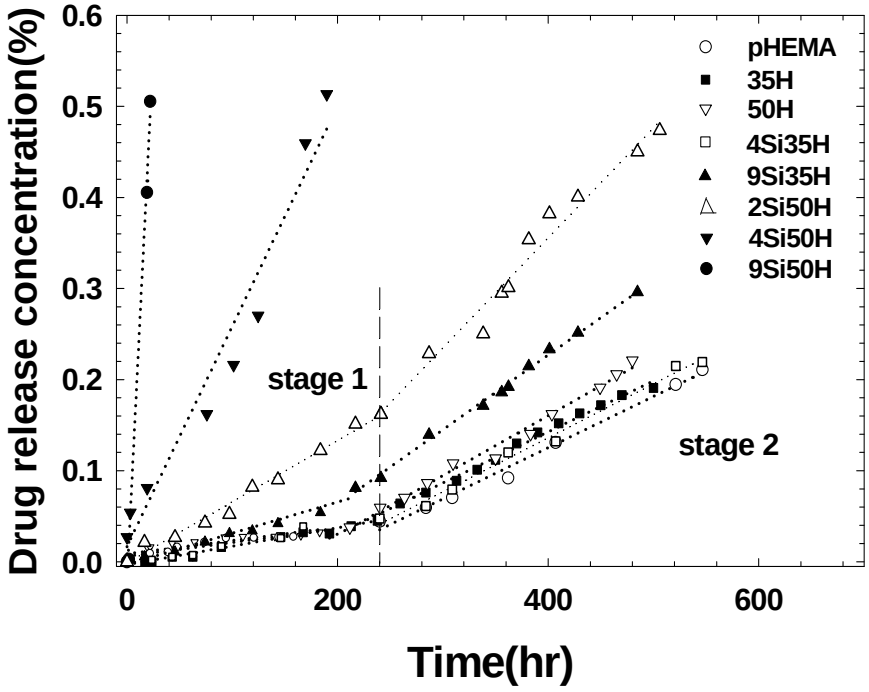

Fig. 4.7 Drug release profiles of pHEMA and SiO_2/pHEMA composites

The partition coefficient is sensitive to the chemical and physical properties of both the

permeant and the matrix system, including those of the polar groups and functional groups of the pHEMA and B_{12}, and the microstructure of the composite. However, it is difficult and impractical to differentiate the influence of individual characters on resultant drug release patterns; alternatively, these can be represented by the partition coefficient of the materials system. As illustrated in Table 2, the partition coefficient of the 0H, 35H, 50H, 4Si35H, 9Si35H, and 2Si50H samples shows a higher value in the second stage of drug release than in the first stage. This slight increase in the drug release rate in the second stage may be due to the complete swelling of the polymer matrix, corresponding to a higher diffusion rate. As evidenced in Fig. 4.8(a), sample 35H showed a dense structure before the swelling test; however, after approximately 20 days of the test, it became highly porous (Fig. 4.8(b)). The same scenario was also observed for samples 50H (Fig. 4.8(c)) and 9Si35H (Fig. 4.8(d)), wherein the latter showed the evolution of a greater number of completely swollen pores than that in the former.

The variation in microstructural evolution is consistent with the drug diffusion characteristic in the second stage where the drug permeability of 9Si35H is higher than that of 35H and 50H. In addition, it was also noted in Fig. 4.7 that the addition of the silica nanoparticles increased the drug release rate in the second stage such as observed in the cases of 50H vs. 2Si50H and 35H vs. 9Si35H. One plausible explanation is that the evolution of these nanopores that underwent enlargement upon complete swelling created larger voids, enabling a greater number of drug molecules to diffuse into the environment. However, the presence of the SiO_2 nanoparticles does not appear to be an effective physical barrier for retarding drug diffusion through the composite membrane in these compositions.

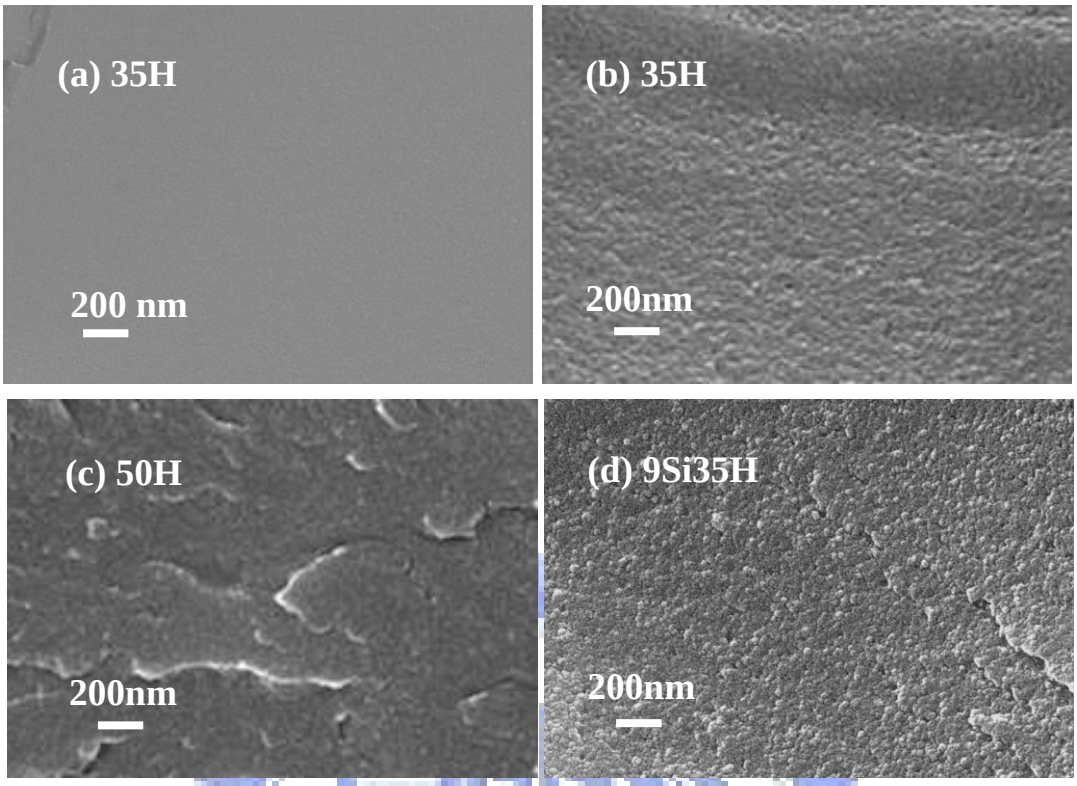

Fig. 4.8 SEM photographs of (a) 35H before drug diffusion and after drug diffusion for (b) 35H, (c) 9Si35H, and (d) 50H

Table 4.2 The permeability [DH] of B_{12} of pHEMA and SiO_2/pHEMA composites

	Two-stage				Only one stage
	Stage 1		Stage 2		
	Permeability $[DH]_1$ ($10^{-7}cm^2/hr$)	Partition coefficient	Permeability $[DH]_2$ ($10^{-7}cm^2/hr$)	Partition coefficient	Permeability [DH] ($10^{-7}cm^2/hr$)
pHEMA	2.31	$5.67*10^{-4}$	4.22	$8.72*10^{-4}$	*
35 H	2.39	$6.72*10^{-4}$	5.28	$2.32*10^{-3}$	*
50 H	2.64	$6.82*10^{-4}$	5.75	$3.88*10^{-3}$	*
4Si35H	2.71	$7.12*10^{-4}$	6.02	$1.32*10^{-3}$	*
9Si35H	4.32	$7.84.*10^{-4}$	8.14	$5.27*10^{-3}$	*
2Si50H	7.29	$6.87*10^{-4}$	13.35	$4.98*10^{-3}$	*
4Si50H		*		*	178
9Si50H		*		*	392

In contrast, for samples with higher water incorporation during the course of synthesis, i.e., typically >35%, the incorporation of a certain critical amount of the SiO_2 nanoparticles

appeared to manipulate drug release, from a two-stage profile (samples 50H and 2Si50H) to a one-stage profile (samples 4Si50H and 9Si50H). Since a higher permeability [DH] was determined for samples 4Si50H and 9Si50H, which is similar to that observed for the second-stage profile of those samples, it is then believed that this one-stage release profile indicates that the release of drug is dominantly controlled by porosity. In other words, higher water and SiO_2 nanoparticles concentrations ensure a higher porosity of the resulting composites, rendering higher release rates and a corresponding higher permeability.

The influence of SiO_2 nanoparticles on the permeability of the resulting composites is illustrated in Fig. 4.9, with 35% and 50% water incorporation during the synthesis. The permeability of the Vitamin B_{12} with the SiO_2 concentration when 50% water was incorporated during polymerization in the starting solution (i.e., 50H, 4Si50H, and 9Si50H). However, this permeability remains relatively unchanged with increasing concentrations of the SiO_2 nanoparticles for samples with 35% water incorporation.

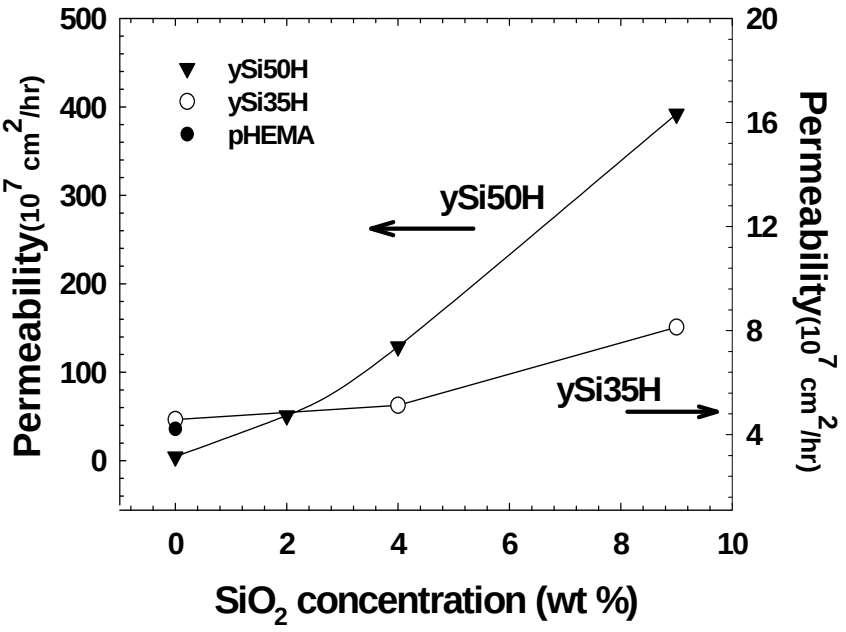

Fig. 4.9 Permeability [DH] of B_{12} at stage 2 of SiO_2/pHEMA composite

According to an earlier study, the critical water concentration for an effective phase separation should be greater than 35% for such an experiment, and the increase in

nanoparticles, corresponding to an increase in nanoporosity, appeared to have little effect on the resultant drug diffusion. As shown in Fig. 4.10, the incorporation of SiO_2 nanoparticles increased the nanopore structure of the SiO_2/pHEMA composite. It was believed to be a compromise between the nanopore (as a diffusion conduit) and nanoparticle (as a physical barrier). However, higher water incorporation enhanced phase separation, which became more pronounced when the nanoparticles were introduced. This resulted in a more porous microstructure and thus enhanced drug diffusion.

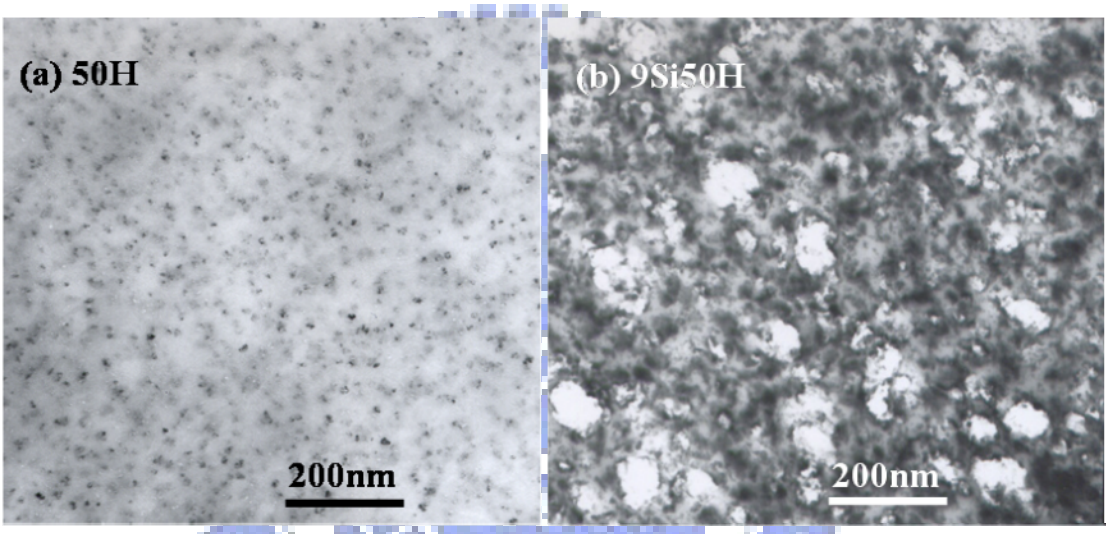

Fig. 4.10 TEM micrographs of SiO_2/pHEMA composite

4.6 Summary

Nanoporous SiO_2/pHEMA composites were prepared by the photopolymerization process. In comparison with neat pHEMA, the addition of SiO_2 nanoparticles revealed a significant effect on the reaction rate of crosslinking during polymerization, resulting in composites with varying nanoporous structures. The composites showed improved tensile strength, and the platelet adhesion property remained as excellent as that of neat pHEMA, which encourages the use of such composites for antithrombotic applications. Drug diffusion characteristics in the composites can be well modulated by controlling the

concentrations of the SiO_2 nanoparticles and water in the starting stage of synthesis. By taking into consideration the aforementioned improved properties, it is suggested that the nanoporous SiO_2/pHEMA composites can be employed as candidate biomaterials for coatings or as bulk devices for a number of biomedical applications

Chapter 5

Inorganic/organic Hybrid – Silanol/pHEMA – Synthesis and Characterization of Silanol/pHEMA Biocomposites for Drug Controlled Release

5.1 Introduction

In this study, silanol group was produced and incorporated with HEMA monomer to form a hybrid membrane for drug controlled release. The hydrolysis and condensation of TMOS was controlled to prepare different silanol sol. The silanol(Si-OH)/pHEMA hybrid was prepared by photopolymerization. The structure and drug release characteristic of hybrid was investigated.

5.2 Fabrication of Silanol/pHEMA Composite

The Silanol/pHEMA hybrid was prepared by employing UV irradiation of 365nm UV light for 90min at room temperature to aqueous solution containing 2.5g 2-hydroxyethyl methacrylate monomer, 0.1 ml of ethylene glycol dimethacrylate as cross linker, 0.03 g UV photoinitiators Darocur 1173 (Ciba) as initiator, and different weight ratio of silanol were added to the reactant. The compositions of the hybrid were shown in table 5.1.

Table 5.1 The compositions of the Silanol/pHEMA hybrid

	Silanol process (molar ratio)		Polymerization process (weight ratio)	
	TMOS	H_2O	Silanol	HEMA
A21	1	16	2.3	1
A11	1	16	1	1
B21	1	32	2.3	1
B11	1	32	1	1

The changes of the silanol degree in sol/gels were observed for a series of sols with TMOS : H_2O : MeOH : HCl molar ratios equal to 1:n:3:0.0005, where n = 16 and 32. Methanol was added to minimize the effects of immiscibility between TMOS and water. The tetramethoxy silane (TMOS) was purchased from Sigma-Aldrich. The maximum silanol degree was determined by the fluorescence spectra of the sols by using fluorescence spectrophotometer with pyranine as a photoprobe to detect and control the hydrolysis of TMOS [155]. The hydrolysis and condensation relation for tetramethoxy silane (TMOS)-derived sol/gels are

Hydrolysis: $\equiv Si{-}OCH_3 + H_2O \Leftrightarrow \equiv Si{-}OH + CH_3OH$ (1)

Water condensation: $\equiv Si{-}OH + \equiv Si{-}OH \Leftrightarrow \equiv Si{-}O{-}Si\equiv + H_2O$ (2)

Alcohol condensation: $\equiv Si{-}OCH_3 + \equiv Si{-}OH \Leftrightarrow \equiv Si{-}O{-}Si\equiv + CH_3OH$ (3)

It was found that the relative water content is the decisive factor determining the fluorescence spectra of the water/alcohol solutions. Fluorescence spectra were measured by a Hitachi F-4500 spectrofluorimeter with a Xe lamp. Excitation was set as 390 nm and spectra were taken in the range 400-600 nm. As shown in Fig. 5.1, the ratio of intensities of emission peaks at 510nm (water) and 430 nm (alcohol) (I_{510} / I_{430}) were used as a measure of the relative hydrolysis degree of TMOS.

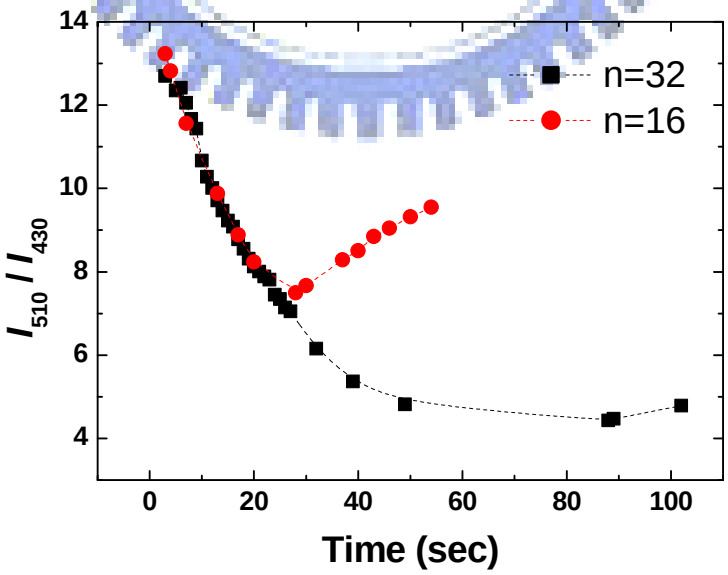

Fig 5.1 Time dependencies of the relative water content in the sol-gel solution of a nominal composition TMOS : H_2O = 1:n, where n=16 and 32.

5.3 Chemical and Physical Characterization

The results of the Mid-IR spectra for the Sianpl/pHEMA hybrids were shown in Fig. 5.2. The infrared spectrum of the hybrid exhibited characteristic vibrations of both silica and pHEMA, such as C=O, carboxylic acids group (COOR), and silicate - oxygen bond (Si-O-Si). Samples A21 and B21 showed the peaks of silicate – oxygen-carbon bond (Si–O–C) at 836 cm^{-1} and 1080-1120 cm^{-1}, which is related to the chemical bonds between pHEMA and silanol [156, 157]. The results also showed the peak of silicate – oxygen-carbon (Si-O-C) indicated that a certain chemical interactions might occur between pHEMA and the silanol. However, not all the silanols were reactive as noted by the –OH peaks at 3120 cm^{-1} and 3420 cm^{-1}. The low frequency of the Si–OH band at 3120 cm^{-1} suggests that the silanols are in a condensed environment interacting with neighboring groups which is consistent with the fact that some silanols are inaccessible to the HEMA monomer during polymerization. The peak at 3120 cm^{-1} may also be due to strongly adsorbed water [158].

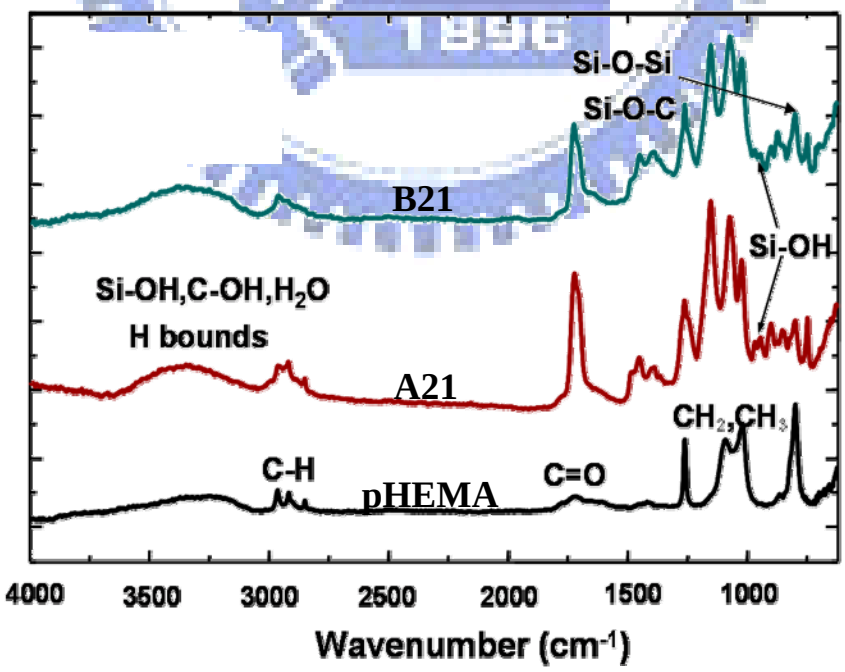

Fig. 5.2 FTIR, Mid-IR, absorption spectra of pHEMA and silanol/pHEMA hybrid

The Near-IR spectra for analyzing the hydroxyl group (OH) of the hybrids [159, 160] were shown in Fig. 5.3, the hydroxyl group in the hybrids is well characterized at this peak at 4892 cm^{-1} [161], which was assigned as a stretching band of the hydroxyl group (OH). It can be seen that the peak intensity increased with the content of silanol and water of hybrid of the sol-gel process. By controlling the hydrolysis of the silane, it allows modulating the hydroxyl group density in the resulting silanol/pHEMA hybrids.

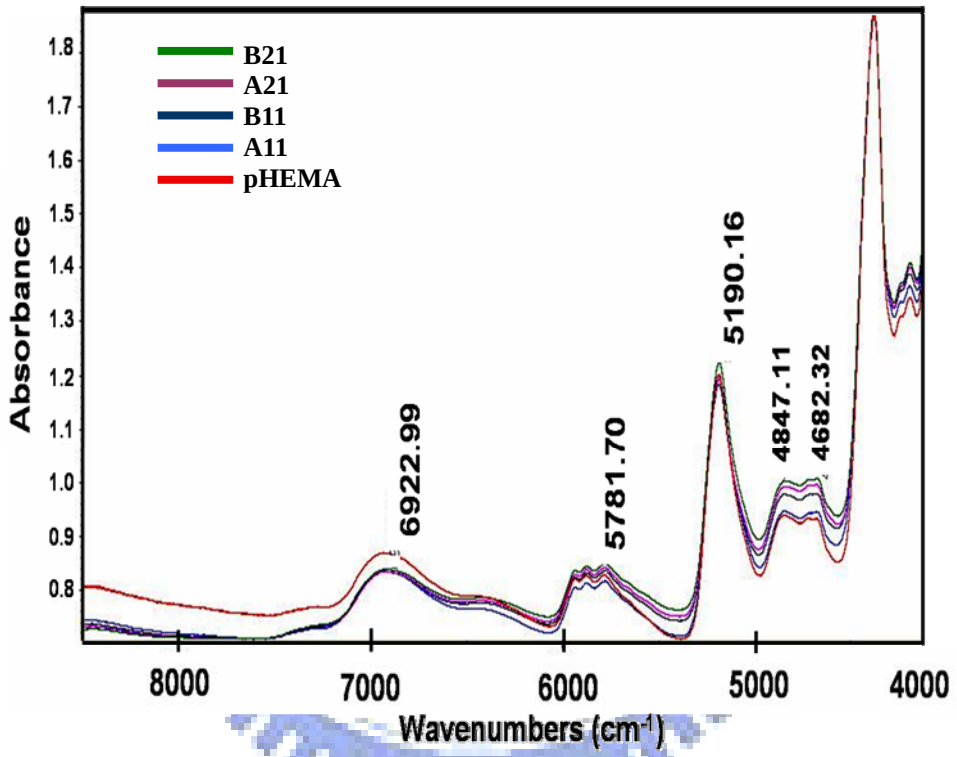

Fig. 5.3 FTIR, Near-IR, absorption spectra of pHEMA and silanol/pHEMA hybrid

Fig. 5.4 shows the cross-sectional microstructure of the silanol/pHEMA composites with different amounts of silanol concentrations during polymerization. It was observed that, in Fig. 5.4 (a) and (b), sample A11 and B11 showed a considerably dense and uniform microstructure with no visually observable voids, which is similar to that of pure pHEMA membrane (not shown in Fig. 5.4). However, when increasing the amount of silanol upon the synthesis of hybrid, i.e., A21 and B21, the resultant samples presented a loose microstructure, as illustrated in Fig. 5.4 (c) and (d). This loose microstructure might be caused by the silicate

from the silanol which could provide a domain region that the monomers near the silicate can be cured at a faster rate under UV irradiation than other those of the bulk regions [162, 163]. Hence, the difference in the rate of polymerization between the “domain regions” and “bulk regions” induced the formation of heterodomains. It is believed that a phase separation should take place once the heterodomains are fully developed, resulting in a loose structure in the final composite.

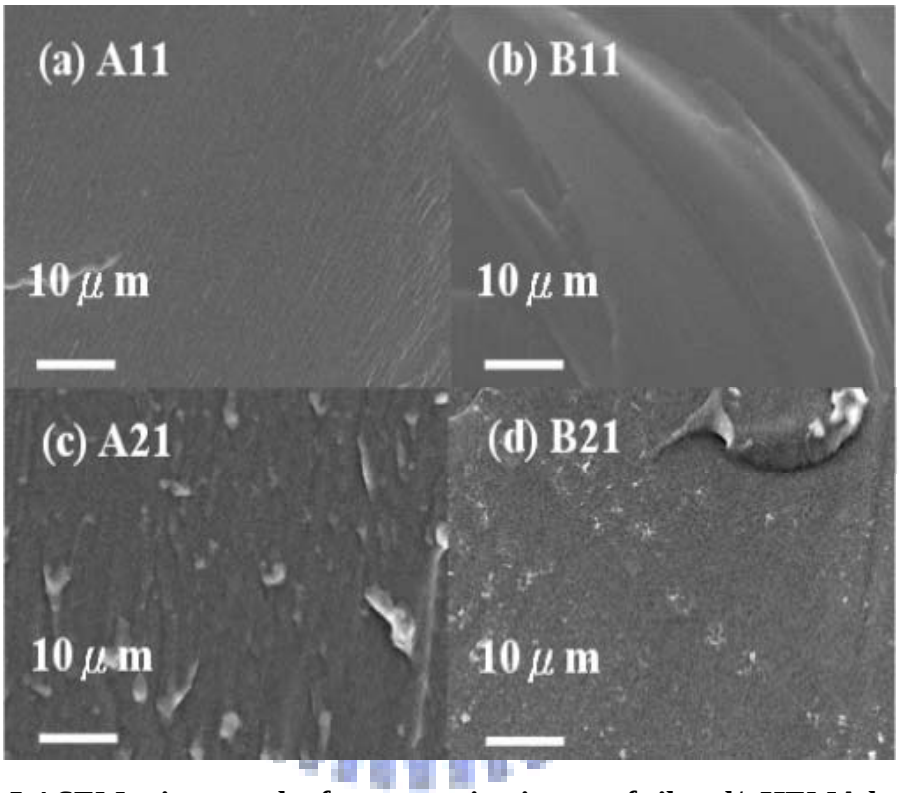

Fig. 5.4 SEM micrograph of cross-section image of silanol/pHEMA hybrid

The thermal decomposition behaviors of silanol/pHEMA hybrids were also investigated. The effect of incorporated silica sol into pHEMA on the thermal behavior of the hybrids was further illustrated in Fig. 5.5 which showed the typical weight loss (TG) curves of pHEMA and silanol/pHEMA hybrid at a heating rate of 10 ^{o}C/min under nitrogen atmosphere .It was observed that the weight loss behavior for all the hybrids showed two-stage degradation. The first stage is due to the evaporation of non-bonded water and

other volatile compounds from room temperature to ~200 ^{o}C. The second stage from 250^{o}C to 500^{o}C is due to both polymer decomposition and loss of hydroxyl groups from the silica. The temperature corresponding to 10 wt% losses was defined as the initial thermal degraded temperature of polymer phase, T_d. From the results, the incorporation of silanol into pHEMA increased the thermal behavior comparing to pure pHEMA. Furthermore, for the same content of silanol of the hybrid, such as sample A21 and B21, there should be more silicate in A21 than in B21 because of the higher weigh ratio of TMOS in silanol. The higher content of silicate of the hybrids also increases the thermal decomposition temperature.

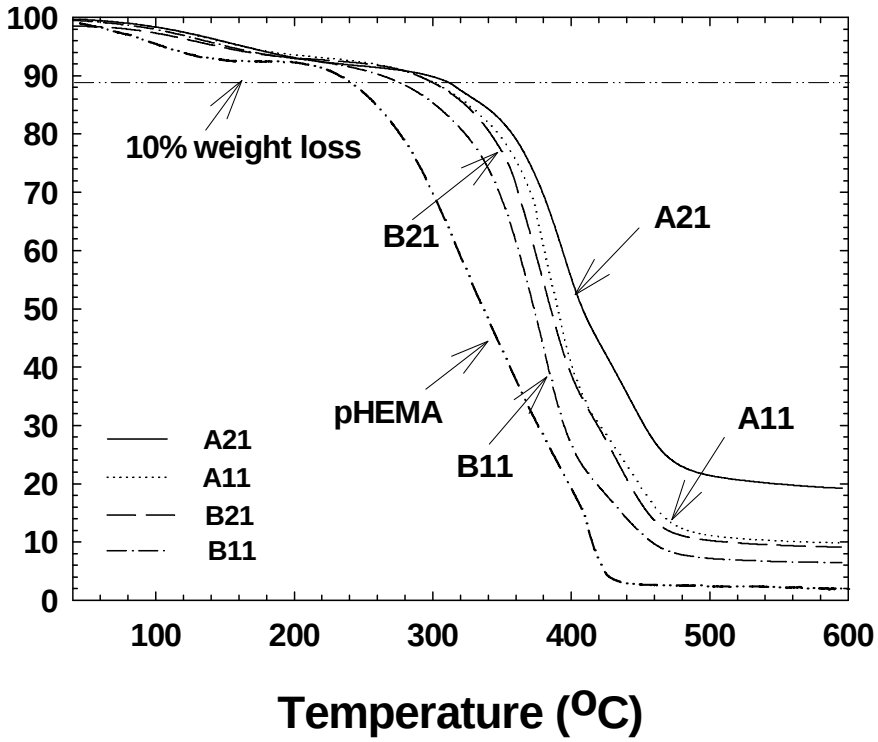

Fig. 5.5 TG thermograms of pure pHEMA and silanol/pHEMA hybrids

5.4 Drug diffusion Characterization

The diffusion profiles of the model drug (2000ppm vitamin B_{12}) through silanol/pHEMA hybrids membranes were shown in Fig. 5.6. The release profiles of vitamin B_{12} for samples pHEMA, A11, A21, B11, and B21 showed a similar pattern. From the

profile, it can be seen that the permeability of vitamin B_{12} is in the range of 3.82×10^{-7} cm^2/hr to 1.73×10^{-5} cm^2/hr and increased in the order of pHEMA < B11 < A11 < B21 < A21. The increase of release profile may be attributed to the variation of the partition coefficient H that is a function of the concentration of the permeant dissolved in the membrane [164]. The partition coefficient is sensitive to the chemical and physical properties of both the permeant and the matrix system, including those of the polar groups and functional groups of the silanol, pHEMA and B_{12}, and the microstructure of the composite. However, it is difficult and impractical to differentiate the influence of individual characters on resultant drug release patterns; alternatively, these can be represented by the partition coefficient of the materials system. As illustrated in Table 2, the partition coefficient of the pHEMA, B11, A11, B21, and A21 samples show different value.

Table 5.2 The partition coefficient of the pHEMA, B11, A11, B21, and A21 samples

	pHEMA	A11	A21	B11	B21
Swelling ratio	42%	53%	71%	49%	65%
Partition coefficient	5.34×10^{-4}	8.14×10^{-4}	2.64×10^{-3}	8.57×10^{-4}	1.72×10^{-3}
Permeability(10^{-7} cm^2/hr)	2.11	4.23	8.13	3.92	5.72

This slight increase in the drug release rate in Fig. 5.6 may be due to the complete swelling of the polymer matrix, corresponding to a higher diffusion rate. Here, it was noted that the water content in the sol-gel process affected the hydrolysis and condensation of TMOS which also varied the drug diffusion characteristic. In addition, as comparing A11 with A21, it was found that with the increase of hydroxyl group of hybrid, the drug release rate was enhanced due to the higher swelling degree of silanol/pHEMA hybrids. Similar results were also observed for the B11 and B21.

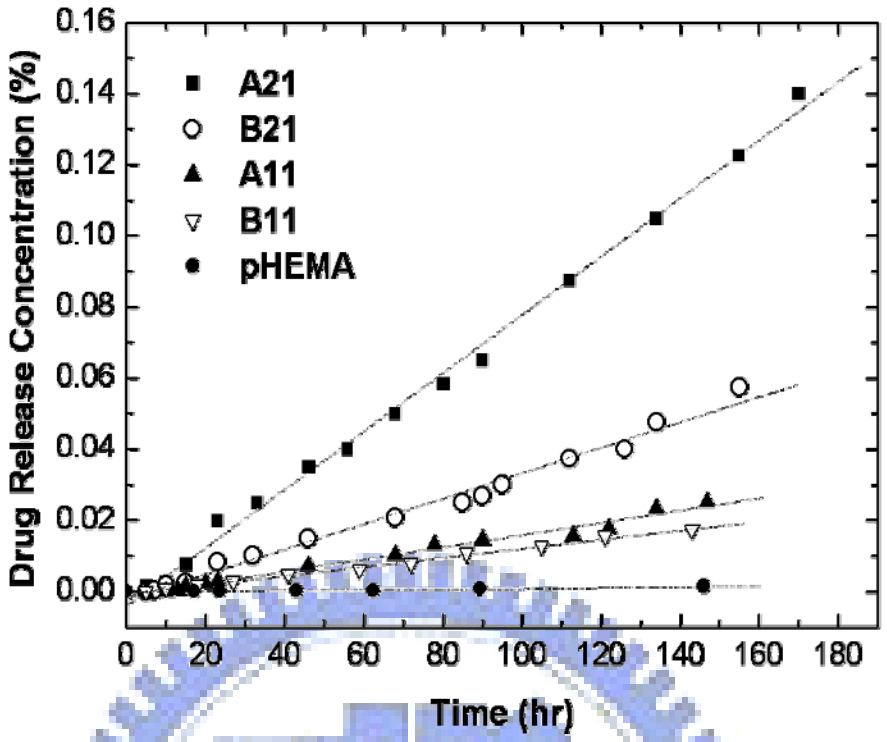

Fig. 5.6 Drug release profile of pHEMA and silanol/pHEMA hybrid

5.5 Summary

In this study, a novel silanol/pHEMA hybrid was achieved by photopolymerization of silica sol (silanol) and HEMA monomer. The hydroxyl group of the hybrid was verified by controlling the hydrolysis degree of silanol and the composition of the hybrid. The drug diffusion profile of silanol/pHEMA hybrid could also be modified by varying the silanol in the range from 2.11×10^{-7} cm^2/hr to 8.13×10^{-7} cm^2/hr. The incorporation of silica sol into pHEMA hydrogel not only enhanced the thermo stability of hydrogel but also increased the swelling degree.

Chapter 6

Metal/organic Hybrid – Cu/pHEMA - Structural Evolution of Cu-pHEMA Hybrid and Cu Release Behavior on the Proliferation of Endothelial Cells

6.1. Introduction

Copper has been well-recognized as a physiologically important element for human health and from a number of clinical practices. Copper deficiency has been known to associate with complications such as Wilson's disease, thrombotic disorder, etc. In the meantime, copper is also a widely known element that is able to enhanced repairing efficacy with optimal dose for skin and bone growth as a result of proangiogenic action that favors the development of new vessels after surgery [18-21]. Copper has been widely known to enhance the antifertility effect of an intrauterine device (IUD); great efforts have been made to improve the copper-containing intrauterine device (Cu-IUD) and to investigate corrosion behavior of copper *in vivo* and *in vitro* [22]. All of those studies, from in-vivo to clinical practices, have pointed out that a stringent control of copper concentration level, either for the maintenance of health or acting as therapeutic purposes, is essentially critical.

Development of Cu-containing composites, although not extensively studied so far, has been reported for years. Shuizhou Cai *et al*. [165] demonstrate that the copper/ low-density polyethylene nanocomposite manufactured by a laser-inductive vaporization condensation technique displayed a near zero-order release after a month of incubation, indicating that the Cu^{2+} release behavior controlled by nanocomposite was remarkably superior to that by microcomposite. In addition, the use of organic-metal compound such as lipophilic Cu complex [133] or metallic Cu particles [134] embedded in the polymeric matrix where a catalytic generation of nitric oxide generated from the composite surface has received

promising outcomes in-vitro where both the lipophilic Cu complex or copper particle were employed as a catalyst to activate the redox chemistry by reduction of the nitrite or S-nitrosothiols into nitric oxide in blood and has successfully mimicking the nitric oxide forming activity of endothelial cell or other cells. The proangiogenic activity of a hyaluronan-based 50% hydrogel (Hyal-50%) enriched with copper ions (Cu(II)) has also been reported where the Cu-containing hydrogel was mixed with freeze-dried bone and inserted in subcutaneous pockets. The angiogenesis results showed a significant higher vascular density in Hyal-50%- Cu(II) and Hyal-50%- Cu(II) plus freeze-dried bone group when compared to other groups [18]. However, limitation of copper ion content and the stability of ion release from the hydrogel system are still heavily concerned.

In a previous publication, we reported the synthesis of a Cu-containing pHEMA hybrid and it was demonstrated outstanding blood compatibility [166]. However, structural evolution and its corresponding release behavior of copper from the hybrid have not been elucidated and are the main objectives of this study. Copper release and its effect on the proliferation or inhibition of human endothelial cells and smooth muscle cells were also investigated.

6.2 Fabrication of Cu-pHEMA Hybrid synthesis

The Cu-pHEMA hybrid was prepared by employing UV irradiation to aqueous solution containing 2.5 grams of 2-hydroxyethyl methacrylate monomer (HEMA, Tokyo Kasei Kogyo Co., Ltd., Japan, analytical grade), 0.1 ml of ethylene glycol dimethacrylate (EGDMA, Sigma-Aldrich, Inc. USA, analytical grade) as cross linker, 0.03 g benzoin methyl ether (BME, Tokyo Chemical Industry, analytic grade) as initiator, 0.1g SiO_2 suspension (ChangChun Inc., Taiwan) for enhancing the strength of the hybrid, and 1 M $CuSO_4$ (Sigma-Aldrich, Inc. USA, analytic grade) solution (with 0.1 wt% polyvinylpyrrolidone, average mol wt 10,000, Sigma-Aldrich, Inc. USA, analytical grade). During the sample preparation, water is required to ionize the HEMA and it can chelate with Cu^{2+} and turn the mixture into a homogeneous solution. The molar ratio of water and

HEMA, in a range of 2, 3, 4, and 6 with various Cu contents, has been employed as a major parameter for hybrid synthesis, namely Hybrid-1-Cu, Hybrid-2-Cu, Hybrid-3-Cu, and Hybrid-4-Cu, respectively. Based on the Hybrid-1-Cu, the Cu(0)-pHEMA hybrids with the Cu concentration of 0.1%, 0.5% and 1.0% by weight were also prepared using the synthesis scheme aforementioned, namely Hybrid-1-Cu01, Hybrid-1-Cu05, and Hybrid-1-Cu10, respectively.

The mixture was vigorously agitated using a magnet during the course of mixture. To remove the dissolved oxygen from precursors, N_2 was purged for approximately 1 min. Then, the mixture was transferred to a sealed transparent plastic holder of 50 mm × 50 mm × 0.5 mm in dimensions, followed by UV irradiation at 365 nm for 2 h and the Cu(II)-pHEMA hybrid were produced. The Cu(II)-pHEMA hybrid were rinsed by distilled water to remove the un-reacted species (e.g., cross-linker, monomer, etc.) and then subjecting to in-situ chemical reduction by immersion the as-synthesized Cu(II)-pHEMA hybrid into 50 ml of 0.5 M hydrazine solution at 40^{o}C for 24 h, to form a final metallic Cu(0)-pHEMA hybrid.

The amount of copper particles in hybrid was qualified by using an analytical semi-micro precision balance (precision: 0.0001g, PRECISA XS225A Series, Switzerland). First, the weight of dried Cu-pHEMA hybrid sample was measured by the analytical balance. Then, the Cu-pHEMA hybrids were immersed in a PBS (phosphate-buffered saline, pH=7.4) solution for dissolving the copper into copper ion. Ultrasonic machine was also used for accelerating the dissolving process. The solution was refreshed until little copper ions in the solution were detectable. The existence of copper ion in the solution was identified by sodium diethyldithiocarbamate trihydrate (copper reagent) (Sigma-Aldrich, Inc. USA.) which is able to form a yellow chelate with the cupric ion. Finally, the residual polymer matrix pHEMA was dried and weighted. The weight of copper particles in the hybrid can

then be determined after the dissolving process and five measurements were carried out for each sample.

6.3 Hybrid Characterization

Figure 6.1 shows the infrared spectra of the neat pHEMA and the hybrid before the stage of chemical reduction was carried out, i.e., Cu(II)-pHEMA hybrid. The FT-IR ATR spectrum of the pHEMA (Fig. 1a) is characterized by stretching bands peaked at 1723 cm^{-1} [ν(C=O)] and 1158 cm^{-1} [ν(C-O)], and a bending mode at 1020cm^{-1} [δ(C-OH)] [167, 168]. The FT-IR ATR spectrum of the Cu(II)-pHEMA hybrid reveals a characteristic peak over a range of 1630 cm^{-1} ~ 1650 cm^{-1} and becomes more pronounced in intensity while increasing both the copper and water concentrations upon polymerization. This indicates that the water molecules coordinated with copper ions forming coordinated complex with hydrogen bonds Cu---(OH), showing a δHOH vibration mode at 1647 cm^{-1}[169]. Therefore, it is clearly showed, from the vibration mode, that the intermolecular coordinated bonding is developed in the hybrid structure.

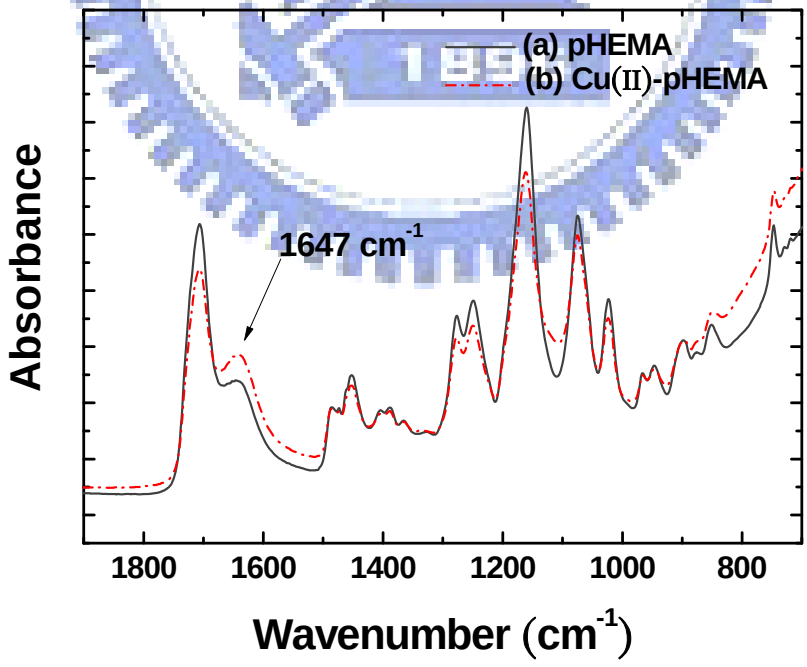

Fig. 6.1 (a) FT-IR ATR spectra of the synthesized pHEMA and (b) Cu(II)-pHEMA hybrid The composition of Cu(II)-pHEMA hybrid was the same with Hybrid-4-Cu05

These results suggest that the coordination reaction between Cu(II) and pHEMA does not interfere the development of the network structure to any appreciable extent, but a form of coordinated bonding which further reinforces the hybrid structure with considerably improved thermal stability as will be discussed in subsequent analysis. Furthermore, the interaction between copper ion Cu(II) and hydroxyl groups originated from pHEMA and water should play a key role in immobilizing, to a certain extent, the development of metallic copper nanoparticles within the hybrid.

It is believed that the interaction between the copper ions and hydroxyl groups, i.e., Cu(II)----O-H, a form of hydrate complex, together with the hydrogen bonds, may further stabilize the hybrid structure. This is further substantiated from the thermogravimetric analysis (TGA) as shown in Fig. 6.2 where the spectra of both the Cu(II)-pHEMA and Cu(0)-pHEMA hybrids are comparatively studied.

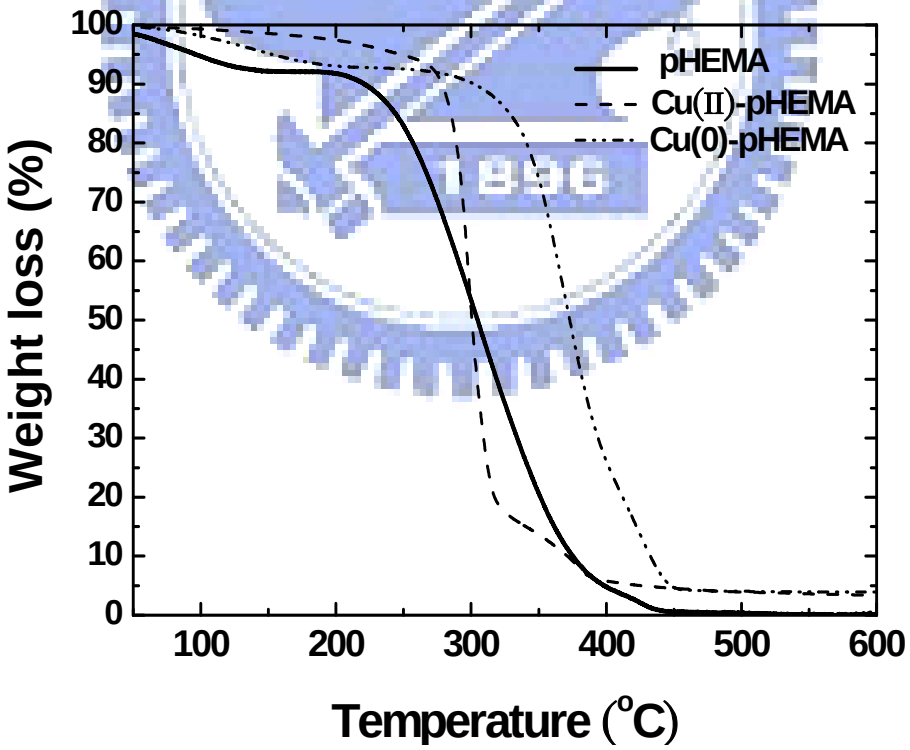

Fig. 6.2 TGA thermograms of the synthesized pHEMA, Cu(II)-pHEMA hybrid, and Cu(0)-pHEMA hybrid. The composition of Cu(II)-pHEMA and Cu(0)-pHEMA hybrid is the same as indicated in Hybrid-4-Cu05

In comparison with the pHEMA, both hybrids, i.e., Cu(II)-pHEMA and Cu(0)-pHEMA, showed a decomposition temperature higher by 52°C and 102°C than pHEMA (243°C), i.e., 295°C and 345°C, respectively. It is also clearly showed that Cu(0)-pHEMA hybrid exhibits superior thermal stability to that of Cu(II)-pHEMA hybrid by an enhancement of the decomposition temperature of 50°C, suggesting a stronger interaction between Cu(0) and pHEMA that further chemically stabilized the resulting Cu(0)-pHEMA hybrid after chemical reduction. The role of the copper, either in ionic or in metallic configuration, not only exhibited an excellent anti-platelet adhesion property as previously observed [166], but also able to enhance thermal stability of the pHEMA matrix through chemical interaction. Such a chemical interaction also implicate a chemical anchorage of the Cu nanoparticle within the network structure of the matrix, which is later found to be effectively in regulating the release of cupric ions from the matrix and will be elucidated in the forthcoming analysis.

6.4 Nanostructural evolution of the Hybrid

XRD analysis, Fig. 6.3, reveals an evolution of crystallinity of the Cu nanoparticles, based on the intensity and sharpness of the diffraction peak at (111) crystallographic plane of metallic Cu [170], depending on water concentration upon hybrid synthesis. The metallic Cu nanoparticle shows improved crystallinity as water concentration increased. However, such an increase in crystallinity may also result from the increase of particle size as shown in Fig. 6.4, where the transmission electron microscoy (TEM) analysis revealed that the size of Cu nanoparticle is increased from an average of ~10 nm to 25 nm in diameter as the molar ratio of H_2O/HEMA increased from 2 to 6.

This finding has been proved earlier that metal ions in some macromolecule-metal complexes have a tendency to evolve agglomerates, owing to their electrostatic or dipole–dipole interactions [171]. However, from our experimental observations, the tendency for cluster formation of the Cu nanoparticles seems to become more pronounced as the molar ratio of H_2O/HEMA was reduced, as shown in Fig. 6.4(a) for the

Hybrid-1-Cu05. However, from the HRTEM image of the marked area in Fig. 6.4(a), Fig. 6.4(c) illustrate that the Cu nanoparticles are still distributed in the pHEMA matrix and display an relatively uniform size of about 3~5 nm in diameter, which is consistent with the observation in XRD which shows a weak and broad peak.

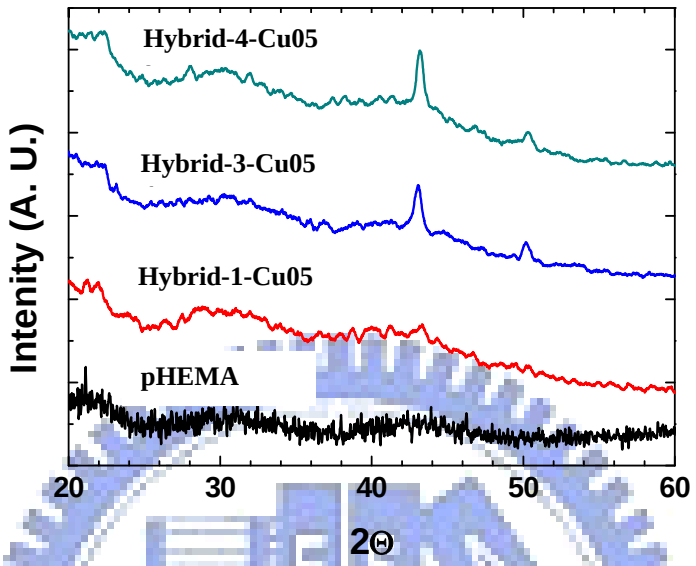

Fig. 6.3 The XRD patterns of pHEMA and Cu(0)-pHEMA hybrids

This is explainable from the viewpoint of materials synthesis where the concentration of Cu is higher for a unit volume of the starting solution mixture with lower water concentration. In the meantime, the degree of swelling of the polymerized HEMA is expected to be lower in the presence of less amount of water, i.e. the lower H_2O/HEMA ratio. These factors will surely give a hybrid with a shorter distance between the Cu, and correspondingly results in a stronger interparticle attraction, and a greater tendency to form clusters within the final hybrid is expected. In contrast, for a higher H_2O/HEMA ratio, the TEM image of Hybrid-4-Cu05 in Fig. 6.4(b) shows that the Cu nanoparticles embedded within the pHEMA matrix are present in a connective particle network. A corresponding magnified TEM image in Fig. 6.4(d) indicates that the Cu nanoparticles appear in a form of primary particle without appreciable aggregation and the particle size of Cu nanoparticle is estimated about 25 nm in diameter, which is very much the same as that (26.7 nm) calculated from Scherrer's equation

$$t = \frac{K * \lambda}{B * \cos\theta_B} \qquad (1)$$

where

t = size of crystallite

K = constant dependent on crystallite shape (0.89)

λ = x-ray wavelength

B = FWHM (full width at half max) or integral breadth

θ_B = Bragg Angle

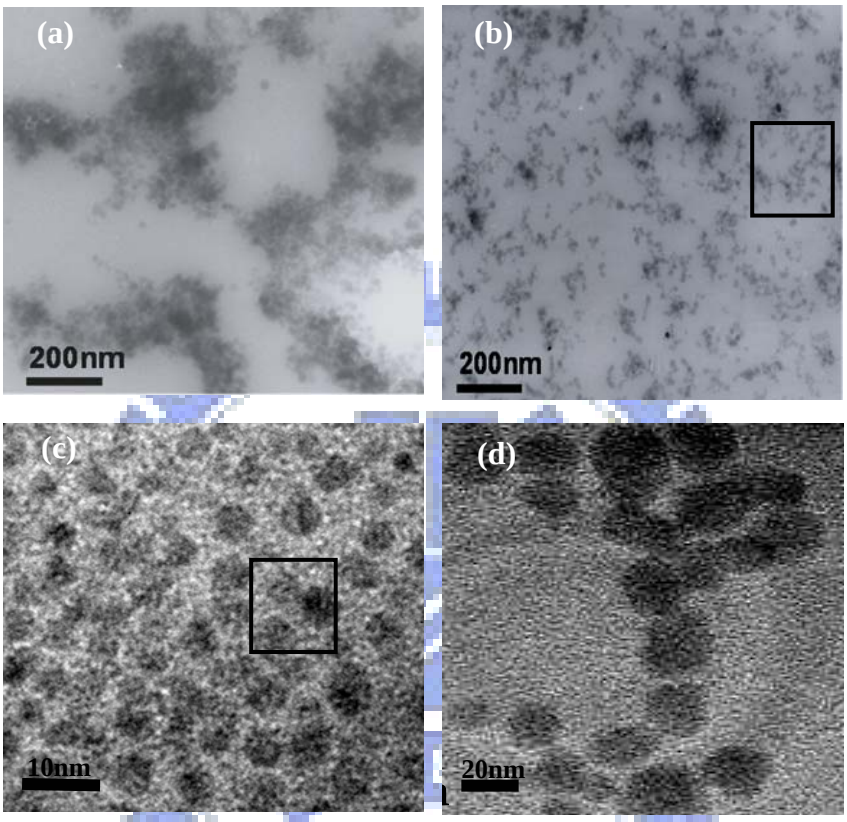

Fig. 6.4 TEM photograph of Cu(0)-pHEMA nanocomposite (a) Hybrid-1-Cu05 and (b) Hybrid-4-Cu05. Both marked area are further magnified in (c) and (d), respectively.

Since the pHEMA is a hydrogel, its molecular structure can be swollen upon water absorption, and this permits an increase in the intermolecular distance of the pHEMA, i.e., increased mesh size, while increasing the H_2O/HEMA ratio, as a result, the network structure of the pHEMA is enlarged, which facilitates further growth of the copper nanoparticles to a larger size, as shown in Fig. 6.5.

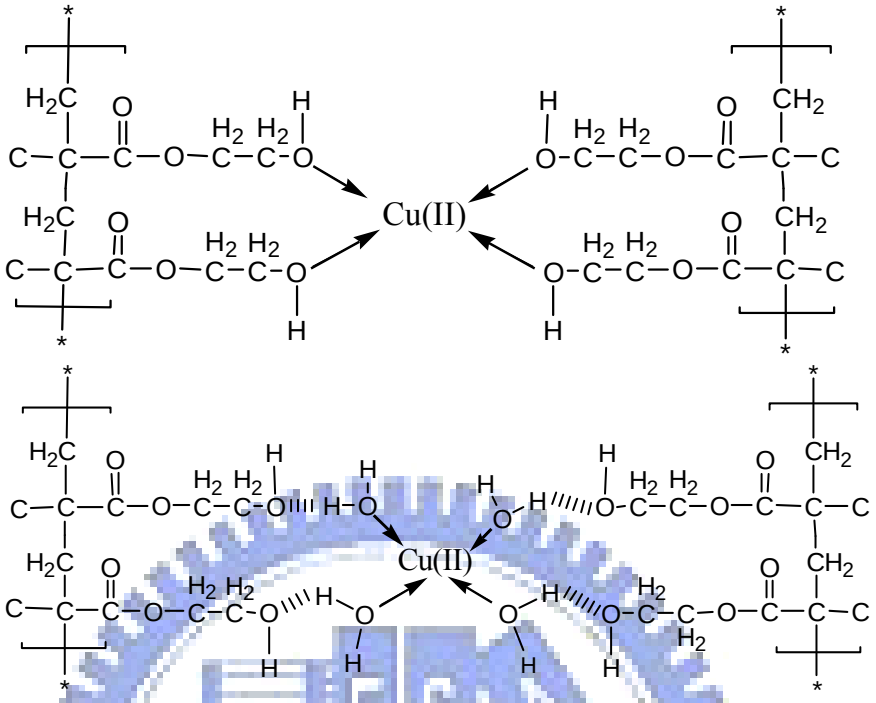

Fig. 6.5 A schematic drawing of the proposed synthesis scheme with the bonding configuration of Cu ions with surrounding environment of Cu(0)-pHEMA hybrid. The Cu(II) ions are assumed to be coupled with the unpaired O of COOR groups along the pHEMA chain or coupled by the unpaired O of H_2O forming a nanophasic Cu domain in place.

Figure 6.6 shows the cross-sectional morphology of the hybrids with various ratio of water to HEMA. It was observed that, in Fig. 6.6(a), Hybrid-1-Cu05 showed a considerably dense and uniform microstructure with no visually observable voids, which is similar to that of pure pHEMA membrane (not shown here). However, as the water concentration was increased upon synthesis, the samples presented a loose microstructure, as illustrated in Fig. 6.6(b) for Hybrid-4-Cu05 sample where a microporous structure, with a pore size over a range of 3-10 μm, was developed. This is because although water is a good solvent for the HEMA monomer, it turned to be a poor solvent upon polymerization, i.e., for the HEMA polymer or pHEMA. Phase segregation between water and pHEMA phases may accordingly cause a change in the resultant microstructure. Therefore it can be concluded that water incorporation not only creates more space for the Cu to grow in size, in the meantime, it also form more porous microstructure in the resulting hybrids.

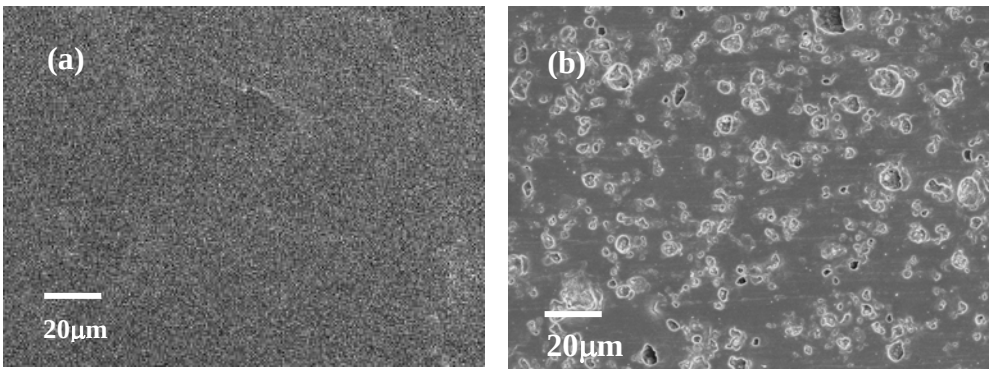

Fig. 6.6 Cross-sectional microstructure of the Cu(0)-pHEMA hybrids (a) Hybrid-1-Cu05, and (b) Hybrid-4-Cu05, where microporous morphology is clearly shown as starting water concentration was increased.

6.5 Cu(Ⅱ) release

Effect of Microstructure

The influence of microstructural variation of the hybrid on the resulting Cu release profile was evaluated using the hybrids with the addition of 0.5 wt% Cu, i.e., Hybrid-1-Cu05, Hybrid-3-Cu05 and Hybrid-4-Cu05, where accordingly higher porosity and larger pore size with increasing H_2O/pHEMA ratio were observed as aforementioned. The cumulative release of Cu(Ⅱ) from the Cu(0)-pHEMA hybrids was measured and given directly in Fig.6.7, where a continuous release for a time duration of 240 hours is attained. The parameters *n* of Hybrid-1-Cu05, Hybrid-3-Cu05 and Hybrid-4-Cu05 calculated from Eq. (2) are 0.602, 0.629, and 0.645 respectively from a highly-correlated linear regression analysis, indicating a non-Fickian diffusion mode. However, for those porous hybrids, e.g., Hybrid-3-Cu05 and Hybrid-4-Cu05, the release mechanism appears to be constant, compared with the dense one, i.e., Hybrid-1-Cu05. In other words, porosity or pore size, i.e., 3-10 um in diameter, evolved seems to have little or no effect on the diffusion mechanism of the hybrids, but the rate constant, *k,* which is increased with the increasing H_2O/HEMA molar ratio from 0.0409 to 0.0747. The presence of porosity should have influenced on the release rate since the porous structure, i.e, Hybrid-3-Cu05 and Hybrid-4-Cu05, allows more surface area of the Cu particles to be exposed to the aqueous solution than that of dense structure, i.e., Hybrid-1-Cu05. Since the exponent n has a relatively constant value for these hybrids with various pore sizes, the value k can then be considered as an index of the release rate of Cu(II). On this basis, the release rate for the porous Hybrid-4-Cu05 is

estimated higher by 82.6% than that of the dense Hybrid-1-Cu05. Therefore, based on the structural evolution and a corresponding tunable release kinetic for the hybrids synthesized in current investigation, the Cu(0)-pHEMA hybrids with tunable technical merits with highly regulated elution of Cu can be well designed for biomedical uses.

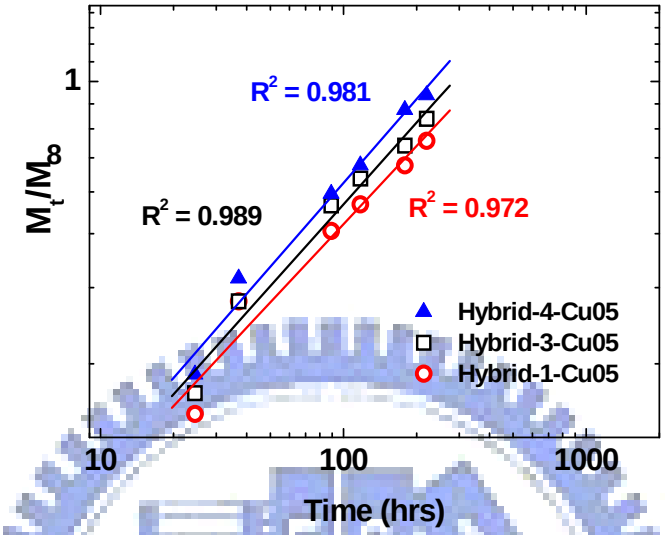

Fig. 6.7 Cu(Ⅱ) release from the Cu(0)-pHEMA hybrids with different H_2O/HEMA molar ratio. The release patterns showed a relatively slow and sustained kinetics with the values of k and n determined according to Eq. (2) for $M_t/M_\infty < 0.6$ (n = 5).

Effect of Particle size and Concentration

Figure 6.8(a) shows the release behavior of cupric ion Cu(II) from Cu-loaded pHEMA hybrids. and composites prepared in this study, namely, the Cu(0)-pHEMA hybrids, i.e., with Cu size of 5~25 nm prepared in-situ. For comparison purpose, the Cu-pHEMA composites with commercial nano-particles (50nm, Sigma-Aldrich, Inc. USA) were prepared by using UV irradiation to aqueous solution containing the same composition as aforementioned Hybrid-1-Cu05, designated as Composite-1-Cu05. The Hybrid-4-Cu05 showed a apparently monotonical decrease with the release time, which is believed to be due to more porous pHEMA matrix as shown in Fig. 6.6(b). In contrast, for Hybrid-1-Cu05, the copper released relatively constantly, i.e., at a concentration of ~ 5.5 ppm over a regular time interval of 24 h, from the very beginning to a time duration of as long as 240 hours. As a larger particle size was used, i.e., Composite-1-Cu-05, although the composite also showed a monotonical decrease over a time period of first 96 hours, followed by a slow reduction up to 240 hours, the slower profile was observed for the Cu released from the

composites, indicating a lower surface area exposed to the surrounding aqueous environment for the larger size of the Cu particles embedded in the pHEMA matrix.

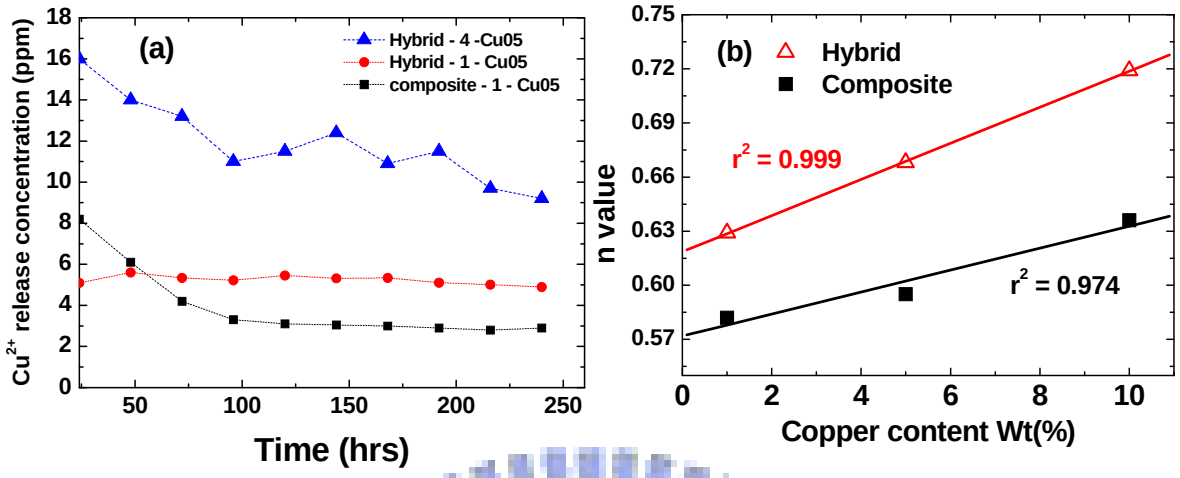

Fig. 6.8 (a) Curves of Cu(Ⅱ) release rates of in-situ Cu(0)-pHEMA hybrids and Cu(0)-pHEMA composites in the PBS. (b) Dependence of n value of different copper content for Cu(Ⅱ) release from Cu(0)-pHEMA composites and in-situ Cu(0)-pHEMA hybrids.

Although no direct evidence for the mechanism of Cu(0) → Cu(II) can be provided in this study, it is generally recognized that an oxidation occurred on the surface of the Cu nanoparticles, following a dissolution of the Cu(II) into the medium. Therefore, the release kinetic is considered as an *apparent kinetic* of Cu(II) release. The diffusion mechanism of the Cu(II) from the hybrids can be characterized using Equation (2) [172-173]:

$$\frac{M_t}{M_\infty} = kt^n \qquad (2)$$

where M_t is the mass of Cu(Ⅱ) released at time t, M_∞ the mass of released Cu(Ⅱ) at time of infinity, k is a proportional constant, and n is a characteristic exponent related to the mode of transport of the solute. This equation is applicable for $M_t/M_\infty < 0.6$. Three modes of diffusion release mechanism were defined from various controlled release systems [174]. Fickian diffusion ($n = 0.5$), in which the rate of diffusion is much slower than the rate of swelling; in this case, the system is controlled by diffusion. The second mode is Case II transport ($n = 1.0$), where the diffusion process is much faster than the swelling process. The controlling step is the velocity of an advancing front, i.e., a swelling-controlled mode. The third is non-Fickian (anomalous) transport ($0.5 < n < 1.0$), which describes those cases where the diffusion and relaxation rates are comparable.

For comparison, a series of Cu(0)-pHEMA hybrids with the same load of copper as that of the composites were prepared. The parameters *n* and *k* calculated from Eq. (2) are listed in Table 6.1. For the hybrids, the parameters *n* of Hybrid-1-Cu01, Hybrid-1-Cu05 and Hybrid-1-Cu10 are 0.629, 0.668, and 0.719 respectively, indicating the release of Cu(Ⅱ) from the Cu(0)-pHEMA hybrids is non-Fickian diffusion, and can be categorized as a combination of both diffusion and swelling controlled modes. In other words, structural evolution upon dilation or relaxation of the hybrid may play certain critical role in determining the resulting release kinetics for the hybrids. This is more pronounced since the Cu particles in the hybrids are the smallest size among other samples and a much higher dissolution rate is heavily expected compared with others. Under such conditions, the length of the pathway and tortuosity of the hybrid structure may play important roles in releasing rate. However, for the composites, namely, Composite-1-Cu01, Composite-1-Cu05 and Composite-1-Cu10, the values of n are 0.582, 0.595, and 0.636 respectively, smaller than the ones from the hybrids, indicating the release of Cu(Ⅱ) from the Cu-pHEMA composite also exhibited a non-Fickian type of diffusion that dominates the release behavior as that of the hybrids.

Table 6.1 The parameters *n* and *k* calculated from Eq. (2) of Cu(0)-pHEMA composites and hybrids.

	k	n	r-square
Composite-1-Cu01	0.0055	0.582	0.985
Composite-1-Cu05	0.0074	0.595	0.982
Composite-1-Cu10	0.0078	0.636	0.972
Hybrid-1-Cu01	0.0018	0.629	0.982
Hybrid-1-Cu05	0.0099	0.668	0.986
Hybrid-1-Cu10	0.0116	0.719	0.969

However, the n value was found to increase linearly with the content of Cu in both the hybrid and composite samples, Fig 6.8(b), suggesting that the Cu release mechanism may apparently be a combination of both diffusion and swelling modes. This is because a certain extent of agglomeration of the Cu particles, for both the hybrids and composites, was observed when the concentration of the Cu was increased from 0.1% to 1.0%. Such a structural inhomogeneity may contribute to the resulting swelling mode of release kinetics. Therefore, we believed that the linear change of the n along with Cu concentration given in

Fig. 6.8(b) indicates a possible transition of release mechanism from diffusion to swelling, resulting in an apparently non-Fickian mode of Cu release.

6.6 Cell behavior

The influence of Cu release and the corresponding concentration on cellular behavior is vital to practical applications. Figure 6.9 shows the growth behavior of the HUVEC with the Cu(II) concentration released from the Cu(0)-pHEMA hybrids for a time duration of 24h and 48h. Copper-induced growth of the endothelial cells was observed and shown to be significant for the hybrids with lower release profile, i.e., Hybrid-1-Cu05 and Hybrid-2-Cu05, in the range of 6~15 ppm daily. After 48-h incubation, a progressive increase of cell numbers which reached 121% of the control group was obtained. However, it seems not applicable for the hybrids with higher water content and porosity, such as Hybrid-3-Cu05 and Hybrid-4-Cu05, where the population of the endothelial cells is reduced to about 80% of the control, albeit not significant to the control group, indicating a higher concentration of Cu(II) released from especially the Hybrid-4-Cu05 prohibit the proliferation of the endothelial cells. Regardless of those biological concerns, in this short-term observation, the Cu-pHEMA hybrid prepared in this investigation has shown promising compatibility and proliferative activity to the endothelial cells. Although preliminary, this study envisions that the copper released form the hybrids shows short-term cytocompatibility at the concentration below certain level, i.e., 15 ppm. A stringent control release of the Cu from the hybrids is therefore critical for biomedical applications and through the manipulation of synthesis scheme, the hybrids capable of delivering optimal dose of Cu can be easily synthesized. However, the mechanism and signal transduction pathways for copper-induced endothelial cell proliferation are not clearly understood. A subsequent study is underway and will be reported shortly.

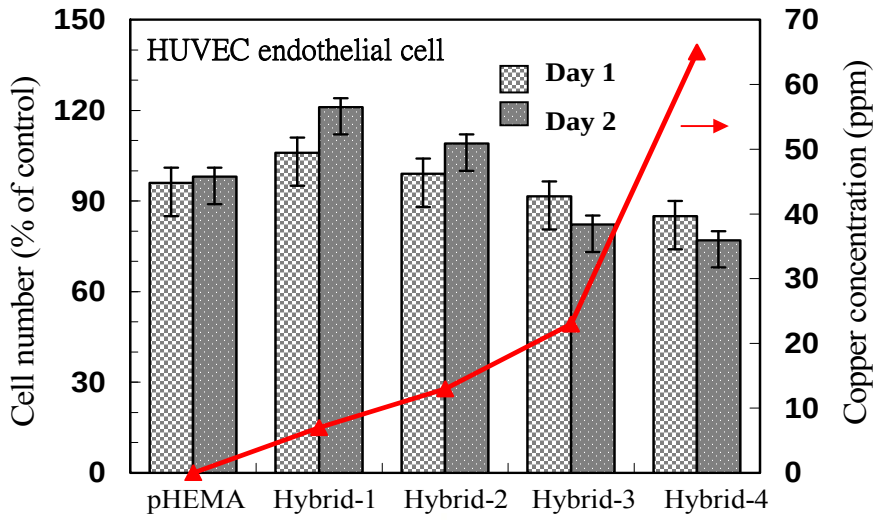

Fig. 6.9 Effect of copper ion on HUVEC proliferation at various time periods. Cell number was determined by AlamarBlue assay.

6.7 Summary

Novel nanocomposites with metallic Cu nanoparticles well-embedded within the pHEMA matrix, forming a well-defined nanostructure have been extensively characterized. The interaction between Cu(II) with the hydroxyl groups within the pHEMA matrix was confirmed by the infrared spectral analysis and a corresponding improvement in the thermal stability of the Cu(0)-pHEMA hybrids. The molar ratio of H_2O/HEMA in the starting synthesis plays a crucial role in the nanostructural evolution of the Cu nanoparticles, wherein a change from amorphous-like Cu or crystalline Cu, corresponding to a size ranging from ~ 5 nm to ~25 nm, has been observed when the ratio of H_2O/HEMA is increased. In addition, the resulting hybrid evolved a microstructural development from dense to porous structure, causing a change in Cu release rate, while the release kinetic is considered to be a non-Fickian diffusion mode or plausibly, a combination of diffusion and swelling modes. Under well control of the hybrid composition, Cu release can be well regulated such as those of dense hybrids, i.e., Hybrid-1 and Hybrid-2, where a Cu(II)-induced proliferation of the HUVEC was observed for a 48-h incubation in vitro, and

agreed with literature report. In contrast, inhibition to the proliferation of the human smooth muscle cell line was observed for a longer incubation time. It may suggest a potential use of the Cu(0)-pHEMA nanocomposite for a number of biomedical applications, such as coating for cardiovascular stents, and will be reported separately.

Chapter 7

Metal/organic Hybrid – Cu/pHEMA –In-Situ Synthesis of Hybrid Nanocomposite with Highly-Order Arranged Amorphous Metallic Copper Nanoparticle in Poly(2-hydroxyethyl methacrylate) and Its Potential for Blood-contact Uses

7.1 Introduction

This has long been highlighted in the area of blood-contacting devices or implants, where topological texture, charging and hydrophilic nature of the hybrid surface are of great concerns [179, 180], and attentions have also largely paid to the electrochemical behavior of the materials surface in order to inhibit the occurrence of thrombosis [181-183]. A general understanding, albeit not yet being officially standardized, for a material showing blood compatibility can be characterized in terms of, for instance, platelet adhesion, fibrinogen deposition, and clotting time. However, it seems that current existing blood-contacting devices in the market are not as good as a true hemocompatible one from the viewpoints of biology and biomaterials science [184]. Development of new biomaterials with improved blood compatibility has continuously attracted great attention, and recently, thromboresistant materials based on inorganic, metals and metal-organic compound have received most attention, which have known to provide more advantages over conventional polymeric materials which are not truly thrombosis-free surface but currently widely available in the market [185, 186]. In situ synthesis of hybrid materials has long been technically attractive for improved property, for instance blood compatibility, due to desirable electrochemical behavior, better physical uniformity and higher chemical homogeneity of both surface and bulk regions. Here, a novel in-situ synthesis method is reported where a hybrid system based on the use of 2-hydroxyethyl methacrylate, i.e.,HEMA, monomers that were photopolymerized in the presence of Cu^{2+} precursor was prepared through an in-situ synthesis, following an in-situ chemical reduction of the Cu^{2+}

precursor to form resulting metallic Cu-containing hybrid. The hybrids were characterized by transmission electron microscopy (TEM), X-ray photoelectron spectroscopy (XPS), and streaming potential measurements. Interaction between blood and hybrids were examined in terms of platelet adhesion test of human whole blood.

7.2 Fabrication of Cu-pHEMA Hybrid

The Cu-pHEMA hybrid was prepared by employing UV irradiation to aqueous solution containing 2.5 grams of HEMA monomer, 0.1 ml of EDGMA as cross linker, 0.03 g BME as initiator, 0.1g SiO_2 suspension, 2 grams H_2O as solvent, and 0.05, 0.08, and 0.20 grams of 1 M $CuSO_4$ solution with 0.1 wt% PVP for different hybrids which were named 5C, 8C, and 20C, respectively. The mixture was vigorously mixed during the course of reaction. To remove the dissolved oxygen from precursors, N_2 was purged for approximately 1 min. Then, the mixture were transferred to a sealed transparent plastic holder of 50 mm × 50 mm × 0.5 mm in dimensions and UV irradiated at 254 nm for 2 h and the Cu(II)-pHEMA hybrid were produced. The Cu(II)-pHEMA hybrid were rinsed by distilled water to remove the un-reacted species (e.g., cross-linker, monomer, etc.) and then subjecting to in-situ chemical reduction by immersion the as-synthesized Cu(II)-pHEMA hybrid into 50 ml of 0.5 M hydrazine solution at 40^{o}C for 24 h, to form a final metallic Cu(0)-pHEMA hybrid.

7.3 Structural Analysis

Figure 7.1a illustrates the nanostructure of the Cu(0)-pHEMA hybrid where the Cu(0) nanoparticles are relatively homogeneously distributed in the pHEMA matrix and show a relatively uniform size of about 2~5 nm in diameter, as shown in Fig. 7.1b, a high resolution image of Cu(0) nano particles in pHEMA matrix. Fig. 7.1c is a selected area electron diffraction pattern, which confirmed that the Cu(0) nanoparticles are poorly crystallized metallic phase, which is due to its relatively small crystallite size. The dimensional restriction of the primary Cu(0) nanoparticles, which according to the work of Huang et al. [187], should exhibit quantum confinement effect, where the electrons may behave in a wave-like rather than a particle-like manner.

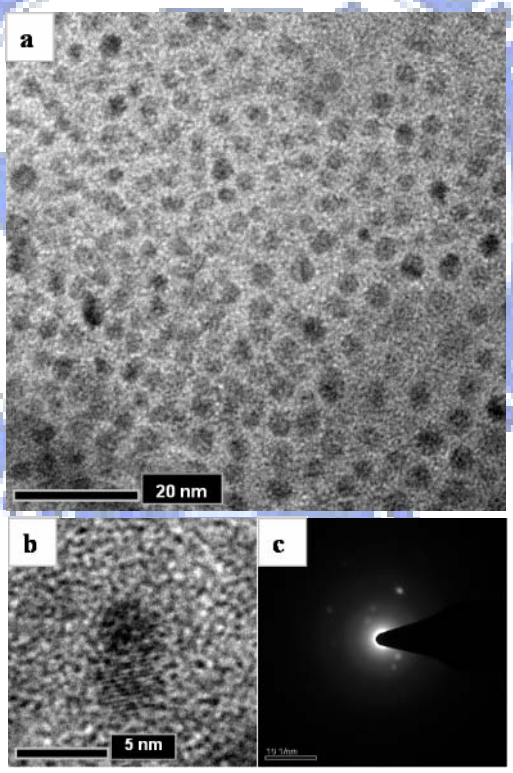

Fig. 7.1 TEM photographs of Cu(0)-pHEMA hybrid showing (a) an orderly packing configuration of Cu(0) nanoparticles distributed in the pHEMA matrix, (b) High resolution image of Cu(0) nano particle in pHEMA matrix where the nanopaticle has a size of about 3 nm in average, and (c) selected area electron diffraction pattern of Cu(0) nano particle, indicated the Cu(0) a poorly crystalline (or amorphous) structure.

Although no direct evidence supports this argument at present, it is reasonably believed that the Cu(0) nanoparticles in the pHEMA matrix should behave as a semi-conductor, rather than that of bulk copper.

The highly-order arrangement of the Cu(0) nanoparticles, having a relatively constant particle-to-particle distance of 8-10 nm, within the matrix suggests to resulting from a possible mechanism evolved upon the synthesis of the Cu(II)-pHEMA hybrid. Upon the hybrid formation, the Cu(II) ions can be anchored by the unpaired electron of O from either the COOR group of the HEMA monomers or H_2O in reaction mixture to form coordination bonds, via for instance, coupling reaction, as schematically shown in Fig. 7.2b. The Cu(II) ions are immobilized in the network structure of the HEMA upon polymerization and remained in place while subjecting to chemical reduction, resulting in the formation of amorphous metallic Cu(0) nanoparticles. This argument has also partially self-evidenced from the nanostructural development as illustrated in Fig. 7.1a where no fractal aggregation of the Cu(0) nanoparticles was observed in the resulting hybrid. In other words, the orderly packed configuration of the Cu(0) nanoparticles in the matrix is, as aforementioned, suggesting that the molecular network structure in the pHEMA matrix is acting as spaciously confined space for Cu(0) formation, as schematically elucidated in Fig. 7.2a. It also proposed an interaction between the Cu(II) ions and hydroxyl groups of pHEMA. Once the Cu(0) nanoparticles being nucleated upon chemical reduction and grew, it evolved in a confined nanometric space defined by the dimension of the pHEMA network (as a nano-cage), rather than agglomerated to form fractal aggregates. This may then result in a regular arrangement of the Cu(0) nanoparticles in the well-defined nanostructural network. Such a highly uniformly distributed Cu(0) nanoparticles in the pHEMA ensures a nanometric-scale uniformity on the hybrid surface upon contacting with blood-clotting proteins, such as fibrinogen, from un-desirable adsorption.

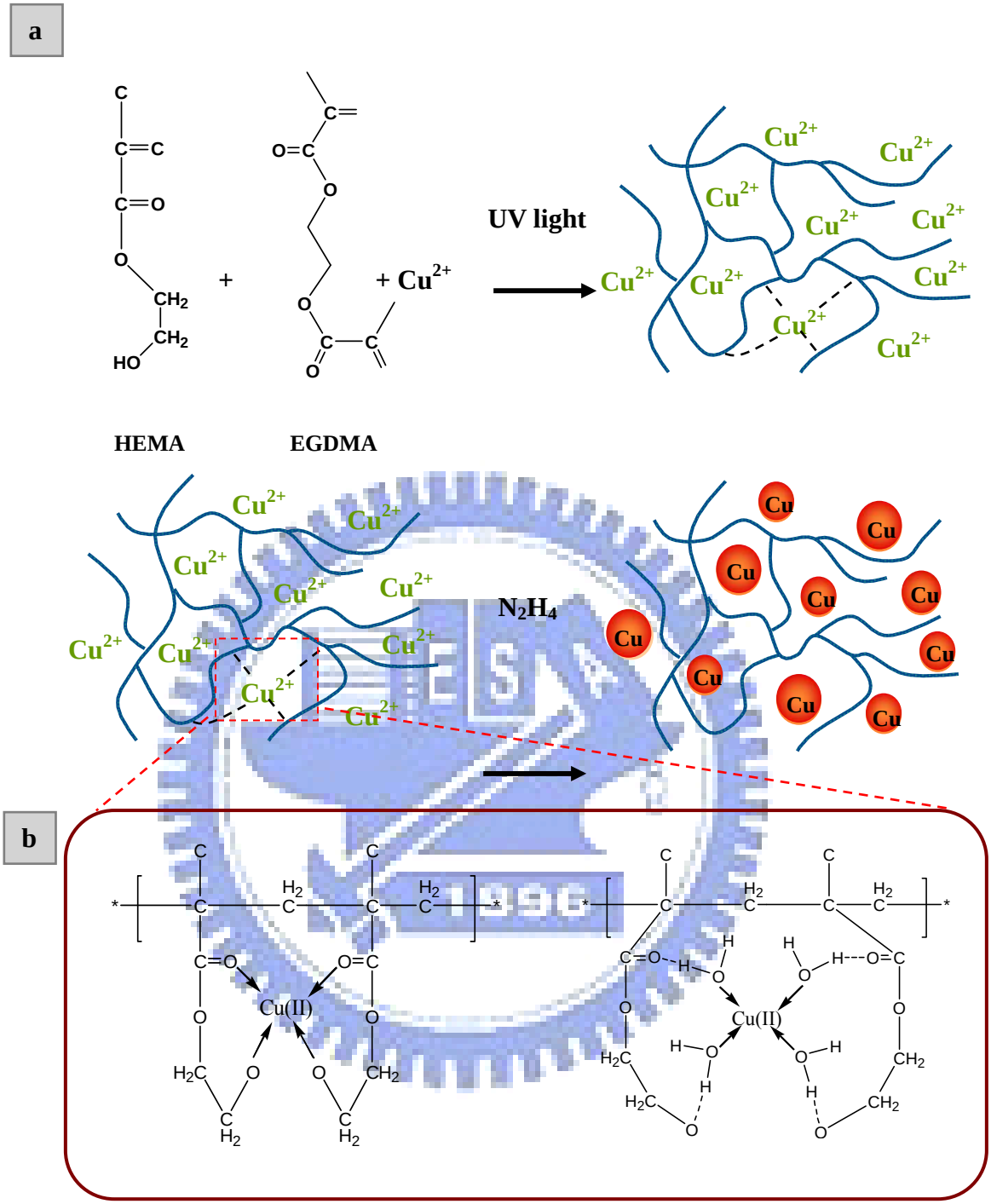

Fig. 7.2 A schematic drawing for the proposed synthesis scheme of Cu(0)-pHEMA hybrid, where (a) the Cu(II) were localized and chemically reduced by N2H4 in-situ to metallic Cu(0) nanoparticles and (b) the Cu(II) ions were assumed to be coupled with the unpaired O of COOR groups along the pHEMA chain network, forming a regularly arranged nanostructure, as illustrated in Fig. 7.1a.

As mentioned earlier [133, 134], copper, in either metallic form or chemical complex, should play a critical role in catalytic nitric oxide generation for improved blood compatibility. It is important to realize the chemical composition of the Cu nanoparticles in-situ prepared and its possible oxidative state of the copper developed in the hybrids since both factors may also determine its electrochemical interaction to protein adsorption or platelet adhesion/aggregation. An XPS analysis on the pristine synthesis of Cu(0)-pHEMA hybrid before and after immersion in PBS is shown in Fig. 7.3 (a) and (b), respectively, where in Fig. 7.3a, the Cu 2p3/2 NPs spectrum of pristine synthesis Cu(0)-pHEMA hybrid shows a peak at 932.79 ± 0.2 eV which is mainly attributed to Cu(0), while a much weaker feature, lying at 933.8 ± 0.2 eV, is attributed to a small amount of CuO. A corresponding fraction of the copper species of respective concentration can be correlated with the area under the spectrum and this determines the metallic form of the Cu(0) to have 83.5% and CuO has 16.5% in the resulting Cu(0)-pHEMA hybrid. This indicates that the copper developed in the Cu(0)-pHEMA hybrid is a mixture of mainly metallic Cu(0) and a small fraction of CuO, after in-situ chemical reduction. The presence of small amount of divalent CuO suggests an incomplete reduction reaction of Cu(II) ions in the matrix. This Cu(II), i.e., CuO, may locate in the inner region of the metallic Cu(0) nanoparticles since the reduction reaction is considered to be a diffusion-controlled process. However, after immersing in PBS for 24 h, the resulting spectra, Fig. 7.3b, indicate that most of the metallic Cu(0) turned into ionic CuO, i.e., Cu(0) has a concentration of 21.1% and CuO, 78.9%, as a result of oxidation. This finding is indicative of the tendency of an electron-giving characteristic of the amorphous metallic Cu nanoparticles in the matrix. The presence of metallic copper nanoparticles, according to a recent report [185], should provide redox ability for thromboresistance.

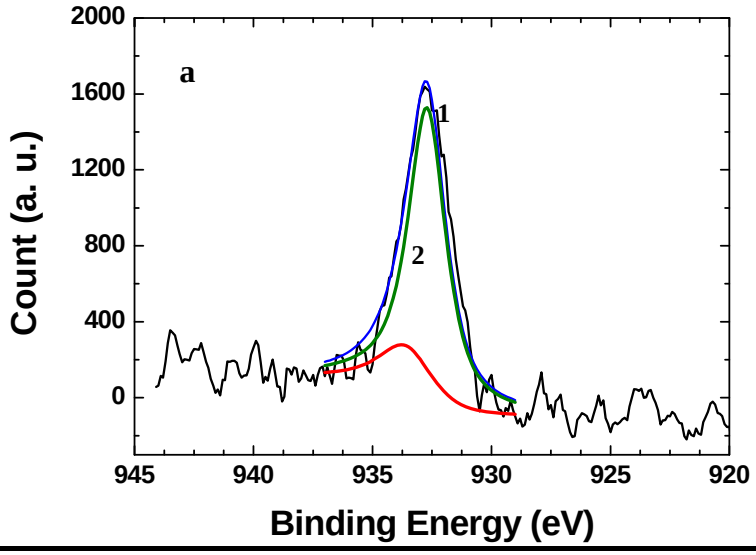

#	Position (eV)	Intensity	FWHM (eV)	Area	Area(%)	Component
1	932.7	1528.1	1.9	3809.8	83.5%	Cu
2	933.8	279.5	3.9	754.5	16.5%	CuO

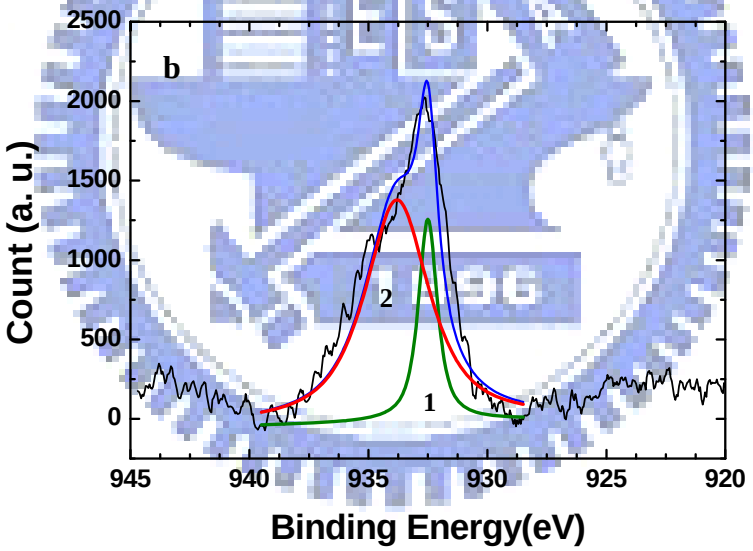

#	Position (eV)	Intensity	FWHM (eV)	Area	Area(%)	Component
1	932.5	1257.565	0.95	1433.8	21.1%	Cu
2	933.8	1378.599	3.2	5361.6	78.9%	CuO

Fig. 7.3 The Cu $2p_{3/2}$ peaks of XPS spectra of (a) as-synthesized Cu(0)-pHEMA hybrid and (b) after immersion in PBS for 24 h. Showing that a metallic Cu(0) was mainly characterized for the as-synthesized hybrid, however, it turned into Cu(II) after PBS immersion, suggesting the Cu(0) nanoparticles being oxidized to copper oxide, Cu(II).

7.4 Zeta potential measurement

Surface charge of the Cu(0)-pHEMA hybrids were determined at pH 7.4 in 10^{-3} M KCl solution. Fig. 7.4 shows the zeta potential of the hybrids with different weight contents of the copper nanoparticles, from 0%, 0.03%, 0.05% to 0.13%, corresponding to samples of pure pHEMA, hybrid 5C, 8C, and 20C, respectively. It can be seen that the surface charge of the neat pHEMA and Cu(0)-pHEMA hybrids showed negatively charged at pH 7.4 and became more negative with an increasing incorporation of the Cu(0) nanoparticle, to a value of as high as -24.6 mV in the range of study.

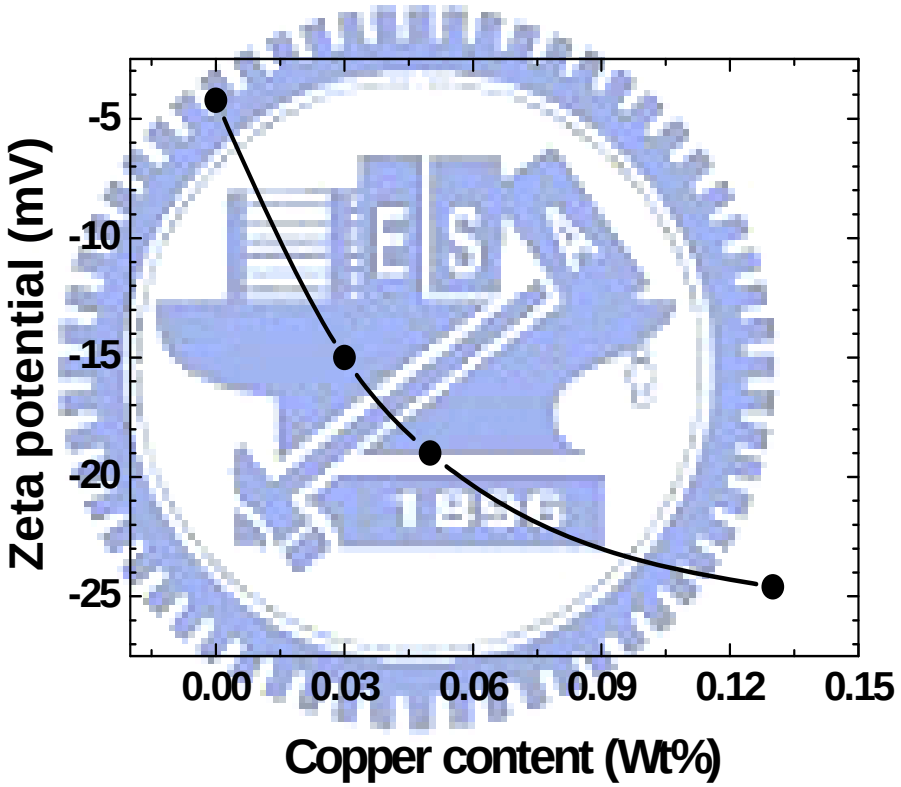

Fig. 7.4 Effect of the nano copper particles on zeta potential of Cu(0)-pHEMA hybrid with different copper particle content (weight %). Concentration of KCl = $1*10^{-3}$ M at pH 7.4

The increment of negative charge of the hybrid surface with the incorporation of relatively small amount metallic Cu nanoparticles suggests to be a result of the highly uniform distribution of the relatively small dimension of the Cu nanoparticles, i.e., a few nanometers, in the hybrid, where higher surface potential of the total Cu nanoparticles, due to relatively

large total surface area, can be cumulatively achieved. Copper nanoparticles of Cu(0)-pHEMA can be oxidized to CuO in aqueous solution as proved by XPS and it was demonstrated that CuO particles show negative surface charge at pH 7.4 [188] which may be due to the formation of hydroxide ions (OH^-) on the surface of CuO-pHEMA hybrid [189]. However, the increment of the surface charge of the hybrids is gradually reduce as the Cu concentration is continuingly increased, suggesting that the increment in the surface potential tends to reach a constant level at pH 7.4. In the case of neutral pH, there are limited hydroxide ions (OH^-) that can be adsorbed on the surface of Cu(0)-pHEMA hybrid where the surface charge ζ then approached constant. Accordingly, surface with increasing negative charge should exhibit improved anti-blood clotting behavior [179], together with redox ability of Cu nanoparticles reported earlier, it further reinforces the argument that the hybrids currently prepared should have improved thromboresistant property.

7.5 Blood and platelet test

The coagulation of blood consists of a cascade of reactions dividing into two pathways: the extrinsic and intrinsic pathways and platelets can accelerate thrombosis through secretion of bulk phase agonists, fibrinogen-mediated platelet–platelet aggregation, and by the acceleration of thrombin production [190]. Therefore, the extent of platelet adhesion to biomaterials is often used as an index of blood compatibility [191]. In this study, platelet adhesion and platelet activation on the surface of the Cu(0)-pHEMA hybrid was one of the main focuses in order to evaluate the hemocompatible properties of the hybrid. Fig. 7.5 shows that a trace amount of platelets adhered on the surface of the Cu(0)-pHEMA hybrid after 2 h immersion with human whole blood, in comparison with the PSF (polysulfonate, as a referenced materials) and pure pHEMA, a controlled group. The PSF showed a considerable amount of platelet adhesion, and pHEMA showed some extent of platelet adhesion, which are agreed with the observations reported in the literature [192, 193]. In contract to those two

well-recognized candidates, the amorphous metallic Cu(0)-pHEMA hybrid exhibits much improved anti-platelet adhesion behavior, where as small as 30% of the adhesion amount of platelet compared to that of neat pHEMA can be observed for the hybrids, and turned to be more significant in comparing to that of PSF, i.e., improved by about 92%.

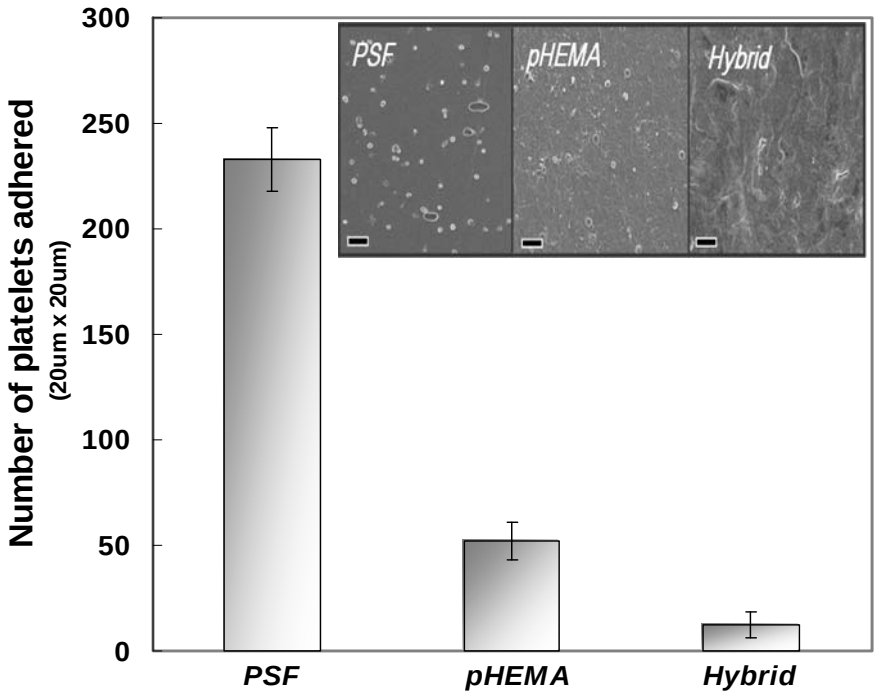

Fig. 7.5 The blood platelet adhesion test showed that the Cu(0)-pHEMA hybrid demonstrated an improved anti-platelet adhesion behavior by ~70% and 92% compared to that of the neat pHEMA and PSF, respectively. (The scale bar of SEM image is 10μm.)

Although the exchange of electrons from blood proteins to the surface of medical devices has been considered to induce blood coagulation [179], the actual mechanism(s) of adhesion behavior of platelets from whole blood to the hybrid surface is not clearly understood at present. In spite of the ambiguity, it is reasonably trusted that the Cu nanoparticles in the pHEMA may trigger an electron-transferring process from the amorphous Cu(0) nanoparticles to blood-clotting proteins. In the meantime, the negatively-charged hybrid surface is expected to inhibit adsorption of the blood-clot-induced protein (fibrinogen, negatively charged), and

this will surely minimize or eliminate protein adsorption/denaturation as a result of electrostatic repulsion and prevent electron transferred from the protein to the negatively-charged hybrid surface. Either the former or latter mechanism or a combination can be effectively inhibiting undesirable platelet adhesion.

It seems able to conclude that the metallic Cu nanoparticle-pHEMA hybrids reported in this communication exhibited outstanding anti-platelet adhesion property compared to neat pHEMA and a widely-used biocompatible material, PSF. The highly-ordered nanostructure offers an unprecedented physical and chemical uniformity of the hybrids, together with its highly negatively-charged property, permitted the hybrids to behave as an outstanding anti-blood-clotting material. The electron-giving potential of the hybrid, as revealed in an earlier electrochemical test [179], together with the XPS spectral variation in Fig. 7.2, also reinforced the thromboresistant character of the hybrids. A further study on the blood compatibility in terms of Cu-catalyzed nitric oxide generation for the hybrids is under investigation through the use of electrochemical method and will be reported shortly.

7.6 Summary

The amorphous metallic Cu nanoparticles with an orderly packing configuration within the pHEMA matrix, forming a well-defined hybrid structure have been successfully synthesized. The oxidation of Cu nanoparticles was confirmed by the XPS analysis. A relatively uniform copper nanoparticles about 2~5 nm in diameter and a relatively constant particle-to-particle distance of 8~10 nm were observed in Cu(0)-pHEMA hybrid structure, suggesting an unprecedented chemical and physical homogeneity can be achieved. The negative surface charge of the Cu(0)-pHEMA hybrid were confirmed by surface streaming potential and is expected to play important role in reducing the absorption of platelets. Thus, those experimental results demonstrate that the Cu(0)-pHEMA hybrid is capable of offering a promising characteristic for thromboresistant applications.

Chapter 8

Metal/organic Hybrid – Cu(0)-pHEMA - Electrochemical behavior of Cu(0)-pHEMA hybrid

8.1 Introduction

Over the last few years, much effort has been directed into developing new materials with specific electrochemical properties that could be used in biosensors, artificial muscles, and drug delivery system. The electric current of redox- reaction of specific enzyme and protein in biological substance could be used as an environmental signal to induce responses of designed action such as in-situ drug release or on–off switching from the implant device. On the other hand, the electrochemical properties of the implant material will also effect on the bio-reaction of the cell and implant materials [194]. For many biomaterials, interfacial charge on polymeric materials was claimed to be relevant for the success of medical devices according to different considerations [195]. Therefore, immobilization of ions, particles, and complex of metals in the matrix of polymeric for varying the electrochemical properties of the intrinsic polymer open up the way for designing the catalysts combining redox ability [196] and provide a variable mechanism of activity in many physiological processes [197].

In this study, copper-containing pHEMA hybrids, Cu(0)-pHEMA, were developed for potential uses in blood-contact applications. An in-situ polymerization process was developed to promote high-affinity nucleation and growth of nano copper particles in the polymer hydrogel which provides an efficient approach toward inorganic/organic nano-hybrids with high-uniformity. These hybrids with different compositions could be produced and characterized in terms of their structure and electrochemical properties of the Cu(0)-pHEMA hybrid. In this chapter, an experimental study of different electro-chemical and physical aspects of electrochemical sensitive Cu(0)-pHEMA hybrid was presented. The electrochemical properties were analyzed by cyclic voltammetry (CV) and alternating current

(AC) impedance measurements. The generation of nitric oxide in aqueous by Cu(0)-pHEMA hybrid was also tested in this study. The nano-sized Cu metal or metal oxide particles could disperse uniformly in polymer matrix and react with ionic group in the aqueous solution by the charge transfer from the interfacial surface of nano copper particles.

8.2 Fabrication of Cu-pHEMA Hybrid

The Cu-pHEMA hybrid was prepared by employing UV irradiation to an aqueous solution containing 2.5 grams of HEMA monomer, 0.1 ml of EDGMA as cross linker, 0.03 g BME as initiator, 0.1g SiO_2 suspension, 0.5 grams H_2O as solvent, and 0.1, 0.3, and 1 grams of 0.5 M $CuSO_4$ solution with 0.1 wt% PVP for different hybrids which were named Hybrid-01, Hybrid-05, and Hybrid-10, respectively. The mixture was vigorously mixed during the course of reaction. To remove the dissolved oxygen from precursors, N_2 was purged for approximately 1 min. Then, the mixture were transferred to a sealed transparent plastic holder of 50 mm × 50 mm × 0.5 mm in dimensions and UV irradiated at 365 nm for 2 h and the Cu(II)-pHEMA hybrid were produced. The Cu(II)-pHEMA hybrid were rinsed by distilled water to remove the un-reacted species (e.g., cross-linker, monomer, etc.) and then subjecting to in-situ chemical reduction by immersion the as-synthesized Cu(II)-pHEMA hybrid into 50 ml of 0.5 M hydrazine solution at 40°C for 24 h, to form a final metallic Cu(0)-pHEMA hybrid.

Cyclic voltammetry (CV)

CV analysis was carried out using the CH instruments potentiostat model 614A. CV scans of Cu(0)-pHEMA hybrids were in aerated Phosphate-buffered saline (PBS) at room temperature from -900 to -300 mV, at a rate of 20 mV/sec versus a Ag/AgCl reference electrode. A three-electrode system was used throughout the study. The working electrode was platinum plate covered with Cu(0)-pHEMA hybrid. Platinum wire served as the counter

electrode in all experiments. Analysis of CV tracings and determination of the oxidation potential and the anodic current are reported.

Alternating current (AC) impedance

An AC impedance measurement technique was employed to investigate the electrochemical kinetics at the semiconductor-electrolyte interface. The measurement was performed at an open-circuit potential and the frequency was varied in the range of 10^5 Hz to 10^{-1} Hz with an imposed voltage of 5 mV AC (CHI, model 614A). These experiments allow the detection of the properties of the films when submerged in an Phosphate-buffered saline (PBS) solution. Since the thin surface film acts as a capacitor when the semiconductor device makes contact with physiological fluids or blood, the time it takes for the reaction to take place is an important characteristic of each type of film. The time constant, τ, is calculated by multiplying of the values of capacitance and resistance obtained from the impedance measurements.

Nitric oxide generation in vitro

The NO-generating ability of Cu(0)-pHEMA hybrid was examined before and after the in vitro studies using a CH instruments potentiostat and nitric oxide detector (Mini Warn, KAOTEN science CO., LTD). Nitrosoglutathione (GSNO) was prepared by the reaction of equal-molar glutathione (GSH) and $NaNO_2$ in 0.06M H_2SO_4. To n glass reaction cell containing 50mL PBS (138mM NaCl, 2.7mM KCl and 10mM sodium phosphate, pH 7.4) was added 1 μM GSNO, 30 μM GSH and 5 μM EDTA (to chelate metal ion contaminates that might otherwise decompose GSNO). The solution was bathed at 37 ^oC and continuously bubbled with N_2. Any NO produced in the test solution was purged from the buffer, carried by the N_2 gas into the nitric oxide detector chamber and monitored in real-time. The different GSNO concentration was controlled by adding 0.05M GSNO solution into reaction cell. The working potential is -0.8 mV versus a Ag/AgCl reference electrode.

8.3 Electrochemical properties

The surface electrochemical behaviors of Cu(0)-pHEMA hybrid were analyzed by cyclic voltammetry (CV) method and alternating current (AC) impedance method. Cyclic voltammogram is presented in Fig. 8.1 for the Cu/pHEMA hybrid in phosphate-buffered saline solution over the potential range of -0.7 to 0.7V at a scan rate of 50mVs^{-1} at 25^{o}C.

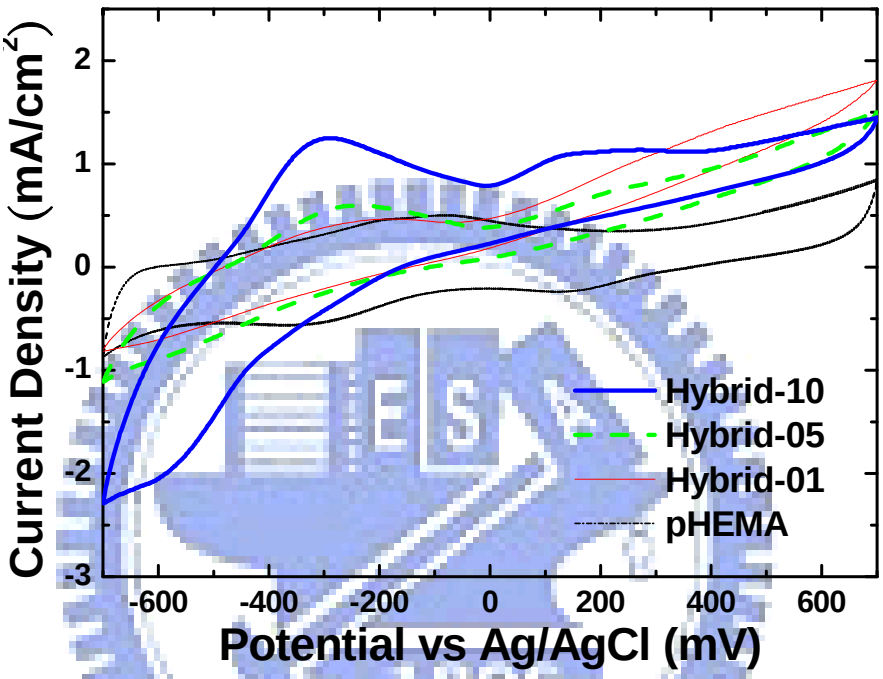

Fig. 8.1 Cyclic voltammograms of pHEMA and Cu(0)-pHEMA in the phosphate-buffered saline solution, v=50mVs^{-1}.

As shown in Fig. 8.1, the Cu(0)-pHEMA hybrid exhibits a higher oxidation current at -310mV when the crystallinity, shown in chapter 6, of the in-situ-formed nano Cu particles is increased. The oxidation peak appeared at a potential of anodic peak is related to the formation of surface-bonded Cu(I) hydrous oxide($[Cu^{+}\bullet nH_2O]_{ads}$) and active Cu(II), respectively [198, 199]. The Cu atoms at an active site probably have a range of energies [200] and some of these, temporarily present (due to energy fluctuations) in a very low lattice coordination state, may be sufficiently active to be oxidized at ca.-0.3V to the Cu (I) or Cu(II) state. The Cu(I) hydrous oxide and active Cu(II) play a major role in the oxidation on the

surface of hybrid at the potential range with respect to the formation of copper oxide. This particular material is easily oxidized and has a higher possibility of absorption hydroxyl group and release electrons in the reaction surface. In addition, from the alternating current (AC) impedance measurement, it can be observed that the incorporation of nano copper particles into pHEMA matrix increases the interface interaction between the solid film and aqueous solution. The AC impedance method was used to calculate the specific capacitance (C_{spec}) and the charge transfer resistance (R_{CT}) of the Cu(0)-pHEMA hybrid. The spectra (i.e., Nyquist plot) for pHEMA and Cu(0)-pHEMA hybrids are presented in Fig. 8.2.

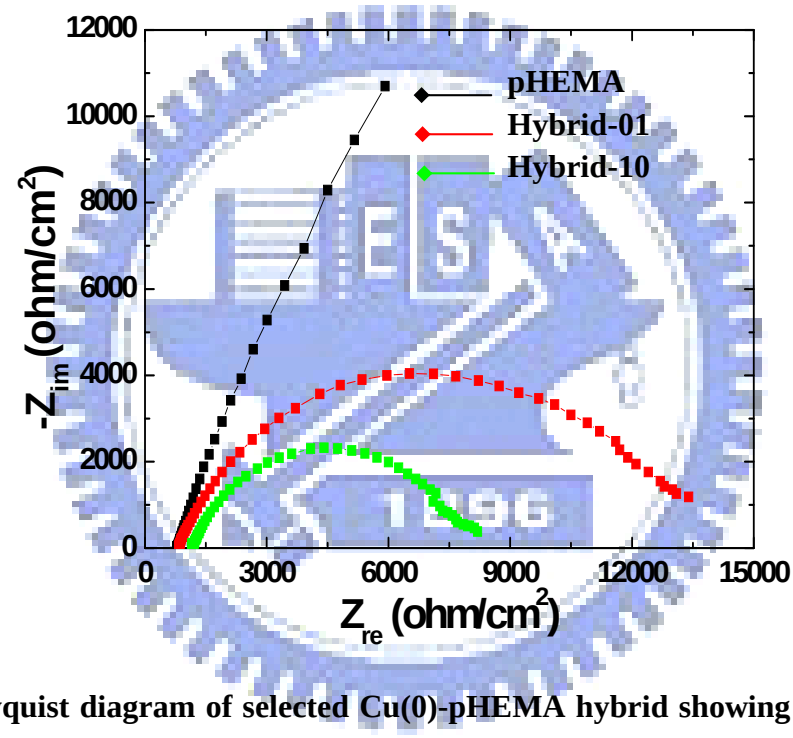

Fig. 8.2 Nyquist diagram of selected Cu(0)-pHEMA hybrid showing various values of time constant.

At high frequency, the spectral feature represents a limiting diffusion process and at low frequency it represents purely capacitive characteristic. For pHEMA, there is no copper nano particle within the polymer matrix, which indicates purely capacitive behavior. On the other hand, the AC spectrum for the Cu(0)-pHEMA hybrids displays a semicircle profile and is indicative of an electric double-layer capacitor behavior. The charge transfer resistances (R_{CT}) of Hybrid-01 and Hybrid-10 sample are estimated to be 11743 and 6438 ohm, respectively. As

the content of nano copper particle in polymer matrix increased, the redox ability of copper raised and promote the oxidation current shown in cyclic voltammograms, where the time constant ($\tau = C_{spec}R_s$) of Hybrid-01 and Hybrid-10 which is about 0.098 and 0.133, respectively was obtained. A material with a higher value of time constant suggests that the probability of thrombosis or platelet adhesion is minimized. However, the copper oxide played a n-type role in the hybrid, it can be seen that the surface charge of the hybrids showed more negative with an increasing incorporation of the copper nanoparticle, to a value of as high as -24.6 mV as given in previous study. Accordingly, surface with increasing negative charge should exhibit improved anti-blood clotting behavior; together with redox ability of Cu nanoparticles reported earlier, it further reinforces the argument that the hybrids currently prepared should have improved thromboresistant property.

Nitric oxide has been widely recognized as a potent vasodilator and inhibitor of platelet adhesion and activation [201-203]. Because it has very short lifetime in blood [204] due to its reactivity with various blood components [205], a more abundant (i.e., micromolar concentrations) and stable form of NO in blood are *S*-nitroso adducts with thiol groups (RSNOs) [206], such as *S*-nitrosoglutathione (GSNO) [207-209]. In order to investigate the NO production from Cu(0)-pHEMA hybrid, the redox properties and the mechanism of copper mediated nitrosoglutathione (GSNO) reduction to nitric oxide (NO) were performed in aqueous system. Fig. 8.3 illustrates the typical current responses to different concentrations of nitrosoglutathione reduced by the Hybrid-10 at an operation voltage of -1.1V (vs. Ag/AgCl) at 25^{o}C. As shown in Fig. 8.3, the reduction currents of hybrid varied with the concentration of nitrosoglutathione. With increasing levels of nitrosoglutathione (GSNO), the amount of NO generation increased. The reduction current of nitrosoglutathione into NO was linear with the nitrosoglutathione concentration as shown in Fig 8.3 (b).

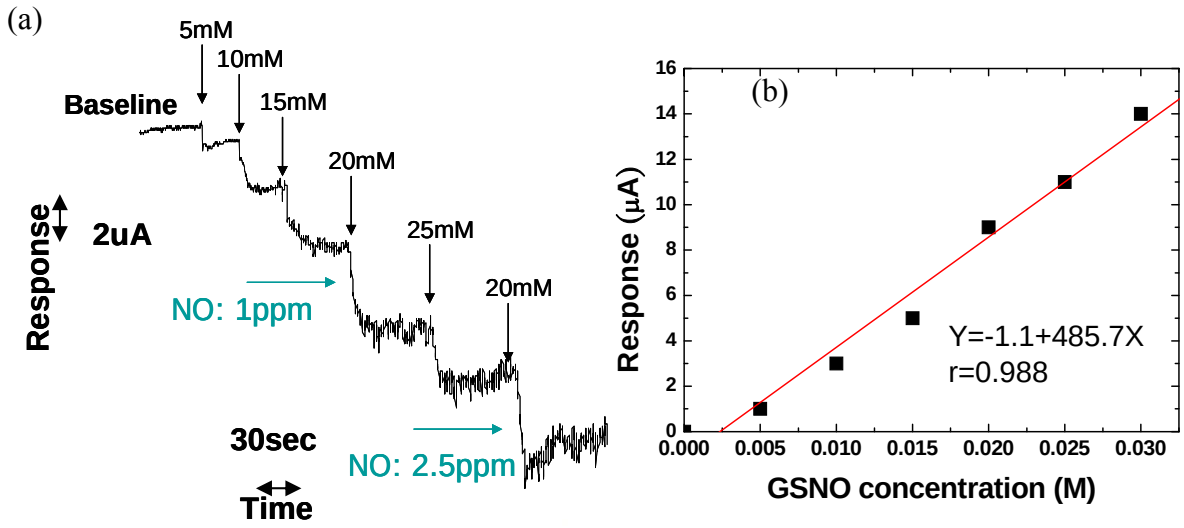

Fig. 8.3 (a) Amperometric responses of NO-generating from Hybrid-10. (b) The correlation between nitrosoglutathione (GSNO) and reduction current.

The reduction current of nitrosoglutathione for Composite-05 micro, Composite-05 nano (synthesis in chapter 6), Hybrid-2, and Hybrid-4 (synthesis in chapter 6) have also been tested. As shown in Fig. 8.4, for the same copper content (about 0.3~0.5 wt %), the in-situ Cu(0)-pHEMA hybrid has higher reduction current than the composite. It might be due to the higher surface area of the in-situ hybrid.

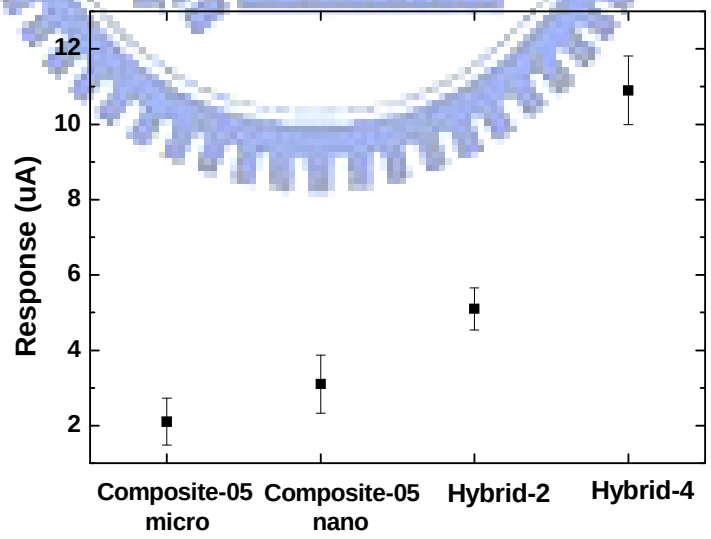

Fig. 8.4 Amperometric responses of NO-generating from Composite-05 micro, Composite-05 nano, Hybrid-2, and Hybrid-4 with 20mM GSNO.

An XPS analysis of Cu(II)-pHEMA hybrid after redox with GSNO was shown in Fig. 8.5., where the Cu 2p3/2 NPs spectrum of the Cu(II)-pHEMA hybrid shows a peak at 933.8 ± 0.3 eV which is mainly attributed to CuO, while two weaker feature, lying at 932.3 ± 0.2 eV and 934.7 ± 0.2 eV are attributed to a small amount of Cu_2O and $Cu(OH)_2$, respectively. A corresponding fraction of the copper species of respective concentration can be correlated with the area under the spectrum and this determines the fraction of the CuO was 77.1%, Cu_2O was 10.3%, and $Cu(OH)_2$ was 12.6% in the resulting Cu(II)-pHEMA hybrid.

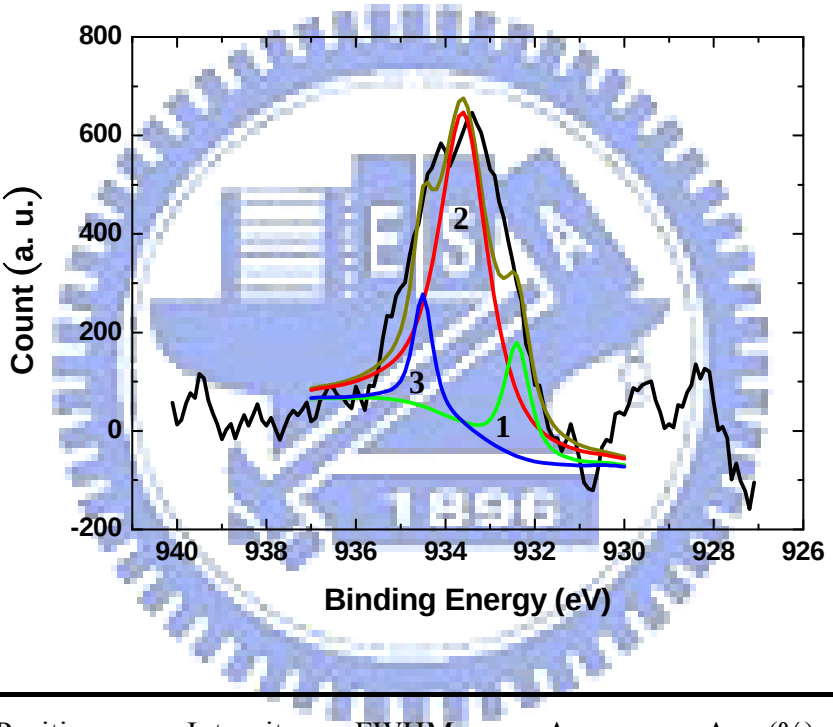

#	Position (eV)	Intensity	FWHM (eV)	Area	Area(%)	Component
1	932.3	196.38	2.8	382.8	10.3%	Cu_2O
2	933.8	623.51	1.7	3347.6	77.1%	CuO
3	934.7	293.66	1.2	546.5	12.6%	$Cu(OH)_2$

Fig. 8.5 The Cu $2p_{3/2}$ peaks of XPS spectra of Cu(II)-pHEMA hybrid after redox reaction with GSNO.

This indicates that the copper oxidized into copper oxide developed in the Cu(II)-pHEMA hybrid is a mixture of mainly CuO and a small fraction of Cu_2O and $Cu(OH)_2$, after electrochemical oxidation. The presence of mainly divalent CuO imparts a negative surface charge to the hybrid (present in chapter 7) which may further prevent the occurrence of the oxidative reaction of fibrinogen as schematically shown in Fig. 8.6, leading to an improved anti-thrombosis character of the hybrid composites.

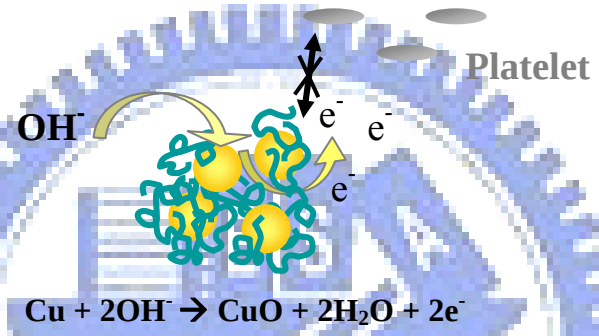

Fig. 8.6 Scheme of the electrochemical reaction for Cu(0)-pHEMA hybrid.

8.4 Summary

An electrochemical activated Cu(0)-pHEMA hybrid was successfully fabricated by in-situ UV-light polymerization and chemical reduction process. The nano copper particles were uniformly dispersed in pHEMA matrix to form a Cu(0)-pHEMA hybrid and alternated the electrochemical properties of the polymer matrix. The particle size in pHEMA matrix would be increased by broadening the network space via controlling the monomer concentration. The oxidation reaction of nano copper particles in pHEMA to form copper oxide was enhanced with the content of the copper nano-particles and followed that the time constant of the Cu(0)-pHEMA hybrid was decreased.

Chapter 9

Conclusions

9.1 Silica-base pHEMA nanocomposites

- In comparison with neat pHEMA, the addition of SiO_2 nanoparticles revealed a significant effect on the reaction rate of crosslinking during polymerization, resulting in composites with varying nanoporous structures.
- The composites showed improved tensile strength, and the platelet adhesion property remained as excellent as that of neat pHEMA, which encourages the use of such composites for antithrombotic applications.
- Drug diffusion characteristics in the composites can be well modulated by controlling the concentrations of the SiO_2 nanoparticles and water in the starting stage of synthesis.
- The hydroxyl group of the hybrid was verified by controlling the hydrolysis degree of silanol and the composition of the hybrid.
- The drug diffusion profile of silanol/pHEMA hybrid could also be modified by varying the silanol in the range from 2.11×10^{-7} cm^2/hr to 8.13×10^{-7} cm^2/hr. The incorporation of silica sol into pHEMA hydrogel not only enhanced the thermo stability of hydrogel but also increased the swelling degree.

9.2 Copper-base pHEMA nanocomposites

- The interaction between the copper ions and hydroxyl groups may further stabilize the hybrid structure. Cu(II)-pHEMA and Cu(0)-pHEMA hybrid exhibits superior thermal stability to that pHEMA of by an enhancement of the decomposition temperature.

- The metallic Cu nanoparticle shows improved crystallinity as water concentration increased. The Cu size is increased from an average of ~10 nm to 25 nm in diameter as the molar ratio of H_2O/HEMA increased from 2 to 6.
- The Cu nanoparticle embedded within the pHEMA matrix is present in a form of primary particle without appreciable aggregation. The tendency of cluster formation of the Cu nanoparticles and further developing into particle network structures seem to become more pronounced as the molar ratio of H_2O/HEMA was reduced.
- While increasing the H_2O/HEMA ratio, the network of the pHEMA is prone to developing a spacious volume for copper nanoparticles to nucleate and grow to a certain size, resulting in a porous structure which provided more spacious volume for the growth of Cu nanoparticles.
- The higher starting H_2O/HEMA molar ratio, the greater extent of the porous structure in the final hybrid obtained, and a greater tendency to form connective Cu nanoparticle network within the matrix phase observed.
- The copper developed in the Cu(0)-pHEMA hybrid is a mixture of mainly metallic Cu(0) and a small fraction of CuO, after in-situ chemical reduction. The presence of small amount of divalent CuO suggests an incomplete reduction reaction of Cu(II) ions in the matrix.
- The crystallinity of the resulting Cu nanoparticles have little influence on release mechanism.
- After a 48 h incubation with 6 ppm copper ion Cu(II) results in a progressive increase of cell numbers which reaches 121% of the control. Without the use of ECGS in medium, the proliferation of HUVEC was still stimulated by the copper, with an increase of cell numbers reaching 106% of the control.
- Cu(II) released from the hybrids showed inhibition effect on human smooth muscle cells, from about 90% to 70% of the control.

- The neat pHEMA and Cu(0)-pHEMA hybrids showed negatively charged at pH 7.4 and became more negative with an increasing incorporation of the Cu(0) nanoparticle.
- The incorporation of nano copper particles into pHEMA matrix increases the interface interaction between the solid film and aqueous solution.

Reference

[1] A. S.Hoffman, *J Control. Release* **1987**, 6, 297.

[2] R. Langer, *Science* **2001**, *293*, 58.

[3] R. Langer and J. P. Vacanti, *Science* **1993**, *260*, 920.

[4] N. A. Peppas, J. Z. Hilt, A. Khademhosseini and R. Langer, *Adv. Mater.* **2006**, *18*, 1345.

[5] F. Brandl, F. Sommer and A. Goepferich, *Biomaterials* **2007**, *28*, 134.

[6] S. Brahim, D. Narinesingh and A. Guiseppi-Elie, *Biomacromolecules* **2003**, *4*, 497.

[7] S. Lahooti, M. V. Sefton, *Tissue. Eng.* **2000**, 6, 139.

[8] M. F. Refojo, *J. Polym. Sci. Part A1 Polym. Chem.* **1967**, 5, 3103.

[9] S. S. Ischenko, V. F. Rosovitskii, A. B. Pridatko, N. V. Babkina, E. V. Lebedev. *J. Appl. Chem.* **1998**, 11, 1929.

[10] S. Miyazaki, H. Endo, T. Karino, K. Haraguchi and M. Shibayama, *Macromolecules* **2007**, *40*, 4287-4295.

[11] O. Okay and W. Oppermann, *Macromolecules* **2007**, *40*, 3378.

[12] T. Ogoshi, Y. Takashima, H. Yamaguchi and A. Harada, *J. Am. Chem. Soc.* **2007**, *129*, 4878.

[13] L. Meng, Y. Lu, X. Wang, J. Zhang, Y. Duan and C. Li, *Macromolecules* **2007**, *40*, 2981-2983.

[14] K. N. M. K. N. Y. Shoichiro Yano, *J. Appi. Polym. Sci.* **1994**, *54*, 163.

[15] L.E. Vera-Avila, E. Garcia-Salgado, M.P.G. de Llasera, A. Pena-Alvarez, *Analy. Biochem.* **2008**, *373*, 272.

[16] S. A. Pellice, D. P. Fasce, R. J. J. Williams, *J. Appl. Polym. Sci.* **2007**, *105*, 2351.

[17] C. Ohtsuki, T. Miyazaki, M. Kamitakahara and M. Tanihara, *J. Eur. Ceram. Soc.* **2007**, *27*, 1527.

[18] G. Giavaresi, P. Torricelli, P. M. Fornasari, R. Giardino, R. Barbucci and G. Leone, *Biomaterials* **2005**, *26*, 3001.

[19] C. K. Sen, S. Khanna, M. Venojarvi, P. Trikha, E. C. Ellison, T. K. Hunt, S. Roy, *Am. J. Physiol, Heart Circ. Physiol.* **2002**, *282*, H1821.

[20] G. F. Hu, *J. Cell. Biochem.* **1998**, *69*, 326.

[21] H. Hoffman, B. McAuslan, D. Robertson, E. Burnett, *Exp. Cell Res.* 102(2), **1976**, 269.

[22] J. M. Bastidas and T. Simancas, *Biomaterials* **1997**, *18*, 247.

[23] O. Wichterle and D. Lim, *Nature* **1960**, *185*, 117.

[24] C. Ohtsuki, T. Miyazaki and M. Tanihara, *Mater. Sci. Eng. C* **2002**, *22*, 27.

[25] J. Song, E. Saiz and C. R. Bertozzi, *J. Eur. Ceram. Soc.* **2003**, *23*, 2905.

[26] C. D. Young, J. R. Wu, T. L. Tsou, *Biomaterials* **1998**, *19*, 1745.

[27] I. Gursel, C. Balcik, Y. Arica, O. Akkus, N. Akkas and V. Hasirci, *Biomaterials* **1998**, *19*, 1137.
[28] B. D. Johnson, D. J. Beebe and W. C. Crone, *Mater. Sci. Eng. C* **2004**, *24*, 575.
[29] P. Kortesuo, M. Ahola, M. Kangas, A. Yli-Urpo, J. Kiesvaara and M. Marvola, *Int. J. Pharm.* **2001**, *221*, 107.
[30] B. Kabra, S. H. Gehrke, S. T. Hwang, W. Ritschel, G.. Kabra, *J. Appl. Polym. Sci.* **1991**, *42*, 2409.
[31] J. Wang, W. Wu, *European Polymer Journal* **2005**, *41*, 1143.
[32] X. Lou, C. V. Coppenhagen, *Polym. Int.* **2001**, *50*, 319.
[33] C. D. Young, J. R. Wu, T. L. Tsou, *J. Memb. Sci.* **1998**, *146*, 83.
[34] H. Tsukeshiba, M. Huang, Y. H. Na, T. Kurokawa, R. Kuwabara, Y. Tanaka, H. Furukawa, Y. Osada and J. P. Gong, *J. Phys. Chem. B* **2005**, *109*, 16304.
[35] S. H. Baek and B. K. Kim, *Colloid Surf. A: Physicochem. Eng. Aspects* **2003**, *220*, 191.
[36] K. Haraguchi, R. Farnworth, A. Ohbayashi and T. Takehisa, *Macromolecules* **2003**, *36*, 5732.
[37] P. G. Emmanuel, *Adv. Mater.* **1996**, *8*, 29.
[38] D. L. T. Norman Herron, *Adv. Mater.* **1998**, *10*, 1173.
[39] Z. Wang and T. J. Pinnavaia, *Chem. Mater.* **1998**, *10*, 3769.
[40] G. Carotenuto, Y.-S. Her, E. Matijevic, *Ind Eng Chem Res* **1996**, *35*, 2929.
[41] M. Lira-Cantu, P. Gomez-Romero, *Chem. Mater.* **1998**, *10*, 698.
[42] J. J. Tunney, C. Detellier, *Chem. Mater.* **1996**, *8*, 927.
[43] Y. Wang, N. Herron, Chem. Phys. Lett. **1992**, *200*, 71.
[44] R. D. Maggio, L. Fambri, R. Campostrini, *J. Sol-Gel Sci. Tech.* **2003**, *26*, 339.
[45] L. David, J. F. Gerard, J. P. Pascault, G. Vigier, P. Hajji, *J. Polym. Sci. B: Polym. Phys.* **1999**, *37*, 3172.
[46] K.-D. S. No-Hyung Park, *J. Appl. Polym. Sci* **1999**, *71*, 1597.
[47] E. J. A. Pope, M. Asami, J. D. Mackenzie, *J. Mater. Res.* **1989**, 4, 1018.
[48] M. N. Bruce, *Adv. Mater.* **1993**, *5*, 422.
[49] P . Judeinstein, C. Sanchez, *J. Mater. Chem.* **1996**, 6, 511.
[50] Y. Chujo, R. Tamaki, MRS Bull. **2001**, 26, 389.
[51] J . WEN, G. L. WILKES, *Chem. Mater.* **1996**, 8, 1667.
[52] Z. H. Huang, K. Y. Qiu, *Polymer* **1997**, 38, 521.
[53] R. O. R. Costa, W. L. Vasconcelos, *J. Non-Cryst. Sol.* **2002**, 304, 84.
[54] B. A. Weisenberg, D.L. Mooradian, *J. Biomed. Mater. Res. Part A* **2002**, 60, 283.
[55] H. M. Chen, X.M. Tian, H. Zou, *Artif. Cells Blood Substit. Biotechnol*. **1998**, 26, 431.
[56] R. M. Laine, *J. Mater. Chem.* **2005**, 15 (35&36), 3725.

[57] S. Jedlicka, J. McKenzie, S. Leavesley, K. Little, T. Webster, J. Paul Robinson, D. Nivens, J. Rickus, *J. Mater. Chem.* 2006, 16, 3221.
[58] C. J. Brinker, G. W. Scherer. Sol–gel science. vol. 1. New York: Academic Press; **1989** pp. 97–152.
[59] R. D. Maggio, F. Rossi, L. Fambri, *J. Non-Cryst. Sol.* **2004**, 345, 591.
[60] B. Samuneva, P. Djambaski, E. Kashchieva, G. Chernev, L. Kabaivanova, E. Emanuilova, I. M. M. Salvado, M. H. V. Fernandes, A. Wu, *J. Non-Cryst. Sol.* **2008**, 354, 733.
[61] P. Bosch, F. D. Monte, J. L. Mateo, D. Levy, *J.Polym. Sci.A: Polym.Chem.* **1996**, 34, 3289.
[62] Y. Wei, D. Jin, C.Yang, M. C. Kels, K.Y. Qiu, *Mater. Sci. Engng. C* **1998**, 6, 91.
[63] T. Xie, C. Zhou, S. Feng, H. Wang, *J. Appl.Polym. Sci. **2000**,* 75, 379.
[64] R. O. R. Costa, L. Wander, *J. Non-Cryst. Sol.* **2002**, 304, 84.
[65] S. L. Huang, W. K. Chin, W. P. Yang, *Polymer* **2005**, 46, 1865.
[66] T. Teranishi, M. Hosoe, M. Miyake, *Adv. Mater.* **1997**, 9, 65.
[67] T. Teranishi, M. Miyake, *Chem. Mater.* **1998**, 10, 594.
[68] M. M. Maye, S. C. Chun, L. Han, D. Rabinovich, C. J. Zhong, *J. Am. Chem. Soc.* **2002**, 124, 4958.
[69] D.Y. Godovsky, *Advan. Polym. Sci.* **2000**, 153, 163.
[70] T. Vossmeyer, E. Deionno, J. R. Heath, *Angew. Chem. Int. Ed.* **1997**, 36, 1080.
[71] K. Mohomed, T. G. Gerasimov, H. Abourahma, M. J. Zaworotko, J. P. Harmon *Mater. Sci. Engng. A* **2005,** 409, 227.
[72] J. J. Michels, M. J. O'Connell, P. N. Taylor, J. S. Wilson, F. Cacialli, H. L. Anderson, *Chem. Eur. J.* **2003**, 9, 6167.
[73] S. Dad, P. Hodge, S.D. Kamau, *React. Funct. Polym.* **2003** 54, 131.
[74] K. Matyjazewski , J. H. Xia, *Chem. Rev.* **2001**, 101, 2921.
[75] K. Zhang, H. Li, S. Zhao, W. Wang, S. Wang, Y. Xu, W. Yu, J. Wang, *Polym. Bull.* **2006**, 57, 253.
[76] Z. P. Zhang, L. D. Zhang, S. X. Wang, W. Chen, Y. Lei, *Polymer* **2001**, 42, 8315.
[77] B. C. Sih, A. Teichert, M. O. Wolf, *Chem Mater* **2004**, 16, 2712.
[78] X. L. Zhao, X. B. Ding, Z. H. Deng, Z. H. Zheng, Y. X. Peng, X. P. Long, *Macromol. Rapid. Commun.* **2005**, 26, 1784.
[79] C. Wang , N. T. Flynn, R. Langer, *Adv. Mater.* **2004**, 16(13), 1074.
[80] Y. Xiang, D. Chen, *Eur. Polym. J.* **2007**, 43, 4178.
[81] Y. Qiu, K. Park, *Adv. Drug Deliv. Rev.* **2001**, 53, 321.
[82] N. A. Peppas, R. Gurny, E. Doelker, P. Buri, *J. Membr. Sci.* **1980**, 7(3), 241.
[83] B. Narasimhan, R. Langer, *J. Control. Release* **1997**, 47, 13.
[84] J. Heller, *J. Control. Release* **1985**, 2, 167.

[85] L. Yang, R. Fassihi, *J. Control. Release* **1997**, 44, 135.
[86] N. A. Peppas, A. R. Khare, *Adv. Drug. Deliv. Rev.* **1993**, 11, 1.
[87] P. Colombo, *Adv. Drug. Deliv. Rev.* **1993**, 11, 37.
[88] G. Astarita, G.C. Sarti, *Polym. Eng. Sci.* **1978**, 18, 388.
[89] G. W. R. Davidson, N. A. Peppas, *J. Control. Release,* **1986**, 3, 243.
[90] N. M.Franson, N. A.Peppas, *J. Appl. Polym. Sci*. **1983**, 28, 1299.
[91] C. S. Brazel, A. Nikolaos, *Polymer* **1999**, 40, 3383.
[92] S. Lu, S. Kristi, *J Control. Release* **1999**, 57, 291.
[93] R. W. Korsmeyer, E. von Meerwall, N. A.Peppas, *J. Polym. Sc.i: Polym. Phys.* **1986**, 24, 409.
[94] H.B. Hopfenberg, H. L.Frisch, *Polym. Lett.* **1969**,7 ,405.
[95] T. K. Kwei, T. T. Wang, H. M. Zupko, *Macromolecules* **1972**, 5, 645.
[96] N. A. Peppas, Hydrogels in Medicine and Pharmacy; CRC: Boca Raton, FL, **1986**.
[97] R. Yoshida, K. Sakai, T. Okano, Y. Sakurai, *Adv. Drug. Delivery. Rev.* **1993**, 11, 85.
[98] S. Ueda, T. Hata, S. Asakura, H. Yamaguchi, M. Kotani, Y. Ueda, *J. Drug Target.* **1994**, 2, 35.
[99] B. G. Stubbe, K. Braeckmans, F. Horkay, W. E. Hennink, S. C. De Smedt, J. Demeester, *Macromolecules* **2002**, 35, 2501.
[100]H. Hongyan, L. X. Cao, J. Lee, *J. Control. Release* **2004**, 95, 391.
[101]A. Gallardo, C. Parejo, J. S. Roma´n, *J. Control. Release* **2001**, 71, 127.
[102]L. Sartore, I. Perone, P. Ferruti, R. Latini, R. Barnasconi, *J. Biomater. Sci. Polym. Ed.* **1997**, 8, 741.
[103]I. Nozawa, Y. Suzuki, S. Sato, K. Sugibayashi, Y. Morimoto, *J. Biomed. Mater. Res.* **1991**, 25, 577.
[104] A. D'Emanuele, *Clin. Pharmacokinet.* **1996**, 41, 241.
[105] T. Okano, Y. H. Bae, H. Jacobs, S. W. Kim, *J. Control. Release* **1990**, 11, 255.
[106]R. Dinarvand, M. Ansari, *J. Membr. Sci.* **2003**, 223, 217.
[107]S. Y. Lin, C. J. Ho, M. J. Li, *J. Control. Release* **2001**, 73, 293.
[108]A. K. Bajpai, D. D. Mishra, *J. Mater. Sci: Mater Med* **2004** 15, 583.
[109]E. Kulik, Y. Ikada, *J. Biomed. Mater. Res.* **1996**, 30, 295.
[110]M. Morra, J. Biomater. Sci., Polym. Ed. **2000**,11, 547.
[111]Y. Iwasaki, Y. Aiba, N. Morimoto, Y. Nakabayashi, K. Ishihara, *J. Biomed. Mater. Res.* **2000**, 52, 701.
[112]T. Okano, S. Nishiyama, I. Shinohara, T. Akaike, Y. Sakurai, K. Kataoka, T. Tsuruta, *J. Biomed. Mater. Res.* **1981,** 15, 393.
[113]N. Yui, K. Sanui, N. Ogata, K. Kataoka, T. Okano, Y. Sakurai. *J. Biomed. Mater.*

Res. **1986**, 20, 929.
[114]D. L. Coleman, D. E. Gregonis, J. D. Andrade, *J. Biomed. Mater. Res.* **1982**, 16, 381.
[115]J. P. Montheard, M. Chatzopoulos, D. Chappard, *J. Macromol. Sci. Polym. Rev.* **1992**, 32, 1.
[116]C. Ohtsuki, T. Miyazaki, M. Tanihara, *Mater. Sci. Engng. C* **2002**, 22, 27.
[117]J. Song, E. Saiz, C, R. Bertozzi, *J. Eur. Ceram. Soc.* **2003,** 23, 2905.
[118]C. D. Young, J. R. Wu, T. L. Tsou, *Biomaterials* **1998**, 19, 1745.
[119]I. Gursel, C. Balcik, Y. Arica, O. Akkus, N. Akkas, V. Hasirci, *Biomaterials* **1998**, 19, 1137.
[120]B. D. Johnson, D. J. Beebe, W. C. Crone, *Mater. Sci. Eng. C* **2004**, 24, 575.
[121]B. Kabra, S. H. Gehrke, S. T. Hwang, W. Ritschel, *J. Appl. Polym. Sci.* **1991**, 42 2409.
[122]G. W. Boss, N. M. Scharenborg, A. A. Poot, G. H. M. Engbergs, T. Beugeling, W. G. van Aken, J. Feijen, *J. Biomed. Mater. Res.* **1999**, 47, 279.
[123]C. W. Chung, H. W. Kim, Y. B. Kim, Y. H. Rhee, *J. Biol. Macromol.* **2003**, 32, 17.
[124]E. Brynda, M. Houska, M. Jirouskova, J. E. Dyr, *J. Biomed. Mater. Res.* **2000**, 2, 249.
[125] X. F. Li, C. F. Chen, Z. F. Li, H. Q. Gu, M. Z. Lu, Y. Z. Han, X. B. Liu, *Die Makromolekulare Chemie.* **2003**, 187(2), 367.
[126]V. Sirolli, S. D. Stante, S. Stuard, L. Liberato, L. Amoroso, P. Cappelli, M. Bonomini, *Int. J. Artif. Organs* **2000**, 23, 356.
[127]Y. C. Nho, O. H. Kwon, *Radiation Phy. Chem.* **2003**, 66, 299.
[128]A. K. Bajpai, S. Kankane, *J. Mater. Sci.: Mater. Med.* **2008**, 19, 1921.
[129]A. K. Bajpai, S. Kankane, *J. Appl. Polym. Sci.* **2007**, 104, 1559.
[130]K. Rezwan, L. P. Meier, L. J. Gauckler, *Biomaterials* **2005**, 26, 4351.
[131]W. K. Lee, J. S. Ko, H. M. Kim, *J. Colloid. Interface Sci.* **2002**, 246, 70.
[132]A. K. Bajpai, D. D. Mishra, *J. Appl. Polym. Sci.* **2008**, 107, 541.
[133]B. K. Oh, M. E. Meyerhoff, *Biomaterials* **2004**, 25(2), 283.
[134]Y. D. Wu, A. P. Rojas, G. W. Griffith, A. M. Skrzypchak, N. Lafayette, R. H. Bartlett, M. E. Meyerhoff, *Sensors And Actuators B-Chemical* **2007**, 121(1), 36.
[135]C. C. Shih, C. M. Shih, Y. Y. Su, R. A. Gerhardt, S. J. Lin, *J. Biomed. Mater. Res. Part A* **2005**, 74A: 325.
[136]M. C. Yang, T. Y. Liu, *J. Membr. Sci.* **2003**, 226, 119.
[137]M. Miyajima, A. Koshika, J.i. Okada, M. Ikeda, *J. Control. Release* **1999**, 60, 199.
[138]J. M. Bastidas, J. Simancas, *Biomaterials* **1997,** 18(3), 247.

[139]J. M. Bastidas, E. Cano, N. Mora, *Contraception* **2000,** 61(6), 395.
[140]C. C Hu, S. Y. Wang, C. L. Li, C. J. Chuang, K. L. Tung, *J. Chem. Eng. Jpn.* **2006**, 39,1283.
[141]S. X. Lu, K. S. Anseth, *J. Control. Release* **1999**, 57, 291.
[142]J. D. Cho, H. T. Ju, J. W. Hong, *J. Polym. Sci. Pol. Chem.* **2005**, 43, 658.
[143]D. S. Kim, K. M. Lee, *J. Appl. Polym. Sci.* **2004**, 92, 1955.
[144]J. E. Elliott, J. W. Anseth, C. N. Bowman, *Chem. Eng. Sci.* **2001**, 56, 3173.
[145]M. Taira, H. Suzuki, H. Toyooka, M. Yamaki, *J. Mater. Sci. Lett.* **1994**, 13, 68.
[146]W. S. Kim, Y. C. Jeong, J. K. Park, *Optics Express.* **2006***,* 14, 8967.
[147]P. Bosch, F. DelMonte, J.L. Mateo, D. Levy, *J. Polym. Sci. Pol. Chem.* **1996**, 34, 3289.
[148]F. Branda, A. Costantini, G. Luciani, L. Ambrosio, *J. Biomed. Mater. Res. Part A* **2001**, 57, 79.
[149]S. M. Murphy, C. J. Hamilton, B. J. Tighe, *Polymer* **1998**, 29, 1887.
[150]A. Barnes, P. H. Corkhill, B.J. Tighe, *Polymer* **1988**, 29, 2191.
[151]M. Tanaka, A. Mochizuki, *J. Biomed. Mater. Res. Part A* **2004**, 68A, 684.
[152]M. Tanaka, A. Mochizuki, N. Ishii, T. Motomura, T. Hatakeyama, *Biomacromolecules* **2002**, 3, 36.
[153]E. Hirota, K. Ute, M. Uehara, T. Kitayama, M. Tanaka, A. Mochizuki, *J. Biomed. Mater. Res.* **2006**, Part A 76A, 540.
[154]R. Baker, Controlled release of biologically active agents, John Wiley & Sons, New York.
[155]M. Wasiucionek, M.W. Breiter, *J. Non-Cryst. Sol.* **1997**, 220(1), 52.
[156]S. L. Huang, W. K. Chin, W. P. Yanga, *Polymer* **2005**, 46(6), 1865.
[157]R. O. R. Costa, W. L. Vasconcelos, *J. Non-Cryst. Sol.* **2002**, 304(1-3), 84.
[158]X. L. Ji, S.C. Jiang, X. P. Qiu, D.W. Dong, D.H. Yu, B. Z. Jiang, *J. Appl. Polym. Sci.* **2003**, 88(14), 3168.
[159]J. Zhang, X.X. Xu, Z.C. Wu, R.J. Yang, C.Z. Zhang, Spectroscopy and Spectral Analysis **2006**, 26(1), 37.
[160]J. Hjartstam, T. Hjertberg, *J. Appl. Polym. Sci.* **1999**, 72(4), 529.
[161]B. Schrader, Infrared and Raman spectroscopy:methods and applications, Weinheim,**1995**
[162]J. E. Elliott, J. W. Anseth, C. N. Bowman, *Chem. Eng. Sci.* **2001**, 56(10), 3173.
[163]J. D. Cho, H. T. Ju, J. W. Hong, *J. Polym. Sci. Part A1 Polym. Chem.* **2005**, 43(3), 658.
[164]R. Baker, Controlled release of biologically active agents, John Wiley & Sons, New York.
[165]S. Z. Cai, X. P. Xia, C. H. Zhu, C. S. Xie, *J. Biomed. Materi. Res. Part B* **2007**,

80B(1), 220.
[166]Y. Y. Liu, T. H. Tung, T. Y. Liu, S. Y. Chen, D. M. Liu, *Acta Biomaterialia*, **2008** (in print).
[167]K. D. F. Vlugt-Wensink, X. L. Jiang, G. Schotman, G. Kruijtzer, A. Vredenberg, J. T. Chung, Z. B. Zhang, C. Versluis, D. Ramos, R. Verrijk, W. Jiskoot, D. J. A. Crommelin, W. E. Hennink, *Biomacromolecules* **2006**, 7(11), 2983.
[168]S. Belfer, A. Bottino, G. Capannelli, *J. Appl. Polym. Sci.* **2005**, 98(1), 509.
[169]A. Perkowska, H. Maluszynska, *J. Mol. Struct.* **1999**, 508(1-3), 111.
[170]S. Deki, K. Akamatsu, T. Yano, M. Mizuhata, A. Kajinami, *J. Mater. Chem.* **1998**, 8(8), 1865.
[171]Y. Hu, Y. Z. Wu, J. Y. Cai, Y. F. Ma, B. Wang, K. Xia, X. Q. He, *Int. J. Molecular Sci.* **2007**, 8(1), 1.
[172]P. L. Ritger, N.A. Peppas, *J. Control. Release* **1987**, 5(1), 37.
[173]J. S. Ahn, H. K. Choi, M. K. Chun, J. M. Ryu, J. H. Jung, Y. U. Kim, C. S. Cho, *Biomaterials* **2002**, 23(6), 1411.
[174]L. Y. Huang, M. C. Yang, *Colloids Surf. B: Biointerfaces* **2008**, 61(1), 43.
[175]P. M. Gullino, M. Ziche, G. Alessandri, Gangloosides, *Cancer Metastaasis Reviews* **1990**, 9, 239
[176]B. R. McAuslan, G.A. Gole, Trans Ophthalmol Soc **1980**, 354.
[177]M. Ziche, J. Jones, P.M. Gullino, *J. Natl. Cancer Inst.* **1982**, 69, 475.
[178]J. Folkman, M. Klagsbrun, J. Sasse, M. Wadzinski, D. Ingber, I. Vlodavsky, *Am. J. Pathol.* **1988**, 130, 393.
[179]R. K. Dey, A. R. Ray, *J. Macromol. Sci., Chem.* **2005**, A42, 351.
[180]T. Goda, K. Ishihara, *Expert Review of Medical Devices* **2006**, 3, 167.
[181]A. Bolz, M. Amon, C. Ozbek, B. Heublein, M. Schaldach, *Texas Heart Institute Journal* **1996**, 23, 162.
[182]P. Baurschmidt, M. Schaldach, *Ann. Biomed. Eng.* **1977**, 1, 261.
[183]Y. Liu, Z. Li, Z. He, D. Chen, S. Pan, *Surf. Coat. Technol.* **2007**, 201, 6851.
[184]B. D. Ratner, *Biomaterials,* In Press, Corrected Proof
[185]I. Topala, N. Dumitrascu, V Pohoata, *Plasma Chem. Plasma Process.* **2007**, 27, 95.
[186]H. P. Zhang,G .M. Annich, J. Miskulin, K. Stankiewicz, K. Osterholzer, S .I. Merz, R. H. Bartlett, *J. Am. Chem. Soc.* **2003**, 125: 5015.
[187]C. Huang, C. Z. Yang, *Appl. Phys. Lett.* **1999**, 74: 1692.
[188]J. Wang, Q. W. Zhang, F. Saito, *Colloids Surf. A-Physicochemical And Engineering Aspects* **2007**, 302, 494.
[189]G. Merga , R. Wilson R, G. Lynn, B. H. Milosavljevic, D. Meisel, *J. Phys. Chem. C* **2007**, 111, 12220.

[190]J. M. Grunkemeier, W. B. Tsai, T. A.Horbett, *J. Biomed. Materi. Res.* **1998**, 41, 657.
[191]G. A. Skarja, J. L. Brash, *J. Biomed. Materi. Res.* **1997,** 34, 439.
[192]F. C. Kung, J.J. Chang, M. C. Yang , *Polym. Adv. Tech.* **2007**, 18, 286.
[193]E. Hirota, K. Ute , M. Uehara, T. Kitayama, M. Tanaka, A. Mochizuki, *J. Biomed. Materi. Res. Pt. A* **2006**, 76A, 540.
[194]Y. H. Kim, D. K. Han, K. D. Park and S. H. Kim, *Biomaterials* **2003**, 24, 2213.
[195]V. Chandrasekhar, A. Athimoolam, V. Krishnan, R. Azhakar, C. Madhavaiah and S. Verma: *Eur. J. Inorg. Chem.* **2005**, 1482.
[196]S. Srinivasan and P. N. Sawyer, *Correlation of the surface charge characteristics of polymer with their antithrombogenic characteristics.* In: A. Rembaum, Shen M, editors, Biomedical polymers, New York: Marcel Dekker **1971**, p. 51.
[197]Y. Tabata, Y. Matsui and Y. Ikada, *J. Control. Release* **1998**, 56, 135.
[198]L. D. Burke,T.G. Ryan, *J. Electrochem. Soc.* **1990**, 37, 1358.
[199]L. D. Burke,G.M. Bruton, J. A. Collins, *Electrochem. Acta* **1998**, 44, 1467.
[200]A. W. Adamson, Physical Chemistry of Surfaces, 3rd ed.,John Wiley, New York, **1976**, p. 244.
[201]J. G. Diodati, A. A. Quyyumi, N. Hussain, L. K. Keefer, *Thromb. Haemost.* **1993**, 70, 654.
[202]L. J. Ignarro, G. M. Buga, K. S. Wood, R. E. Byrns, G. Chaudhuri, *Proc. Natl. Acad. Sci. U.S.A.* **1987**, 84, 9265.
[203]M. Radomski, R. Palmer, S. Moncada, *Proc. Natl. Acad. Sci. U.S.A.* **1990**, 87, 5193.
[204]P. L. Feldman, O. W. Griffith, D. J. Stuehr, *Chem. Eng. News* **1993**,71, 26.
[205]K. Wong, X. B. Li, Transfus. *Apheresis Sci.* **2004**, 30, 29.
[206]J. P. Wallis, *Transfus. Med.* **2005**, 15, 1
[207]J. S. Stamler, O. Jaraki, J. Osborne, D. I. Simon, J. Keaney, J. Vita, D. Singel, C.R. Valeri, J. Loscalzo, *Proc. Natl. Acad. Sci. U.S.A*. **1992**, 89, 7674.
[208]D. Giustarini, A. Milzani, R. Colombo, I. Dalle-Donne, R. Rossi, *Clin. Chim. Acta* **2003**, 330, 85.
[209]D. Jourd'heuil, K. Hallen, M. Feelisch, M.B. Grisham, *Free Radic. Biol. Med.* **2000**, 28, 409.